Research Institute for Farm Animal Biology (FBN), Department of Nutritional Physiology, Dummerstorf, Germany

and

Rostock University Medical Center, Department of Medicine II, Division of Gastroenterology and Endocrinology, Rostock, Germany

# Metabolic alterations and early development of sarcopenia in a murine model of cholestatic liver disease

Dissertation for the attainment of the academic degree of

Doctor of Medical Sciences

(doctor rerum humanarum, Dr. rer. hum)

of the University of Rostock

Submitted by

**Ottavia Agrifoglio**

**Reviewers:**

**Prof. Dr. Cornelia C. Metges**: Research Institute for Farm Animal Biology (FBN) - Dummerstorf (FBN)

**Prof. Dr. Robert Jaster**: Rostock University Medical Center, Department of Medicine II, Division of Gastroenterology and Endocrinology, Rostock, Germany

**Prof Dr. Ali A. Aghdassi**: Greifswald University Medical Center, Department of Gastroenterology, Hepatology, Endocrinology, Nephrology and Rheumatology

**Submission year:** 2025

**Defense year:** 2026



https://doi.org/10.18453/rosdok_id00005753

*To mum, dad and Anto,*

*to Michael and Teresa*

**INDEX**

**Zusammenfassung**

Alle chronischen Lebererkrankungen im Endstadium bilden im Verlauf eine Leberzirrhose aus. Dies gilt auch für die cholestatischen Lebererkrankungen. Mangelernährung und Sarkopenie, der fortschreitende Verlust von Muskelmasse und Muskelkraft, sind die häufigsten Komorbiditäten von zirrhotischen Patienten und verschlechtern deren Lebensqualität und schlussendlich die Prognose.

Die Mangelernährung wird durch verschiedene Faktoren ausgelöst, hauptsächlich Entzündung, aber auch Appetitlosigkeit, verringerte Nahrungsaufnahme, Verdauungsschwierigkeiten und Malabsorption. Die Sarkopenie wird durch ein Ungleichgewicht zwischen Abbau und Aufbau im Skelettmuskel hervorgerufen. Abbaumechanismen stehen dabei im Vordergrund. Nichtsdestoweniger sind die Mechanismen, die Sarkopenie in zirrhotischen Patienten auslösen, und das Zusammenspiel zwischen der Sarkopenie selbst und der Mangelernährung noch nicht geklärt. Das liegt auch an der Schwierigkeit, die entsprechenden Mediatoren auf molekularer Ebene zu identifizieren.

Um Einblicke in diese Mechanismen zu erlangen, haben wir ein Modell für cholestatische Lebererkrankungen in C57BL/6J-Mäusen etabliert, denen zu diesem Zweck die Gallengänge ligiert wurden. Die Mäuse wurde in drei Gruppen randomisiert: (1) Die ligierten Tiere (BDL-Gruppe), (2) eine Gruppe mit einer Schein-Operation ohne Gallengangligatur (sham-Gruppe), und (3) die Kontrollgruppe ohne jegliche Operation. Nach der OP wurden täglich Gewicht und Gesundheitszustand der Mäuse erfasst. Die Muskelkraft wurde mittels Griffstärkemessgerät und die Muskelmasse mittels Magnetresonanztomografie ermittelt. In Stoffwechselkäfigen wurden die Stickstoffbilanz und der Gesamtenergieverbrauch mittels isotopmarkiertem Wasser gemessen. Die Mäuse wurden nach 7, 10 oder 14 Tage postoperativ durch zervikale Dislokation geopfert. Danach wurden Blut, Verdauungsorgane (Leber, Pankreas, Dünn- und Dickdarm) und Muskeln (Musculus Gastrocnemius und Quadrizeps femoris) entnommen. Mit Gewebeproben der nach 7 und 14 Tagen geopferten Mäuse wurde die fraktionelle Proteinsyntheserate (FPSR) mittels $^{2}H_5$-Ring-Phenylalanine ($^{2}H_5$-Phe) und der *flooding dose* -Methode ermittelt. Es wurden Plasmakonzentrationen von Entzündungsmarkern, Aminosäuren, Metaboliten und Enzymen, die mit Leberschädigung in Verbindung stehen, bestimmt., Außerdem wurden die Urinkonzentrationen von Stickstoffmetaboliten und Aminosäuren gemessen. Das Muskelgewebe wurde histologisch untersucht und mittels q-RT-PCR die Genexpression analysiert.

Die Ligatur der Gallenwege löste eine cholestatische Lebererkrankung mit begleitender Fibrose, Nekrose, Entzündung, erhöhten Aktivitäten der Alaninaminotransferase, Aspartataminotransferase und alkalischen Phosphatase, sowie erhöhten Plasmaspiegeln von Bilirubin und Cholesterol aus. Die BDL-Mäuse zeigten eine Mangelernährung, die mit einer reduzierten Nahrungsaufnahme, Gewichtsverlust, sowie einer reduzierten Stickstoffbilanz und einem verminderten Gesamtenergieverbrauch verbunden war. Interessanterweise ist die reduzierte Stickstoffbilanz nicht nur auf eine reduzierte Nahrungsaufnahme zurückzuführen, sondern auch auf einen durch die Entzündung ausgelösten katabolen Status der Tiere, der dann zu einem massiven Stickstoffverlust führt. Die BDL-Mäuse zeigten erhöhte Werte für Entzündungsmarker wie IL6R-α, TNFRI, TNFRII, und VEGF bereits am siebten postoperativen Tag. Außerdem war die Expression von Genen, die mit Muskelschwund und Katabolismus assoziiert sind, im Muskelgewebe der BDL-Mäuse schon am siebten Tag erhöht. Diese Messungen, sowie die verringerte Muskelkraft und Muskelmasse, erhöhte Urinwerte von 3-Methyl-Histidin (ein Metabolit des Aktins und dadurch ein Marker für Muskelabbau) und eine reduzierte FPSR im M. Gastrocnemius und Quadrizeps, deuten insgesamt auf einen sarcopenen Zustand der BDL-Mäuse hin. Dieser wird durch erhöhte Plasmakonzentrationen von konjugierten Gallensäuren, welche zusätzlich Entzündungsreaktionen und Muskelabbau stimulieren, verschlechtert. Der Muskelabbau beeinflusst den Gesamtenergieverbrauch, da dieser in BDL-Mäusen am wahrscheinlichsten auf einen reduzierten Energieverbrauch der Muskeln zurückzuführen ist. Außerdem wiesen die BDL-Mäuse veränderte Blutplasmaspiegel von Aminosäuren auf, wie etwa erhöhte Taurin- und erniedrigte Argininkonzentrationen.

Insgesamt zeigten die BDL-Mäuse Anzeichen einer Mangelernährung und Entzündungsreaktion, sowie Veränderungen im Energie- und Proteinhaushalt, die mit der primären Leberschädigung einhergingen. Die negative Stickstoffbilanz und der Proteinabbau waren hauptsächlich im Muskel lokalisiert und verschlimmern dadurch vermutlich den Krankheitsverlauf.

Zusammenfassend belegt die Studie, dass Mangelernährung und Sarkopenie bei cholestatischen Lebererkrankungen parallel auftreten und sichgegenseitig verstärken. Außerdem zeigt sich die Sarkopenie frühzeitig und ist ein multifaktorieller Prozess, der durch die Entzündung, einen systemischen pro-inflammatorischen und katabolischen Status, eine reduzierte Proteinsynthese, einen gesteigerten Muskelabbau, muskeltoxische Gallensäuren und ein Ungleichgewicht an Aminosäuren unterhalten wird.

## 1. SUMMARY

Liver cirrhosis (LC) is the common end-stage of all progressive and chronic liver diseases, including cholestatic liver disease (CLD). Malnutrition is one of the main comorbidities of LC, and it is often present in cirrhotic patients together with sarcopenia, worsening the prognosis and the quality of life of LC patients. Malnutrition in LC is caused by several factors, including inadequate food intake, loss of appetite due to inflammation and gastrointestinal conditions, and nutrient malabsorption. Sarcopenia is triggered by an unbalance between skeletal muscle protein synthesis and degradation, in favour of catabolic processes. However, the mechanisms underlying sarcopenia in LC and the interplay between malnutrition and sarcopenia are still unclear, also due to the fact that the molecular mediators are hard to identify.
To gain mechanistic insights into the development of sarcopenia, a C57BL/6J mouse model of CLD, using the bile duct ligation (BDL) surgery, has been established. The mice were randomly assigned to three different groups: the BDL surgery group, the Sham surgery group or the no surgery group (controls). After surgery, their weight and health conditions were monitored daily. Muscle strength was measured using a grip strength meter, and muscle volume was assessed using MRI. Mice were sacrificed via cervical dislocation either 7, 10 or 14 days after surgery, according to the experimental procedure. Metabolic cages (MC) experiments were performed to assess nitrogen balance (N-BAL) and total energy expenditure (TEE) using doubly labelled water. At d10, mice were sacrificed via cervical dislocation and blood and muscle were collected. Fractional protein synthesis rate (FPSR) of different tissues was assessed on post-operative days (d) 7 and d14 with the flooding dose method, using $^{2}H_5$ ring-phenylalanine ($^{2}H_5$-Phe). Mice were sacrificed via cervical dislocation either 7,10 or 14 days after surgery, according to the experimental procedure; and blood, splanchnic organs and muscle tissue of the quadriceps femoris (M. quadriceps) and gastrocnemius (M. gastrocnemius) were collected. Plasma concentrations of inflammatory markers, amino acids, metabolites, and enzymes associated with liver damage, and urinary concentrations of nitrogen metabolites and amino acids were measured. Muscle tissue was used for histological investigations and gene expression analyses via q-RT PCR.

The BDL surgery caused CLD, associated with fibrosis, necrosis, inflammation, and elevated activity of alanine aminotransferase, aspartate aminotransferase and alkaline phosphatase, as well as high concentrations of levels of bilirubin and cholesterol. Furthermore, the BDL mice showed signs of malnutrition, reflected in the reduced feed intake, progressive weight loss and

decreased N-BAL and TEE. Interestingly, the lower N-BAL showed by the BDL mice is not only a direct consequence of the decreased feed intake, as it can also be caused by an accelerated catabolic situation due to inflammation, which led to severe nitrogen loss. The BDL mice exhibit indeed inflammation, already in the early stages of the disease, as shown by the increased plasma concentrations of pro-inflammatory markers such as IL6R- α, TNFRI, TNFRII, and VEGF at d7. Furthermore, the BDL mice have an increased expression of genes associated with muscle atrophy and catabolism in M. quadriceps and M. gastrocnemius which is detected already at d7. These data, together with lower muscle strength and mass, increased concentrations of urinary 3-methyl-histidine (a marker of muscle protein breakdown, coming from actine degradation), and a decreased FPSR in both M. quadriceps and M. gastrocnemius point to a sarcopenic state in the BDL mice. This condition is further exacerbated by the high concentrations of circulating conjugated bile acids, which not only trigger further inflammation but also induce muscle atrophy. The muscle atrophy affects the TEE, as the BDL lower TEE is reasonably due to a diminished muscle energy expenditure. Moreover, the BDL mice displayed altered circulating concentrations of amino acids, such as low arginine concentration and increased taurine concentration. To summarize, the BDL mice showed signs of malnutrition, alteration of protein and energy metabolism as well as inflammation, mostly associated to liver injury. Specifically, the N loss and the protein catabolism are mainly localized in the muscle and are worsened by inflammation.

In conclusion, the study shows that malnutrition and sarcopenia are present in parallel in CLD, and that they trigger each other in a sort of vicious circle. Furthermore, sarcopenia occurs early in CLD, and it is a multicausal process, involving inflammation, a systemic pro-inflammatory and catabolic state, reduced protein synthesis, degradation of muscle proteins, muscle toxicity of bile acids and amino acid imbalance.

# 2. INTRODUCTION

## 2.1 Liver as a central organ in metabolism regulation

The liver plays a crucial role in several metabolic functions, including amino acid regulation, fat storage, glucose synthesis, storage and breakdown, bile acid production and bilirubin metabolism.

### 2.1.1 Liver and protein metabolism

The main tasks of the liver in the protein metabolism refer to amino acid (AA) synthesis, interconversion and deamination, as well as plasma protein and urea synthesis. Dietary proteins are degraded in the digestive tract and the hepatocytes uptake of the resulting AAs occurs via several transporters (either sodium-dependent or -independent). The activity of the transporters is mostly influenced by the concentrations of glucagon and insulin[1]. Once internalized in the hepatocytes, the AAs can be disposed for hepatic protein synthesis or can be degraded by removal of the amino group via reversible transamination processes. Among the transaminase reactions, the one to form glutamate is particularly important, as glutamate is oxidatively deaminated to yield ammonium ion ($NH_4^+$). This ion is toxic even at low concentrations and thus it must be metabolized by entering the urea cycle, by reacting with $CO_2$, and adenosine triphosphate (ATP) to produce carbamylphosphate[2]. The urea cycle is an energy-dependent pathway occurring in the mitochondria and in the cytosol of the hepatocytes and converts toxic ammonia in urea. During the cycle, important intermediates such as ornithine, arginine and citrulline are also produced[3]. In general, substrate supply regulates the hepatic AA metabolism short-term, while in the long-term it is regulated by both substrate supply and glucagon, which activates AA transporters to increase the uptake. However, liver disease patients have disturbances of protein metabolism, depending on the stage and aetiology of the disease. It has been shown that liver disease patients have higher circulating concentrations of aromatic AAs, while the circulating branched chain AAs are present in lower concentrations than in healthy subjects[2]. Cirrhotic patients may also present high concentrations of leucine, marking protein breakdown and decreased protein synthesis in response to a meal[2]. These alterations clinically manifest as muscle wasting, protein-caloric malnutrition and low hepatic plasma proteins[2].

### 2.1.2 Liver and lipid metabolism

Hepatic lipid metabolism mainly revolves around fatty acids (FA). In fact, in the case of carbohydrates abundance, hepatocytes can convert them into FA; but they can also absorb dietary FA from the bloodstream and store them as triacylglycerol or cholesterol esters in lipid droplets. However, if there is an excess of fat storage the liver can develop consequences such as steatosis and fatty liver[2, 4]. In the liver, FA can be used for lipid biosynthesis or to produce energy through oxidation processes[2]. Specifically, lipogenesis is the synthesis of FA and triglycerides from non-lipid precursors, usually carbohydrates. In the fed state, the glycolysis converts glucose into pyruvate, which is to be used in the tricarboxylic acid cycle to produce citrate, which is e further converted to acetyl-CoA, the precursor of FA, by ATP citrate lyase[5]. The regulation of the hepatic lipid metabolism occurs at a genetic level, and it relies on two transcription factors: peroxisome proliferator-activated receptor α and the sterol regulatory element-binding protein 1-c. The first is a regulator of the key enzymes involved in the FA oxidation pathways, while the latter controls the expression of genes involved in lipogenesis[6, 7]. Imbalances between lipid availability and consumption might lead to hepatic lipid accumulation, which in the long term could cause lipoperoxidative stress, non-alcoholic fatty liver diseases, steatosis and eventually liver cirrhosis (LC)[2].

### 2.1.3 Liver and carbohydrate metabolism

Hepatic carbohydrate metabolism primarily involves glucose. One of the main functions of the liver is keeping the blood glucose levels in a physiological range, as blood glucose concentrations change depending on a fasted or fed state[8, 9]. In the hepatocytes, glucose is phosphorylated to glucose-6-phosphate, which not only maintains the intracellular glucose concentrations low but also serves as an intermediate compound for several pathways, including the glycogen synthesis, glycolysis and pentose phosphate pathway. Hepatic carbohydrate metabolism is regulated by insulin and glucagon, respectively down- and upregulating glucose biosynthesis. Furthermore, the hepatocytes have glucose-sensitive signalling pathways, mostly relying on the glucose kinase enzyme, working through a wide range of glucose fluctuations and thus allowing efficient trapping of glucose in hepatocytes in response to glycaemic changes. However, in the case of liver disease, the glucose metabolism is altered with reduced glucose and insulin uptake following carbohydrate administration. This alteration in the long term leads to peripheral insulin resistance[2].

### 2.1.4 Liver and bile acids metabolism

The liver is the only organ that can synthetize bile acids. The bile acid biosynthesis can occur via two different pathways: the classic and the alternative pathways. The first one initially provides the hydroxylation, isomerization, reduction, and dihydroxylation of the cholesterol's steroid rings in the cytosol and the endoplasmic reticulum, and then the steroid side chain oxidation in the mitochondria and the oxidative cleavage of the side chain in peroxisomes. The latter firstly oxidates the steroid side chain, then modifies the steroid rings and eventually provides an oxidative cleavage of the steroid side chain[10]. The bile acids formed through cholesterol modifications are subsequently conjugated mainly to taurine and glycine, increasing their ionization, amphipathic characteristics and solubility, but also to glucuronide. Afterwards, they are secreted into the bile through the bile acids export pumps. Once in the gallbladder, they bind to cholesterol and form micelles to avoid both cholesterol precipitation and epithelial injury due to bile acids toxicity. In the postprandial state, bile is secreted into the intestinal tract under the signal of the pancreatic hormone cholecystokinin. Most of the conjugated bile salts are reabsorbed in the ileum and colon and de-conjugated back to primary bile acids, cholic and chenodeoxycholic acid, by the bile salt hydrolase of the intestinal microbiota. In the gut, primary bile acids are converted to secondary bile acids. A portion of the secondary bile acids is finally excreted with the feces, but part of them is also reabsorbed in the colon and brought back to the liver via the bloodstream to contribute to the circulating bile acid pool[11].

## 2.2 Chronic Liver Diseases

Chronic liver disease alludes to a disease process that involves progressive destruction and regeneration of liver parenchyma, culminating to fibrosis and cirrhosis. The main causes of chronic liver diseases include alcohol associated liver disease (AALD), metabolic dysfunction-associated steatotic liver disease (MASLD), and cholestatic liver disease (CLD). Specifically, AALD is one of the main cause of liver disease worldwide[12] and accounts for around 27% of liver-related deaths globally[13]. It includes different phenotypes that go from asymptomatic disease to advanced stages with a high mortality rate. In fact, about 90% of alcohol abusers develop liver steatosis, but only about 10-20% of them will further progress to LC[14]. Cirrhotic patients are at risk to further develop either to decompensated LC (20-40%) or hepatocellular carcinoma (3-10%)[15]. On the other hand, advanced fibrosis can also lead to alcoholic hepatitis in about 10-35% of patients[16]. Interestingly, alcohol consumption plays a role also in the pathogenesis of MASLD. Alcohol has an effect on the MASLD progression to LC, and

metabolic risk factors such as obesity impact the natural history of AALD[17, 18]. MASLD can be diagnosed in adults suffering from hepatic steatosis and in the presence of obesity or overweight, type 2 diabetes mellitus (T2DM), or at least two risk metabolic conditions. Its detection can be performed via imaging techniques, blood biomarkers, or liver histology[19, 20]. Specifically, MASLD is the most frequent cause of chronic liver disease and accounts for most liver-associated morbidity and mortality[21], as it affects about 30% of the worldwide adult population and its prevalence increased from 22% in the early 90s to 37% in 2019[22]. Interestingly, the increasing prevalence of MASLD matches the increasing prevalence of obesity and overweight[21]. However, other important comorbidities for MASLD are cardiovascular diseases, which represent the main cause of mortality in MASLD patients – especially those with advanced liver fibrosis[23], and T2DM. In fact, T2DM patients often suffer from steatotic liver disease (SLD), with many of them developing advanced LC[24].

Among the liver diseases not associated with alcohol abuse or metabolic conditions, CLD affects about 20% of the general population[25]. CLD is triggered by the blockage of bile flow from the liver to the duodenum. The stagnation of bile due to cholestasis results in the accumulation of bile salts, bilirubin, and other toxic compounds coming from the clearance of the liver, and thus in cellular damage which initiates the hepatic inflammatory and fibrogenic processes. These processes include: necrosis of hepatocytes and cholangiocytes, activation of macrophages, release of pro-inflammatory cytokines, neutrophils infiltration, hepatocytes and cholangiocytes proliferation, stellate cell activation and subsequent fibrosis, secondary biliary cirrhosis, and ultimately liver failure or progression into liver cancer[26]. The two most common types of CLD are primary biliary cholangitis (PBC) and primary sclerosing cholangitis (PSC). Although both PBC and PSC are slow progressive chronic diseases that lead to LC, the etiology of these two forms are different, as PBC's hallmark is the granulomatous destruction of small intrahepatic bile ducts[27, 28], while PSC is mainly characterized by inflammation and fibrosis of both intrahepatic and extrahepatic bile ducts and subsequent stenosis[29, 30]. Specifically, PBC has a silent onset with no hepatic dysfunctions and only minimal alterations of liver histology, which progresses to a long period of asymptomatic liver dysfunction and, eventually, cirrhosis and end-stage liver failure[31, 32]. Therapy with ursodeoxycholic acid (UDCA) has been proven effective in ameliorating liver functions in patients with PBC, however, the risk of progression to LC is still present in about one-third of the patients under treatment[33]. On the other hand, PSC can have a heterogeneous natural course, with asymptomatic initial phases of the disease, which is incidentally diagnosed via blood tests presenting altered hepatic parameters in 10-60% of the patients[34–36]. Contrary to the PBC, the PSC doesn't have a gold standard therapy as no

medicament has been shown to improve long-term outcomes[37]. However, UDCA has shown some beneficial effects by improving serum biliary enzyme levels[38]. Overall, chronic insults to the liver can lead to impaired function, caused by inflammation, necrosis, fibrosis, hepatocellular dysfunction, and vascular remodeling, eventually culminating in LC[39]. If the cause of primary injury is mitigated, reversibility of the process is possible, however, the more the severity of fibrosis and progression of the disease are advanced, the fewer are the possibilities of a disease regression[40] (Figure 1).

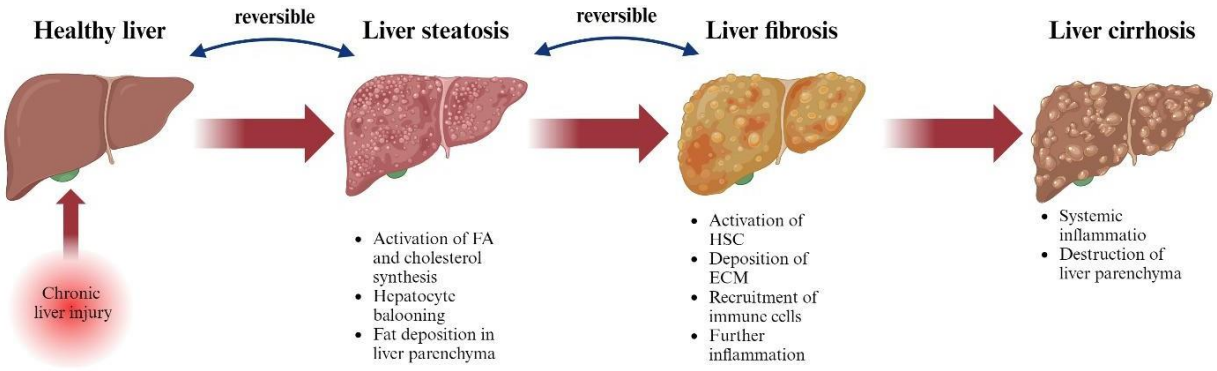


**Figure 1:** Liver damage progression to liver cirrhosis (LC). Chronic liver injury leads to an enhanced fatty acid (FA) and cholesterol synthesis, which causes an excess of fat deposition in the hepatocytes (liver steatosis). Liver steatosis triggers oxidative stress and the activation of pro-inflammatory and pro-fibrogenic pathways, which lead to the recruitment *in situ* of immune cells, the activation of hepatic stellate cells (HSCs) and the consequent deposition of extra cellular matrix (ECM) (liver fibrosis). The chronic inflammation state and the continuous ECM deposition due to wound-healing processes eventually culminate in a state of non-reversible destruction of liver parenchyma and systemic inflammation (liver cirrhosis). If the primary causes of injury are alleviated and treatment is tempestively performed, it is possible to have a regression of the condition. However, if the disease progression and fibrosis are too advanced a regression is not possible[40]. Figure created with Biorender.com.

### 2.2.1 Liver Cirrhosis

LC is the end stage of all progressive and chronic liver diseases. According to the Cirrhosis Collaborators of the Global Burden of Disease, LC increased its health burden since 1990 and in 2017 caused 1.32 million deaths globally[41], accounting for 3.5% of all deaths worldwide[42]. In particular, MASLD is becoming one of the main causes of liver disorders, contributing to exacerbating the burden of obesity and metabolic syndrome. On the other hand, the cases of alcoholic liver disease are also increasing worldwide (especially in Europe) and account for around 27% of liver-related deaths globally[13]. Specifically, LC is triggered by chronic liver insults that can result in impaired functions of the organ due to inflammation, necrosis, fibrosis,

hepatocellular dysfunctions, and vascular remodeling, eventually culminating in LC[39]. The inflammation in LC originates as a mild inflammatory response, a mechanism aiming to protect hepatocytes from injuries and repair tissue damage. However, when inflammation becomes too intense or the resolution phase fails, it becomes chronic and is accompanied by an important loss of hepatocytes. Furthermore, this leads to an activation of hepatic stellate cells (HSCs). This process causes the accumulation of collagen and other extracellular matrix (ECM) components, eventually leading to the destruction of hepatic parenchyma and innervation, and impaired liver function[43, 44]. Under normal circumstances, immune response in the liver is mediated by macrophages, Kupfer and dendritic cells, as well as natural killer and T-killer cells (NK and NKT, respectively) and circulating pro-inflammatory molecules such as cytokines, chemokines, acute phase proteins, and complement factors. Nevertheless, in case of further damage, circulating monocytes can be recruited in the hepatic parenchyma, to generate macrophages or myeloid and dendritic cells[45].

### 2.2.2 Pathogenesis of liver cirrhosis

Liver injury triggers the activation of ECM-secreting myofibroblasts, which are not normally present in a healthy liver and are the primary source of accumulation of ECM [46]. Investigations on the hepatic fibroblasts have identified liver-resident activated hepatic stellate cells (HSCs) and portal fibroblasts (PFs) as their main sources since they make up approximately 90% of the collagen-producing cells[47]. However, it must be considered that HSCs and PFs are activated under different kinds of stresses: in fact, the HSCs primarily respond to toxic liver injury, while the PFs are activated by cholestatic liver fibrosis[47, 48]. Murine models of LC induced by bile duct ligation (BDL) have shown PFs account for about 70% of the myofibroblasts at the onset of cholestatic liver injury (5 days after BDL), while the HSC are activated with disease progression (17 days after BDL) to eventually become the biggest portion of the myofibroblast population (20 days after BDL)[47]. However, other cell populations, such as bone marrow-derived cells, fibrocytes, and mesenchymal stem cells (MSCs) are also known to contribute to the onset of the disease[46, 49, 50]. Hepatocytes also contribute to the onset of fibrosis by expressing fibrogenic factors such as Notch, osteopontin, Transforming Growth Factor β (TGFβ), NADPH-oxidase4, TAZ, and Indian Hedgehog[51–54]. Furthermore, with the progression of the disease, the damaged hepatocytes secrete exosomes containing RNA able to activate the quiescent HSCs[55]. The chronic insults to the liver eventually lead to inflammation, which is a requirement for fibrosis. The pathogenesis of toxin-induced fibrosis changes according to the

triggering factor. In the case of non-alcoholic liver steatosis (NASH), mainly associated with metabolic syndrome, a two-hit etiology has been hypothesized[56]. The first hit is due to dietary-induced obesity and/or excessive accumulation of triglycerides, cholesterol, and fatty acids in hepatocytes (inducing the expression of caspase 2), as well as alteration in the release of adiponectin, leptin, or resistin, causing insulin resistance and inflammation[57, 58]. The second hit is associated with the production of reactive oxygen species, gut-derived LPS, mostly due to changes in the intestinal permeability, and additional release of pro-inflammatory (TNF, IL-6, IL-1β, IL-17 and leptin) and profibrogenic cytokines (TGFβ), leading to HSCs activation[56, 59, 60]. In the case of alcoholic liver disease, the liver injury is directly attributed to alcohol, which activates fatty acids and cholesterol synthesis via the sterol regulator binding protein (SREBP) 1 and SREBP2 pathway, which enhances the hepatic synthesis of fatty acids and triglycerides, causing an increase of hepatic fat droplets, ballooning degeneration and Mallory-Denk bodies formation in injured hepatocytes[61–63].

### 2.2.3 Liver cirrhosis and inflammation

Systemic inflammation in LC is due to the persistent stimulation of immune cells, which produce elevated amounts of pro-inflammatory cytokines. These cytokines, together with enhanced expression of cell activation markers are detectable in the serum of cirrhotic patients[64]. Systemic inflammation is commonly diagnosed as the presence of systemic inflammatory response syndrome (SIRS), a state of alterations of most of the clinical and biochemical parameters of the body, such as heart and respiratory rate, white cell count, and body temperature. Eventually, it can lead to organ failure[64]. There are several circulating immune cells involved in systemic inflammation in LC, mostly neutrophils, monocytes, T-lymphocytes, and B-lymphocytes. While the neutrophils are responsible for the oxidative burst[65], the monocytes are the primary source of TNF-α production together with T-lymphocytes[66]. T-lymphocytes are also major producers of interferon-γ (INF- γ) and interleukin (IL)-7 [67, 68]. In general, the activated circulating immune cells are responsible for elevated serum concentrations of pro-inflammatory markers, including TNF-α and TNF-α receptors I and II, IL-1β, IL-6, IL-17, and INF- γ[66–70] (Figure 2). In liver diseases, the upregulation of these markers in immune cells is triggered by pathogen-associated molecular patterns (PAMPs) and damage-associated molecular patterns (DAMPs), which are produced and released by the leaky gut due to increased intestinal permeability, and the necrotic liver respectively. PAMPs and DAMPs activate specific receptors, such as the toll-like and the nucleotide-binding

oligomerization domain-like ones, that in turn activate the expression of surface molecules on the immune cells (cytokine receptors and/or adhesion molecules) and the overexpression of cytokines. Among the cytokines produced by the immune cells, chemokines and growth factors play a crucial role in recruiting and activation of further inflammatory cells. These processes take place first in gut-associated lymphoid tissue and mesenteric lymph nodes. However, locally activated cells spread to the rest of the body via the bloodstream, causing a systemic inflammatory response[64]. Furthermore, fibrosis in the liver is driven by the activation of the HSCs and deposition of ECM due to hepatocyte injury, inflammation, and activation of the innate immune system. The HSC are activated by macrophages, including Kupffer cells secreting TGF-β, which is known as the most effective fibrogenic factor. In fact, upon hepatocytes' apoptosis, neutrophils are recruited in the damaged liver and start secreting cytokines and cell-free DNA, which have also a strong pro-inflammatory effect[71–73] (Figure 2).

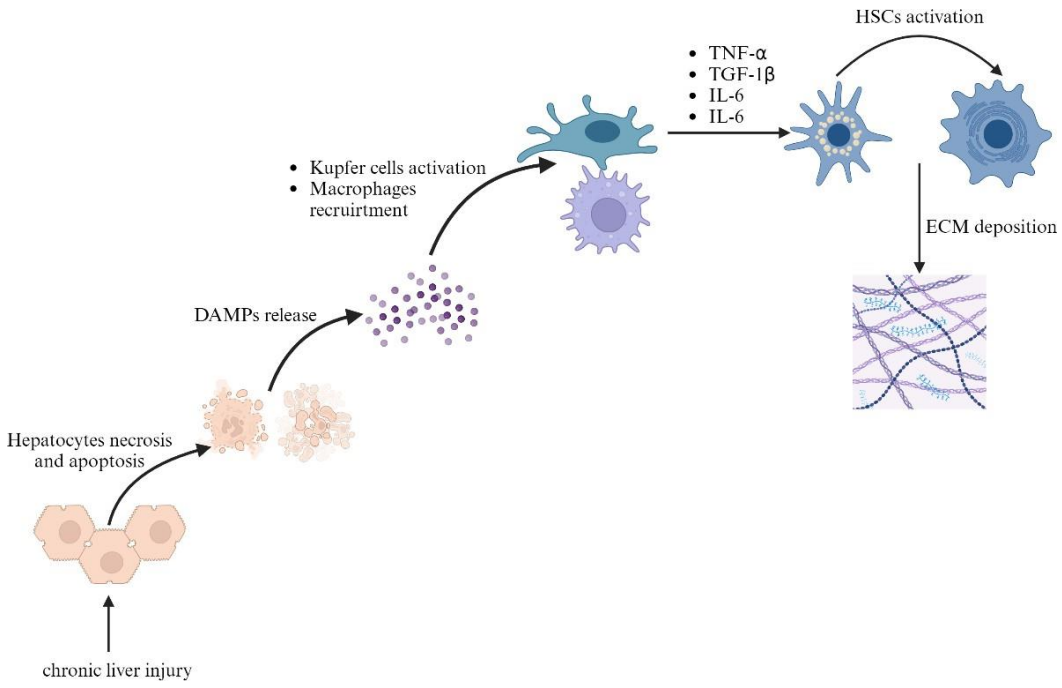


**Figure 2**: Pathophysiological processes of liver cirrhosis (LC). Chronic insults to the liver lead to apoptosis and necrosis of hepatocytes and subsequent release of damage-associated molecular patterns (DAMPs). DAMPs trigger the activation of Kupffer's cell and the recruitment of macrophages, which secrete pro-inflammatory factors and cytokines. Cytokines and pro-inflammatory factors lead to hepatic stellate cells (HSCs) activation. Activated HSCs are the primary responsible of extra cellular matrix (ECM) deposition. Figure created with Biorender.com.

### 2.2.4 Complications and treatments of liver cirrhosis

Although LC can be compensated for years, it takes constant monitoring to avoid the worsening of the condition and the following consequences and complications that can turn out to be fatal. Most of the fatal complications are driven by portal hypertension, caused by increased intrahepatic resistance and increased portal venous flow[74]. In general, patients with compensated LC have a better prognosis and life expectancy than those with the decompensated disease, whose mean survival is around 9 years[75]. During the compensated stage, mainly concerning the fat deposits and early ECM deposition in the liver parenchyma, the process can be considered reversible[76]. Several studies based on animal models showed the reversibility of the process. Most attempts are based on the increase of the fibrinolytic activity of the macrophages via the fibrinolytic matrix metalloproteinase[50, 77], or on the apoptosis or inactivation of the HSCs[78, 79]. Although most of the data about fibrosis reversibility come from experimental preclinical settings, results from clinical settings are also available and encouraging[80]. The most common complication of LC is ascites[75]. It is known that about 15% of patients with ascites have a life expectancy of one year[81], however intrahepatic portosystemic shunt (TIPS) can improve patients' survival[82]. The presence of oesophageal varices is another main complication of LC, present in about 85% of patients with decompensated disease[83] and represents one of the most life-threatening complications. The mortality rate for patients suffering from variceal hemorrhage after six weeks is at least 20% [84]. Treatments include anti-hypertensive medications, as well as endoscopic interventions or TIPS in cases of uncontrolled bleeding[74, 85]. Portal hypertension and sodium retention in LC patients can also lead to hepatorenal syndrome (HRS). HRS is a form of kidney impairment, characterized by a decrease in renal blood flow and glomerular filtration rate[86]. The main pharmacological treatments for HRS consist of the administration of anti-hypertensive drugs and albumin to improve renal perfusion[87], however, in case of treatment failure, TIPS is the most used method[88]. Nevertheless, liver transplantation is the definitive way to possibly reverse HRS[86]. Another complication of LC is hepatic encephalopathy (HE). One of the key drivers of HE in LC patients is the toxic levels of ammonia in the bloodstream, reaching the brain due to the inability of the liver to metabolize it[89]. Treatments for HE include nutritional support[90] and pharmacological therapy with lactulose and antibiotics[91, 92]. Nevertheless, lactulose ameliorates the symptoms but still fails to improve the survival rate[93]. However, once a cirrhotic decompensated state has been established, a complete regression to a healthy liver is not possible, although some strategies and treatments can ameliorate the condition[76]. Theoretically, the main treatment for decompensated LC is targeting the primary causes of complications, suppressing inflammation,

normalizing the blood circulation, and restoring the liver structure by fibrosis regression. However, despite the encouraging results of preclinical trials, none of these approaches resulted to be practicable in clinical settings[94, 95]. While liver transplantation remains the only available treatment for advanced decompensated LC[76], correcting the patients' life style to target the main risk factors is up to date the most used strategy to improve life expectancy and survival rate.

### 2.3 Animal models of liver cirrhosis

Animal models have a key role in preclinical studies of diseases as they can provide significant insights into the pathological mechanisms. Furthermore, animal studies are useful in developing new treatments and therapeutic approaches. However, it should be considered that, due to clear biological differences, animal models can imitate only selected characteristics of the human disease, thus it is extremely important to choose the appropriate one to address specific research questions [96]. Ideally, an animal model should be chosen taking into account the following focal points: 1) it should reproduce the morphological features seen in human patients; 2) the disease progression should be as similar as possible as in human patients; 3) the model must be reproducible and with a low mortality rate; 4) the pathology must be reversible; 5) it must permit pathophysiological alterations and sequelae[97]. Up to date, several animals are used for experimental models of LC, but the most common are mice and rats[98–103]. However, there can be differences between rodents and animals with closer evolutionary relationships to humans, especially when it comes to investigating inflammatory and metabolic responses[104]. In this context, pigs are emerging as a good model for preclinical research, due to their anatomical and physiological similarity with humans[105]. Rabbits are also a good model for liver diseases (especially for viral hepatitis)[106], and small primates are also emerging as preclinical models, as they are a good compromise between costs and similarity to human phisiology[107]. Nevertheless, rats and mice remain the most common models due to the low cost, ease of handling and breeding, and short life span[108]. Specifically, mice with a C57Bl/6 background are widely used for preclinical models of LC, since they develop obesity, insulin resistance, and fatty liver[109]. The main types of *in vivo* models for LC are: chemical, dietary, and surgical[110]. Among the chemical methods, the most widely used are the injection of carbon tetrachloride ($CCl_4$) and thioacetamide (TAA). The first one is a toxic radical metabolite produced by the cytochrome P-450 in the hepatocytes. $CCl_4$ damages the hepatocytes by inducing lipid peroxidation and impairing the structure of their plasma, lysosomal and mitochondrial membranes. The damage results in severe centrilobular necrosis[111, 112]. The necrosis triggered

by a single $CCl_4$ administration is reversible and activates wound-healing processes, however, when it becomes chronic there is a progression to liver fibrosis and cirrhosis[113]. On the other hand, the TAA is not toxic. However, its intermediate thioacetamide-S-oxide is a reactive oxygen species causing cellular harm and hepatocyte necrosis[96]. TAA effects are particularly pronounced in rats[114]. Diet is also a way to induce liver damage. Among the most common methods are alcohol in drinking water, high-fat diets (HFD), and the Lieber-DeCarli (LdC) diet. Alcohol in drinking water represents the simplest method to induce LC. Basically, the water given to the mice is supplemented with alcohol and its quantity is rising over the experimental period[115]. With this method mice develop steatosis in about 10 weeks and oxidative stress, steatosis, mild fibrosis, inflammatory cell infiltrates, increased hepatic injury, and depletion of cellular antioxidant defense in some months[116]. On the other hand, it takes rats about 29 weeks to show fatty liver, inflammation, focal necrosis, and perivenular fibrosis[117]. The HFD model is based on the principle that the high amounts of fats in the feed will increase the free FA levels, causing hepatic insulin resistance, decreased FA oxidation, de novo lipogenesis in hepatocytes, weight gain, and eventually hepatic steatosis[118]. The mice models of HFD are designed to mimic the human pathophysiology of liver fibrosis and the diet composition is variable, thus also the pathological findings can vary[119]. Lastly, the LdC diet consists of a liquid feed supplemented with ethanol. Like with the alcohol in drinking water method, the amount of alcohol increases over the experimental period. Furthermore, the feed is supplemented with essential fat-soluble vitamins (A, D, E, K) and water-soluble vitamin B12, minerals, and fibers[115]. This method is mostly used to investigate alcoholic liver disease and over a 12-week experimental period leads to the development of fatty liver, mild inflammation, and moderate liver damage without fibrosis[120]. However, to overcome these limitations, the Tsukamoto-French method was established. This method is based on the direct infusion of the LdC diet supplemented with ethanol directly in the stomach of the animal, using a catheter and an infusion pump[121].As far as surgical models are concerned, the most common is BDL. This model has been well established in rodents since 1932[122], becoming one of the most common techniques to induce CLD[123], which can progressively culminate in LC in response to cholestatic obstruction[124, 125]. The surgical obstruction of the common bile duct leads to the accumulation of bile in the liver, causing hepatic damage, inflammation, and eventually fibrosis and cirrhosis[126]. Normally, this surgery technique is performed through a midventral laparotomy, followed by the isolation of the common bile duct above the duodenum and its double ligation[111]. BDL triggers the proliferation of biliary epithelial cells as well as oval cells. The consequences are proliferation of the bile ductules, cholestasis, inflammation and fibrosis,

which causes secondary biliary cirrhosis culminating in liver failure[126, 127]. BDL procedure and the consequent CLD are very often associated with muscle wasting, diminished muscle weight, and decreased number of muscular fibers as well as scarce muscular strength and resistance[128, 129]. Other surgical models include portocaval anastomosis, single and multi-step anhepatic models, and partial hepatectomy. The portocaval anastomosis is used to mimic a generalized liver failure and it is based on the hepatic artery ligation and partial hepatectomy, with ischemia or portacaval shunt. The anhepatic models are based on the total loss of liver function. The single step has mostly been performed on rats, rabbits, dogs, and pigs[130–133] and it consists of ligation of the hepatic artery and the common bile duct. The blood flow is maintained via a shunt or anastomosis between the intrahepatic inferior vena cava and the portal vein, caudally, and the suprahepatic inferior vena cava, cranially[133–135]. On the other hand, the multi-step approach was established to be used on rats, and it is based on the posterior hepatic lobes via ligation of the portal branches, followed by the resection of the two anterior hepatic lobes after two weeks[136]. Models of partial hepatectomy have been performed in rats, mice, pigs, and baboons and normally involve about 70-95% of the total liver mass[105]. A 70% resection usually corresponds to the 20–30% recommended to avoid post-operative liver failure after hepatic resection of an otherwise healthy liver[137].

## 2.4 Skeletal muscle physiology

Skeletal muscle plays a pivotal role in the uptake and storage of glucose[138]. Glucose is stored as glycogen, which can be easily degraded to glucose to provide the muscle with substrates for ATP synthesis, necessary for muscle contraction, even in case of inadequate dietary intake. Several enzymes are responsible for maintaining a correct ATP pool, and among these, creatine kinase and adenylate kinase play pivotal roles. In the presence of ADP, the enzyme creatine kinase allows the degradation of phosphocreatine in creatine with the formation of ATP. On the other hand, the enzyme adenylate kinase is able to produce a molecule of ATP and one of AMP starting from two ADP molecules. This is important because AMP represents an indicator of energy capacity in the skeletal muscle. An increase of AMP concentrations activates 5'-adenosine monophosphate kinase, which enhances glycogenolysis and glucose uptake in the skeletal muscle. At this point, glucose can be phosphorylated in glucose-6-phosphate and initiate the glycolytic process yielding pyruvate. The pyruvate can either translocate to mitochondria and enter the tricarboxylic acid cycle or be converted to lactate[139, 140]. Being glucose essential for muscle contraction, there are several pathways responsible for its

mobilization, depending on the muscle fiber type. Fast-twitching fibers present a myosin heavy chain (MHC) isoforms MHCIIa and MHCIIb which shorten fast and thus allow a faster muscle contraction[141]. This kind of muscle fibers depends on anaerobic metabolism (glycolysis), which can easily and rapidly generate ATP for a quicker contraction. However, glycolysis produces less ATP than the aerobic pathways, causing the fast fibers muscles to be fatigued soon[142]. On the other hand, slow-twitching fibers are characterized by the presence of MHC isoform MHCI. These fibers shorten slower than the fast ones and have an aerobic metabolism, with high capillary density and the presence of oxidative enzymes which make them more resistant to fatigue[143]. Anyway, skeletal muscle represents a storage site for glucose, which is stored as glycogen and can be easily mobilized in case of inadequate dietary intake, either in an anaerobic or aerobic manner. However, while the liver (and to a certain extent the kidney as well) can mobilize glucose and release it into the circulation, the skeletal muscle uses it only for its own metabolic needs[142]. Furthermore, the skeletal muscle is a storage site of AA. Roughly 75% of the protein body pool is stored in the skeletal muscle and the AA coming from the proteolysis can be mobilized in case of further supply needs for gluconeogenesis and the glycogenesis[142]. Alanine and glutamine are among the main AA mobilized in case of proteolysis. The first enters the circulation by skeletal muscle and is internalized in the liver where it serves for gluconeogenesis, the latter is used as a gluconeogenic precursor, independently of the insulin/glucagon ratio[144].

In general, proteostasis (the balance between protein synthesis and protein breakdown) is the main factor in the maintenance of muscle mass[145]. Proteostasis is the result of the fine regulation of pathways associated with muscle growth and muscle catabolism. The main growth factor regulating muscle growth is insulin-like growth factor 1 (IGF-1), which enhances protein synthesis by activation of the PI3K/Akt/mTOR pathway. The PI3K/Akt pathway is also relevant in preventing muscle atrophy, as it inhibits the Forkhead box 0 proteins (Fox0), responsible for the ubiquitin/proteasome system (UPS) activation. Another way in which the PI3K/Akt pathway prevents muscle atrophy is the inhibition of the Smad pathways, which regulate the muscle-atrophy-associated myokine myostatin[146] (Figure 3). In particular, myostatin belongs to the TGF-β family and is an inhibitor of protein synthesis[147–149].

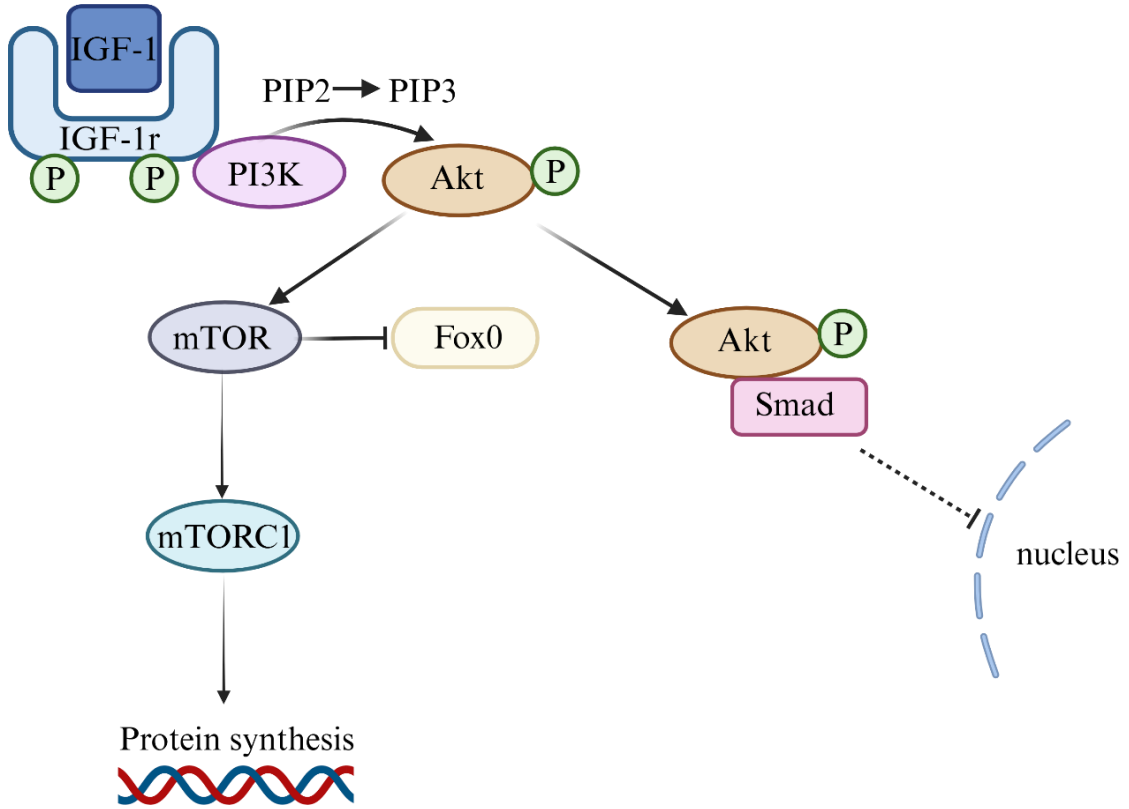


**Figure 3:** IGF-1 pathways regulating skeletal muscle protein synthesis. Insulin-like growth factor 1 (IGF-1) binds to its receptor (IGF-1r), recruiting phosphoinositide 3-kinases (PI3K). PI3K phosphorylates phosphatidylinositol 4,5-bisphosphate (PIP2) to phosphatidylinositol-3,4,5-trisphosphate (PIP3). PIP3 phosphorylates the protein kinase B (Akt), triggering the activation of the mammalian target for rapamycin (mTOR). This brings to the formation of the mTOR complex 1 (mTORC1) and subsequent protein synthesis. Akt phosphorylation also traps Smad, preventing its translocation in the nucleus and the transcription if myostatin. Arrows indicate activation, capped lines indicate inhibition. Created with Biorender.com.

On the other hand, muscle degradation is regulated by three main proteolytic systems: caspase-mediated protein cleavage, ATP-dependent ubiquitin-proteasome system and autophagy[150, 151]. The two latter systems are stimulated by the nuclear localization of the Forkhead box 0 proteins (Fox0), triggered by the inactivation of Akt. Once in the nucleus, Fox0 induces the expression of atrogin1 and Trim63 (also called MuRF1), the main atrophy-related ubiquitin ligases, responsible for muscle degradation[152] (Figure 4).

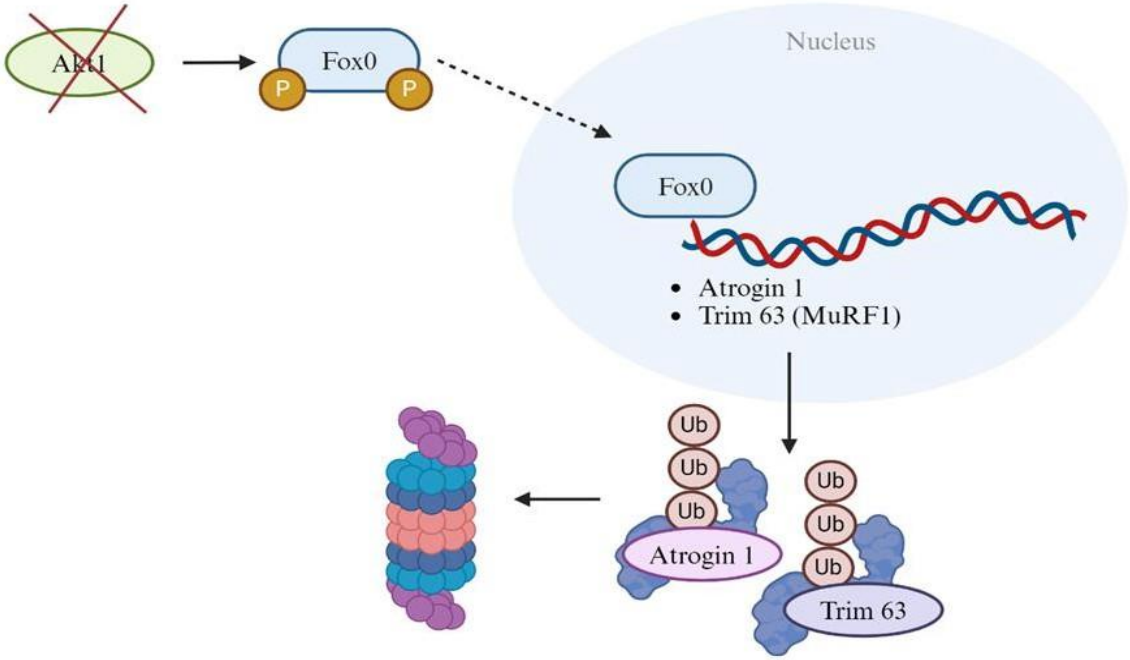


**Figure 4**: Skeletal muscle degradation process. When Akt1 is inhibited, Fox0 is not phosphorylated and translocates in the nucleus. In the nucleus it activates the expression of Atrogin1 and Trim63 (MuRF1). Atrogin1 and Trim63 are the main atrophy-related ubiquitin ligases and lead to proteolysis via the ubiquitin-proteasome system. Created with Biorender.com.

Ubiquitin-proteasome system and autophagy-mediated proteolysis can also be activated by myostatin[149].

### 2.4.1 The liver - skeletal muscle crosstalk

The crosstalk between the liver and the skeletal muscle plays a pivotal role in maintaining glucose and lipid homeostasis, thus its alterations can lead to conditions such as insulin resistance[153], often present in patients with advanced liver disease[154]. IL-6, one of the main mediators of inflammation, is also involved in insulin resistance both in the liver and skeletal muscle[155], and therefore relevant to the disturbance of the liver-muscle axis. Short and transient physical activity leads to an increase in IL-6 concentrations, which can enhance muscle growth[156]. On the other hand, after intense and prolonged muscular efforts IL-6 stimulates hepatic glucose production[157]. Furthermore, the liver clears high circulating levels of IL-6 coming from physical activity[158]. Skeletal muscle is also involved in the compensatory mechanisms of ammonia clearance when the damaged liver is unable to do it. Specifically,

skeletal muscle can convert ammonia to glutamine via glutamine synthase, but in case of damaged muscle tissue, this pathway cannot work properly leading to ammonia accumulation and toxicity and worsening the conditions of cirrhotic patients – also increasing the risk of hepatic encephalopathy[159]. Moreover, the liver and the skeletal muscle can secrete hepatokines and myokines which can affect the target tissue. In the case of decompensated LC, the liver secretes fibroblast growth factor 21 (FGF-21), which contributes to sarcopenia and impaired myogenesis by inhibiting the PI3K/Akt pathway[160]. On the other hand, myostatin not only inhibits muscle growth, but it can affect HSC by increasing the expression of procollagen type 1 and thus playing a role in the fibrogenic process[161]. Another factor that contributes to the disturbances of the liver-skeletal muscle axis is gut microbiota. It is known that in cirrhotic patients inflammation causes altered gut permeability leading to dysbiosis, which is associated to increased frailty and sarcopenia[162].

## 2.5 Protein and energy metabolism

### 2.5.1 Amino acids and protein metabolism

The AA are organic chemical compounds containing both an alpha amino and a carboxyl group as functional groups. Among more than 300 AA existing in nature, only 20 are proteinogenic. Among these, isoleucine, leucine, lysine, methionine, phenylalanine, threonine, tryptophan and valine are “indispensable”, meaning that the organism is not able to synthesize them itself and thus they need to be ingested with food. The indispensable AA are also needed as precursors for the “conditionally indispensable” AA (histidine, arginine, cysteine, glutamine, glycine, proline, tyrosine, asparagine). The remaining four proteinogenic AA (alanine, aspartic acid, glutamic acid, and serine) are synthesized by the human organism itself, starting from available precursors such as acetyl CoA or pyruvate[163]. However, some AA not involved in protein synthesis also play crucial roles in cell metabolism. They are not only precursors for a variety of compounds such as glucose, lipids, ketone bodies, and nucleotides but they can also play a role against oxidative stress and prevent accumulation of ammonia[163]. For instance, the urea cycle takes place in the liver, and it is responsible not only for arginine synthesis but also for ammonia detoxification via conversion to urea. In fact, the ammonia produced from protein catabolism or gut microbiota enters the urea cycle as carbamylphosphate to be used for the conversion of ornithine to citrulline by the ornithine carbamyltransfrease. The following steps

of the urea cycle lead to the synthesis of arginosuccinate first and arginine afterward. Arginine is further used to produce urea and to be reconverted to ornithine by the enzyme arginase[3]. Under physiological conditions, the organism has a constant pool of free AA, sustained by the protein breakdown, as well as endogenous synthesis and AA taken up with food. Any excess that cannot be used to synthesize proteins is dismantled to form intermediates of the Krebs' cycle. Specifically, glucogenic AA are degraded to pyruvate (alanine, cysteine, glycine, serine, threonine, and tryptophan), α-ketoglutarate (arginine, glutamate, glutamine, histidine, and proline), succinyl-CoA (isoleucine, methionine, and valine), fumarate (aspartate, phenylalanine, and tyrosine) and oxaloacetic acid (asparagine, aspartate) and are used for the synthesis of glucose. On the other hand, ketogenic AA are degraded in acetyl-CoA (isoleucine, leucine, threonine, and tryptophan) and acetoacetate (leucine, lysine, phenylalanine, and tyrosine) and eventually used for the synthesis of ketone bodies and fatty acids[164].

### 2.5.2 Energy metabolism

Fats, carbohydrates, and proteins are the major energy sources, with proteins being the main nitrogen and carbon suppliers and fats and carbohydrates producing energy via oxidation. Energy production relies on the oxidation–respiration chain, which releases water and promotes the conversion of ADP to ATP. Taking this into account, the oxidation of proteins is not favorable as it produces nitrogenous compounds that can be toxic if accumulated in exceeding quantities. Generally, when energy production exceeds energy consumption, the surplus is stored as glycogen reserves in muscles and liver. However, glycogen reserves are only short-term energy storage, whereas the long-term reserves are the subcutaneous fat reservoirs produced by the *de novo* lipogenesis [165]. Despite this, the adipose tissue represents the main energy reservoir in the body. It has a lower metabolic rate compared to the fat-free mass (FFM), constituted by the smooth and skeletal muscles, the connective tissue, water, and the bone[166]. For this reason, FFM plays a central role in the total energy expenditure (TEE), which is the energy expended during oxidation of energy-yielding macronutrients within a 24-hour period[167]. TEE is determined by body size and composition as well as behavioral and environmental factors. In fact, TEE is the sum of three major components: resting energy expenditure (REE), diet-induced energy expenditure (DEE), and physical activity-induced energy expenditure (AEE). While DEE accounts for about 10% of the TEE, AEE is variable and depends mostly on the lifestyle, and REE accounts for 60-70% of TEE[167, 168]. Interestingly,

FFM is the parameter that mainly affects REE meaning that most of the oxidative processes take place in the metabolically active tissues[167].

## 2.6 Malnutrition and sarcopenia

### 2.6.1 Characteristics of malnutrition

Malnutrition is defined by the World Health Organization as "deficiency, excesses or imbalances in a person's intake of energy and/or nutrients" [169] and it is often observed in patients suffering from chronic and severe diseases, worsening their conditions and prognosis. In German hospitals 1 out of 4 patients is malnourished and usually, this condition is associated with longer hospital stays, malignant diseases, and several comorbidities[170]. However, the diagnosis of malnutrition can be difficult, as it also depends on the clinical picture, which can be very variable. Up to date, there are two main methods to diagnose malnutrition: the GLIM and the ESPEN. According to the GLIM criteria (Table 1), for a patient to be defined as "malnourished", they should show at least one of the phenotypical criteria (non-volitional weight loss, low body mass index, and reduced muscle mass) and one etiological criterion (reduced food intake or assimilation, and inflammation or disease burden)[171].

| **Phenotypic criteria** | | | **Etiological criteria** | |
|---|---|---|---|---|
| **Weight loss (%)** | **Low body mass index (Kg/m²)** | **Reduced muscle mass** | **Reduced food intake or assimilation** | **Inflammation** |
| >5% within the past six months or >10% beyond six months | <20 if <70 years<br>or<br><22 if >70 years<br><br>Asian population:<br><br><18.5 if <70 years<br>or<br><20 if >70 years | Reduced by validated body composition measuring techniques | ≤50% of energy requirements<br>> 1 week<br>or<br>any reduction for >2 weeks, or any chronic gastrointestinal condition that adversely impacts food assimilation or absorption | Acute disease/injury or chronic disease-related |

**Table 1**: Classification of malnutrition according to the phenotypic criteria modified after Jensen et al. (2019)[171]

Malnutrition can further be classified as moderate or severe according to the grade of the phenotype On the other side, the ESPEN criteria diagnose malnutrition when the body mass index is below 18.5 kg/m² or unintended weight loss occurs together with a reduction of body mass index or fat-free mass index. According to these criteria, malnutrition can be classified as

type 1, which is disease-related with inflammation; type 2, which is disease-related malnutrition without inflammation; and type 3, which is unrelated to any disease[172].

### 2.6.2 Characteristics of sarcopenia

Sarcopenia is a progressive and generalized skeletal muscle disorder, associated with adverse outcomes including falls, fractures, physical disability, and mortality[173]. For a long time, this condition has been mostly associated with aging. However, lately, several contributing factors have been found. It has been established that sarcopenia can also begin earlier in life[174–176] and that people affected by sarcopenia need optimal care as this condition has several personal, social, and economic burdens when untreated[177]. It has been estimated that 32% of patients suffering from digestive disease are affected by this condition[178]. The assessment of sarcopenia can be done using several parameters such as muscle strength, but the grip strength measurement and the chair stand test are among the most widely used methods[179–181]. Muscle quantification using non-invasive techniques such as MRI and computed tomography is also one of the most common methods to assess sarcopenia [181]. According to the triggering cause, sarcopenia can be divided into two different types: primary sarcopenia is due to aging, whereas secondary sarcopenia is due to pathologies and can occur as a consequence of a systemic disease, especially ones invoking inflammation processes[182]. However, independently of the sarcopenia subtype, one of the main pathological causes is the imbalance between protein synthesis and degradation: under physiological circumstances, skeletal muscle mass is maintained by a balance between protein synthesis, protein breakdown, and regenerative capacity regulated by muscle satellite cell function[183]. In sarcopenic patients, the balance is shifted towards protein degradation.

### 2.6.3 Malnutrition and sarcopenia in liver cirrhosis

There are plenty of reasons for cirrhotic patients to be malnourished: negative energy balance due to poor food intake, loss of appetite due to inflammatory cytokines or alcohol-associated anorexia, presence of ascites causing early satiety because of gastric accommodation and impaired stomach expansion, abdominal pain as well as nausea and bloating[184–186]. Furthermore, patients affected by CLD often suffer from fat malabsorption, due to inadequate bile release[187]. Altered fat digestion also leads to vitamin deficiency; in fact, CLD patients are frequently lacking in vitamin A (33.5%), vitamin D (13.2%), vitamin K (7.8%), and vitamin E (1.9%)[188]. The etiology of cirrhotic malnutrition is multifactorial[189]. However, it is known that

the type of malnourishment in cirrhosis is primarily a protein-caloric subtype[190] and that sarcopenia represents one of the key features of malnourishment in patients with advanced decompensated chronic liver disease[191]. In fact, malnutrition and sarcopenia are often present in parallel in liver diseases and manifest clinically as malnutrition-sarcopenia syndrome[192]. The hallmarks of malnutrition-sarcopenia syndrome are a combination of diminished nutrient intake, inflammation, decreased body weight, and reduced muscle mass, strength, and physical function[192]. Cirrhosis mimics a state of accelerated starvation, with a defective adaptive response to fasting caused by the impairment of liver function, which differs from the fed state and the normal physiological conditions. In fact, in fed state carbohydrates and glucose are the main substrate for oxidation and production of energy, and the main muscle metabolic activity in this case is protein synthesis. Furthermore, under physiological conditions, the glycogen stored in the liver serves as a substrate for the glycogenolysis. However, in the case of LC the protein pool in muscle is degraded to produce substrates for gluconeogenesis. In fact, gluconeogenesis and fatty acid oxidation in the liver are elevated due to the short supply of glycogen. Thus, alanine, lactate, and glycerol (coming respectively from muscle protein breakdown, glycogen degradation, and adipose tissue), are delivered to the liver to serve as glucogenic substrates[193, 194]. Moreover, in starvation and depletion of carbohydrates and glucose, fatty acids become the main substrate for energy production. However, some tissues will not be able to use fatty acids and need to increase the rate of gluconeogenesis, thus glucogenic AA are degraded to serve as a substrate for the process. Hence, it is clear that a chronic fasted state like LC results in protein depletion, which added to anabolic resistance causes an impairment in the restoration of the protein pool and thus muscle loss[195–198]. Furthermore, in LC skeletal muscles should also compensate for the liver's inability of ammonia detoxification. This process happens in the mitochondria and glutamine is essential. Glutamine formation depends on the glutamate, produced from α-ketoglutarate. However, hyperammonaemia causes a shortage of glutamate, thus in skeletal muscle, the branched chain AA (BCAA) are catabolized to provide carbon skeletons for the three carboxylic acids, needed to restore α-ketoglutarate and to maintain appropriate levels of glutamate for ammonia clearance and glutamine formation. Glutamine is released in the bloodstream in exchange with BCAA. Hence, in conditions of hyperammonaemia, elevated BCAA uptake and muscle metabolism lead to the depletion of BCAA required for protein synthesis[199–202]. In general, a hyperammonic state induced by LC can affect skeletal muscle. Specifically, ammonia triggers the activation of myostatin via the NF-κB-dependent pathways, resulting in impaired muscle growth and protein turnover; oxidative stress and impairment of the mitochondrial functions

via shortage of α-ketoglutarate; and phosphorylation of the eukaryotic initiation factor 2 (eIF2), which impairs protein synthesis[203, 204]. In addition to this, cirrhotic patients' conditions are usually worsened by insulin resistance, due to Insulin-like Growth factor-1 (IGF-1) decrease[205]. Interestingly, IGF-1 is not only associated with muscle growth and protein synthesis via activation of the mTOR pathway, but is also able to negatively regulate the myostatin pathway[206, 207], so it is not surprising that sarcopenic cirrhotic patients often display IGF-1 deficiencies[208]. However, studies reported that in case of cholestatic damage cholangiocytes start secreting IGF-1 in an attempt to restore the damaged tissue[209].

# 3 AIMS OF THE STUDY

The literature presented in the introduction highlights how malnutrition and sarcopenia are multicausal processes, where inflammation, accelerated catabolism, and nutrients malabsorption play a crucial and intertwining role. In LC patients, the liver injury mimics a state of accelerated starvation that exacerbates the two comorbidities. This is caused by the inability of the liver to adequately compensate the damage, because of its impaired liver function. It is known that the malnutrition-sarcopenia syndrome worsens the prognosis of the disease and negatively impacts patients' expectancy and quality of life, however the mechanisms underlying sarcopenia in LC and its interplay with malnutrition remain unclear. This is due to the difficult identification of specific molecular mediators and biomarkers. In this context, the aim of this study was to investigate on the development of sarcopenia from the initial phases of cholestatic liver damage, using a 14-days experimental period murine C57BL/6J BDL model. Specifically, it was hypothesized that sarcopenia is an early event in CLD. In this regard, AA patters, molecular markers for inflammation and muscle damage, as well as plasma metabolites associated to liver damage and malnutrition were analysed. Furthermore, to gain deeper insights into the molecular pathways and mechanisms involved in sarcopenia, gene expression patterns in muscle quadriceps femoris and muscle gastrocnemius were analysed. All the data were measured at different time points (7-, 10- and 14-days post-surgery) to allow monitoring of the disease state over time. Furthermore, this comprehensive data acquisition can represent a starting point for setting up future mechanistic and interventional studies.

# 4 METHODS

This doctoral thesis is part of the multicentric project EnErGie, thus all the methods described in this section have been performed by different researchers in different research centres. The surgical methods and the whole animal trial were performed in the Institute of Experimental Surgery of the Rostock University Medical Centre. The BDL surgery method was established by Dr. Sarah Rohde and later on carried out by Dr. Luise Ehlers, both from the Department of Medicine II, Division of Gastroenterology, Rostock University Medical Center. Daily monitoring (including muscle strength measurements) and the Luminex assay were performed by the employees of the laboratory of the Department of Medicine II, Division of Gastroenterology, Rostock University Medical Center. MRI measurements were carried out by the Core Facility "Multimodale Kleintierbildgebung" of the Rostock University Medical Center. Metabolic cages and fractional protein synthesis experiments were performed by me in collaboration with Dr. Ehlers. The derivatization $^{2}H_5$-Phe in splanchnic tissue and muscle, as well as their $^{2}H_5$-Phe enrichment measurement using a gas chromatography mass spectrometry (GC-MS) system, were performed by me with the collaboration of Mrs. Meike Statz at the Research Institute of Farm Animal Biology (FBN), Dummerstorf. Preparation of feces and urine samples for nitrogen content determination to calculate N-BAL, as well as RNA extraction from muscle, q-RT PCR experiments, and muscle histology experiments were performed by me at the FBN. Measurements of the N concentrations in feces and urine were performed by Mr. Thomas. Geick and Mrs. Katharina Groth. Measurements of isotope enrichment in plasma and urine were performed by Mrs. Kirsten Karpati and the TEE calculations were performed by Dr. Solvig Görs at the FBN Dummerstorf. Plasma concentrations of IGF-1, IGFBP-1, and IGFBP-3 were performed by Mrs. Birgit Mielenz. Measurements of NEFA and CK were performed by Mrs. Susanne Dwarf at the FBN Dummerstorf. Clinical chemistry measurements were performed at the Institute for Clinical Chemistry and Laboratory Medicine of the Rostock University Medical Centre. AA measurements and total energy expenditure calculations were performed at the FBN by Dr. Solvig Görs. Bile acids analyses were performed at the Greifswald University Medical Centre. Experiment planning, data curation, and evaluation have been performed by me in collaboration with Dr. Luise Ehlers, Dr. Solvig Görs, Dr. Quentin Sciascia, and Prof. Robert Jaster.

## 4.1 Animal model

C57BL/6J mice were purchased from Charles River Laboratories (Sulzfeld, Germany) and bred in the local animal facility of the Rostock University Medical Center. The study protocol was approved by the Landesamt für Landwirtschaft, Lebensmittelsicherheit und Fischerei Mecklenburg-Vorpommern (LALLF/MV; approval no. 7221.3-1.1-046/18). All animals were treated following the German Animal Protection Act (TierSchG) and the European Union Directive, 2010/63/EU. The mice had *ad libitum* access to water and rodent chow diet (V1534-0; 19% crude protein, 3.3% crude fat, 4.9% crude fiber, 16.3 MJ ME/kg diet; ssniff Spezialdiäten GmbH, Soest, Germany). One week before surgery until the end of the experimental period, an additional 50 g of feed was provided daily in the form of a mixture of 30% dry V1534-0 feed and 70% water.

At approximately 17 weeks of age, male mice were randomly assigned to the experimental groups BDL, sham surgery, and no surgery (controls). Before surgery, the mice were anesthetized with isoflurane (5% for induction, 1.5% for maintenance), and carprofen (Pfizer GmbH, Berlin, Germany) at 5 mg/kg body weight (BW) was injected subcutaneously for pain prevention. The surgical procedure for BDL consisted of the common bile duct being exposed after midline laparotomy, ligated three times with a 5-0 polyester suture (Ethicon, Norderstedt, Germany), and transected between the two most distal ligations. The sham surgical procedure consisted of the common bile duct being exposed but neither ligated nor cut. The abdominal wall was closed in two layers using 6-0 prolene (Catgut, Markneukirchen, Germany)[210]. After the surgery, mice were daily monitored, and their BW and wellbeing were assessed. Analgesia was continued with metamizol (Ratiopharm GmbH, Ulm, Germany) dissolved in drinking water (1.25 mg/mL) until the end of the experiment.

On days 7-14 after surgery (as specified below), the animals were sacrificed by an overdose of ketamine/xylazine hydrochloride followed by cervical dislocation. Blood was collected from the retro-orbital venous sinus in Lithium heparin tubes and centrifuged at 3,000 × g for 20 min at 4 °C to obtain plasma. Splanchnic tissues (jejunum, colon, liver, and pancreas) and quadriceps femoris and gastrocnemius muscles (M. quadriceps and M. gastrocnemius, respectively) were collected, and their wet weight was determined. All samples were stored under appropriate conditions until they were assayed as detailed below.

### 4.1.1 Muscle strength measurements

Skeletal muscle strength was determined non-invasively using a BIO-GS3 grip strength meter (Bioseb, Vitrolles, France). For this purpose, the device was set up horizontally, the mice were

held by the tail and lowered towards the device. The mice were allowed to grasp the triangular pull rod and were then pulled backward in the horizontal plane. The force exerted on the rod just before the mouse lost its grip was recorded as peak tension. Each animal was measured three times per time point and the mean value was used for further calculations.

### 4.1.2 Magnetic resonance image (MRI) of the quadriceps muscle

MRI measurements of the M. quadriceps were performed for all animals at three time points: one day before surgery (d-1), 6 days after surgery (d6), and 13 days after surgery (d13). The volumes of the left and right M. quadriceps were determined in anesthetized mice (1.5-2.5 % isoflurane in oxygen). The respiratory rate (between 35 and 50 breaths/min) and body temperature of the animals were continuously monitored during the scan (triggered by respiration). The MRI was performed with a 7 Tesla MRI machine (Bruker BioSpec 70/30, gradient system: BGA 12 S HP, 86 mm volume coil in transmit mode, 2 x 2 receive surface coil, all Bruker Biospin GmbH, Ettlingen, Germany) using coronal T1 weighted FLASH sequences and T2 weighted TurboRARE sequences. T1w FLASH (cor): TR: 313 ms, TE: 2.9 ms, field of view: 32.0 x 35.2, matrix size: 256 x 281, in-plane resolution 125 x 125 µm, FA: 50°, 4 averages, slice thickness: 0.8 mm, 23 to 26 slices depending on the size of the mouse, no slice gap, TA: approx. 5:50 min depending on the respiration rate and consequent trigger. T2w TurboRARE (cor): TR: 1968 ms, TE: 25 ms, field of view: 32.0 x 35.2, matrix size: 256 x 281, in-plane resolution 125 x 125 µm, RARE factor: 8, 4 averages, slice thickness: 0.8 mm, 23 to 26 slices, no slice gap, TA: approx. 4:40 min depending on the respiration rate and consequent trigger. Images were analysed using ITK-Snap software (version 3.8.0, Penn Image Computing and Science Laboratory "PICSL", University of Pennsylvania, USA). Volume evaluation was based on slice-wise independent placement of the regions of interest in each muscle using a T2-weighted image series of coronal slices. Muscle volumes on both sides were scored in $mm^3$, and the average was calculated and related to d-1.

### 4.1.3 Nitrogen balance (N-BAL) and total energy expenditure (TEE) assessment in metabolic cages

Before and after BDL or sham surgery, mice were individually placed in metabolic cages (TECNIPLAST GmbH, Hohenpeißenberg, Germany), three times for 24 h each: from d6 to d5 before surgery (d-6/-5), from d2 to d3 after surgery (d2/3) and from d9 to d10 after surgery

(d9/10). On d2 after surgery, mice were injected i.p. with 8 mg/g BW $^{2}H_2O$ (99.8 atom% 2H, Chemotrade, Leipzig, Germany) plus 12 mg/g BW $H_2{}^{18}O$ (97 atom% $^{18}O$, Eurisotop, Paris, France), sterilized by filtration through a 0.2 µm sterilized NALGENE® 4 mm nylon syringe filter (Thermo Scientific, Fisher Scientific GmbH, Schwerte, Germany) to determine TEE. Blood was collected on d10, and mice were euthanized as described above. During the three MC trials, feed and water intake as well as BW were monitored, and urine and feces were preserved. Urine was collected over 24 h in three different tubes: a 15 mL tube, containing 150 µL of 50% sulfuric acid to prevent the loss of volatile N compounds and thus to be used to calculate N-BAL, N excretion, and urinary AA; and two 2 mL tubes containing no acid at two different time points from 1.5 to 2.5 h and from 22.5 to 24 h after the start of the MC trial, to be used for the measurement of $^{2}H$ and $^{18}O$ enrichment and to calculate TEE. To calculate the N-BAL, the dry matter of feed, urine, and feces was determined by drying the samples at 55 °C (urine and feed overnight, feces 24 h) and measuring the N concentration with an elemental analyzer (Thermo-Fisher Scientific GmbH, Waltham, MA, USA) in pre-dried tin capsules (IVA-Analysentechnik GmbH und Co. KG, Meerbusch, Germany). Subsequently, the 24 h N-BAL was calculated from the N concentrations in feed ($N_{feed}$), urine ($N_{urine}$), and feces ($N_{feces}$) as follows:

$$\text{N-BAL (g)} = N_{feed} - (N_{urine} + N_{feces})$$

The TEE was assessed by isotope dilution using the doubly labeled water method[211]. The isotope ratios $^{2}H/^{1}H$ and $^{18}O/^{16}O$ corrected for isotopic background in the non-acidified urine samples and the plasma samples collected on d10 were analyzed by gas isotope ratio mass spectrometry (DELTA Plus XL, Thermo Quest, Bremen, Germany) coupled with a gas bench (GasBench II, Finnigan, Bremen, Germany)[212]. Tracer enrichments in plasma samples were equivalent to that of the 22.5 – 24 h urine samples collected at d10. If a d10 22.5 - 24 h urine sample could not be collected, the d10 plasma enrichment was used for TEE determination instead. The production of $CO_2$ ($rCO_2$) was calculated using the total water pool (W) and the rate constants for $^{18}O$ (ko) and $^{2}H$ (kh) excretion:

$$rCO_2 \text{ (mol } CO_2\text{/d)} = [(W/2078)\,(1.01\,ko - 1.04\,kh)] - [0.0246\,(1.05W\,(1.01\,ko - 1.04\,kh)]$$[213]

The $rCO_2$ was used to calculate the TEE according to the Brouwer equation[213, 214], using a respiratory quotient (RQ) of 0.94 (mean RQ value taken from Guidotti et al., 2013)[211] and taking into account the urinary N loss (NU) as follows:

$$TEE\ (Kj/(g\times d)) = 5.16\ rCO_2 + 16.18\ rCO_2/\ RQ - 5.90\ NU$$

## 4.2 Histological assessment

Liver, M. quadriceps, and M. gastrocnemius tissues underwent several histological procedures to assess the damage provoked by the BDL (haematoxylin/eosin (H/E) and direct red staining in the liver) as well as the signs of muscle damage induced by the CLD (H/E and ammonium sulfide staining in the M. quadriceps and M. gastrocnemius). The detailed protocols are described in the following paragraphs.

### 4.2.1 Haematoxylin / Eosin (H/E) staining

H/E staining allows for a comprehensive assessment of an organ by simultaneously staining cell nuclei and tissue, giving an overview of the organs' conditions. H/E staining was performed on liver, M. quadriceps, and M, gastrocnemius tissues, albeit with different procedures. The liver was collected and embedded in a 4% formaldehyde solution (Grimm med Logistik GmbH, Torgelow, Germany) overnight. Afterward, the samples were processed in an automated tissue processor (Thermo Fisher Scientific, USA) and embedded in paraffin. Liver sections were then cut into 4 µm thick sections, transferred to a microscope slide and dried overnight at 55 °C. Subsequently, the sections were stained according to the protocol in Table 2.

**Table 2. H/E staining protocol for liver sections**

| Solution | Time of incubation | Procedure |
|---|---|---|
| Xylene | 10 min | Deparaffinisation |
| Xylene | 10 min | Deparaffinisation |
| 96% Ethanol | 5 min | Washing |
| 96% Ethanol | 5 min | Washing |
| 70% Ethanol | 3 min | Washing |
| Distilled water | 2 min | Washing |

| | | |
|---|---|---|
| Haematoxylin | 1 min 15 sec | Nuclei staining |
| Running water | 1 min | Staining fixation |
| Distilled water | 5 sec. | Rinsing |
| Eosin + 2% acetic acid | 1 min | Tissue staining |
| Distilled water | 5 sec | Rinsing |
| 70% Ethanol | Briefly rinse | Removing water excess |
| 96% Ethanol | Briefly rinse | Removing water excess |
| 96% Ethanol | Briefly rinse | Removing water excess |
| Xylene | 30 seconds | Removing water excess |
| Xylene | 30 seconds | Removing water excess |

The M. quadriceps and M. gastrocnemius were treated differently. Right after the extraction, the muscles were snap frozen in liquid nitrogen and stored at -80°C. For the histological analyses the muscles were cut at their thickest part in 12 µm sections using a cryostat microtome (CM3050 S, Leica, Bensheim, Germany) and mounted on a microscope slide. The H/E staining was performed according to the protocol in Table 3.

**Table 3. H/E staining protocol for frozen muscle sections**

| Solution | Time of incubation | Procedure |
|---|---|---|
| 4% Formol-calcium | 5 min | Fixation |
| Distilled water | 5 min | Washing |
| Haematoxylin | 5 min | Nuclei staining |
| Running water | 20 min | Rinsing |
| Distilled water | 5 min | Rinsing |
| Eosin + 3 drops of acidic acid | 10 min | Tissue staining |
| Distilled water | 3 min | Rinsing |
| 70% Ethanol | 1 min | Removing water excess |
| 96% Ethanol | 1 min | Removing water excess |
| Absolute ethanol | 3 min | Removing water excess |
| Xylene | 10 min | Removing water excess |

In the case of the liver sections, the H/E staining allowed the assessment of the presence of necrotic tissue, inflammation, bile duct proliferation, and fibrosis. In the case of the muscle

sections, it allowed the count of the nuclei and fibers, as it is shown that a decrease in nuclei number is a sign of sarcopenia[215, 216]. To count nuclei and fibers, the H/E-stained samples were photographed in six randomly selected areas, using a light microscope with an integrated camera (Nikon Microphot SA, Nikon, Tokyo, Japan) at 20 x magnification. Nuclei and fibers were counted using the Cell^F imaging software (OSIS, Münster, Germany).

### 4.2.2 Sirius red staining

Sirius red staining is used to stain collagen fibers, to assess the presence of liver fibrosis. Liver sections were cut and dried as described in the paragraph above. The detailed staining protocol was performed according to Table 4.

**Table 4. Sirius red staining protocol for liver sections**

| Solution | Time of incubation | Procedure |
|---|---|---|
| Xylene | 10 min | Deparaffinisation |
| Xylene | 10 min | Deparaffinisation |
| 96% Ethanol | 5 min | Deparaffinisation |
| 96% Ethanol | 3 min | Deparaffinisation |
| 70% Ethanol | 2 min | Deparaffinisation |
| Distilled water | At least 2 min | Deparaffinisation |
| Haematoxylin | 8 min | Nuclei staining |
| Distilled water | Briefly | Rinsing |
| Running water | Up to 10 min | Rinsing |
| Sirius red | 1 h | Collagen staining |
| Distilled water + 0.5% acetic acid | 1 min | Rinsing |
| Distilled water + 0.5% acetic acid | 1 min | Rinsing |
| Absolute ethanol | Briefly rinse | Removing water excess |
| Absolute ethanol | Briefly rinse | Removing water excess |
| Xylene | Briefly rinse | Removing water excess |
| Xylene | Briefly rinse | Removing water excess |

### 4.2.3 Ammonium sulphide staining

This staining allowed the count of capillaries and fibers in frozen sections of muscle tissue. The sections were cut 12 µm thick as described above and then stained according to the protocol in Table 5.

**Table 5. Ammonium sulphide staining protocol for frozen muscle sections**

| Solution | Time of incubation | Procedure |
|---|---|---|
| 4% Formol-calcium | 5 min | Fixation |
| Distilled water | 5 min | Washing |
| Incubation solution* | 90 min (37 °C) | Incubation |
| Distilled water | Briefly | Rinsing |
| 2% Cobalt chloride | 5 min | Capillary staining |
| Distilled water | Briefly | Washing |
| 1% Ammonium sulphide | 3 min | Capillary staining |
| Distilled water | Briefly | Washing |
| Eosin | 3 min | Tissue staining |
| Distilled water | At least 3 h | Removing dye excess + avoiding contraction wrinkles |

*Incubation solution: 3% Na-β-Glycerol phosphate + Barbital + Distilled water + 2% $CaCl_2$ + 5% $MgSO_4$

Fibers and capillaries were counted using the Cell^F imaging software (OSIS, Münster, Germany).

## 4.3 Concentrations of free AAs in plasma and urine

Two µL of plasma and acidified urine were ten-fold diluted with ultra-pure water and 40 mM phosphate buffer (pH 7.45), respectively. To allow fluorescence detection, primary AA were derivatized with ortho-phthaldoaldehyde and 3-mercaptopropionic acid, while secondary AA were derivatized using fluorenylmethyloxycarbonyl chloride. Both plasma and urinary free AA were analysed by reverse-phase HPLC system 1260 Infinity II with the G7129A autosampler, the G7112B binary pump, G7116A multicolumn thermostat, and G1321A fluorescence detector (Agilent Technologies, Germany). Separation occurred on a Gemini 250 × 4.6 mm 5 µm reversed-phase C18 110 Å column, with a pre-column 4 × 3 mm C18 (both Phenomenex, Aschaffenburg, Germany)[217] by gradient dilution with a nonpolar phase, consisting of 45 %

methanol, 45 % acetonitrile and 10 % water at pH 7.45. An AA standard mix (Sigma-Aldrich, Germany) and an additional standard mix, consisting of asparagine (Reanat, Hungary), glutamine (Serva, Germany), and tryptophan (Reanat, Hungary), were used for quantification at concentrations of 5 µM, 10 µM, 20 µM, and 50 µM, respectively. A linear standard curve was calculated, and the slope was used for the determination of the plasma AA concentration, subtracting blank values and using a dilution factor of 10. Amino acid concentration (µmol/L) was calculated using the area under the peaks with the HP ChemStation software (Agilent Technologies, Waldbronn, Deutschland), according to the following equation (with dilution factor = 10):

$$[AA]\ (\mu mol/L) = [(Area_{sample\ peak} - Area_{blank})/(Standard\ curve\ slope)] \times dilution\ factor$$

### 4.4 Concentration of urinary N-metabolites

Acidified urine samples were prepared as described in paragraph 4.3. Subsequently, they were diluted 1:50 with ultrapure water to analyse urea, while a 1:10 dilution with 20 mM phosphate buffer (pH 6.5) was used to analyse allantoin, creatine, creatinine, hippuric acid, and uric acid. Urea was analysed with a 1260 Infinity series HPLC system consisting of the temperature-controlled G1329A autosampler, the G1311C 1260 quaternary pump, and the G1362A 1260 refractive index detector (all from Agilent Technologies, Waldbronn, Germany). A Rezex RCM monosaccharide column (300 × 7.8 mm, Phenomenex Inc., Aschaffenburg, Germany) column was used. Five µL of sample was added to the column at a constant 60 °C. The mobile phase was ultrapure water, which ran over the column at a flow rate of 0.5 mL/min. The same HPLC system was used for the measurements of allantoin, creatine, creatinine, hippuric acid, and uric acid, however, a Synergi 4 µm Hydro-RP 80 Å column (250 × 4.6 mm, Phenomenex Inc., Aschaffenburg, Germany) and the G1315D diode array detector (210 nm or 230 nm) (Agilent Technologies, Waldbronn, Germany) were used. Five µL of samples were added to the column at 25 °C. Phosphate buffer (20 mM, pH 6.5) was used as the eluent, which flowed over the column at a rate of 1 mL/min. A gradient elution was used to ensure sufficient separation of the AA with narrow peaks in a short analysis time. For this purpose, acetonitrile was added to the phosphate buffer, starting with 0 % at 5 min and going up to 10 % within 25 min. For the calibration, the urea (108487, Merck Chemicals GmbH, Darmstadt, Germany), allantoin (A-7878, Sigma Aldrich), creatine (91705, Chemapol), creatinine (91703, Chemapol), uric acid (229K17724817, Merck Chemicals GmbH, Darmstadt, Germany), and hippuric acid standard (71796, Berlin Chemie, Menarini) in concentrations of 10, 50, 100, 250 and 500 µM were used.

The concentration of the N-metabolites (mmol/L) was calculated using a linear standard curve, according to the equation:

$$[\text{N-metabolites}]\ (\text{mmol/L}) = [(\text{Area}_{\text{sample peak}} - \text{Area}_{\text{blank}}) / (\text{Standard curve slope})] \times \text{dilution factor}$$

The dilution factors were set to 10 for urea and 50 for allantoin, creatine, creatinine, hippuric acid, and uric acid. The HP ChemStation and LC Open Lab programs (Agilent Technologies, Waldbronn, Germany) were used to evaluate the areas under the peaks.

### 4.5 Clinical chemistry and plasma metabolites concentrations

Activities of aspartate aminotransferase (ASAT), alanine aminotransferase (ALAT), alkaline phosphatase (AP), pseudo-cholinesterase (PCHE), and lipase; the plasma levels of albumin, glucose, direct bilirubin, cholesterol triglycerides (TG), uric acid (UA), and urea; as well as plasma concentrations of Na, K, Ca, and Mg were determined using the chemistry analyser DxC 700 AU (Beckman Coulter, Krefeld, Germany) and systems reagents from Beckman Coulter for this analyser. Creatine kinase (CK) and non-esterified fatty acids (NEFA) were measured with an automatic enzymatic analyser (ABX Pentra 400 Clinical Chemistry Analyser, Horiba medical, Montpellier, France) using commercial kits (ABX Pentra CK NAC CP (Horiba medical, Montpellier, France); NEFA-HR (2) Assay (Fujifilm Wako Chemicals Europe GmbH, Neuss, Germany)). ELISA assays were used to determine plasma levels of IGF-1 (mouse IGF-I; Mediagnost, Reutlingen, Germany), IGF-1 binding protein (BP) 1 and 3 (mouse IGFBP-1; DuoSet Quantikine ELISA kit and mouse IGFBP-3; DuoSet Quantikine ELISA kit (R&D Systems Inc., Minneapolis, USA)), and myostatin (GDF-8/Myostatin Quantikine ELISA kit (R&D Systems Inc., Minneapolis, USA)) according to manufacturer's instructions. Plasma levels of epithelial growth factor (EGF) and its receptor EGFR, hepatocyte growth factor (HGF), fibroblast growth factor 21 (FGF-21), interleukin 6 receptor alpha (IL-6Rα), tumour necrosis factor receptor I (TNFRI) and TNFRII, and vascular endothelial growth (VEGF) were determined with a bead-based multiplex assay using the Luminex technology. Therefore, a mouse-specific magnetic Luminex multiplex assay from Bio-Techne (Minneapolis, MN, USA) was employed according to the instructions of the manufacturer. The Luminex 100/200 device was operated via the xPONENT® 3.1-Software (Luminex Corporate, Austin, USA).

### 4.6 Assessment of bile acids concentration using targeted LC-MS/MS profiling

Targeted metabolomics profiling of the plasma samples was performed with a MxP® Quant 500 kit (BIOCRATES LifeSciences AG, Innsbruck, Austria) which was run on a LC-MS/MS AB SCIEX 5500 QTrap™ mass spectrometer (AB SCIEX, Darmstadt, Germany) with electrospray ionization coupled with a HPLC system (Agilent 1260 Infinity Binary LC, Santa Clara, United States). Ten µL of plasma were processed according to the manufacturer's instruction using a fully automated assay combined flow injection (FIA) and mass selective detection. The isotope-labelled internal standards were partially integrated into the kit plate for metabolite quantification. After the measurements, the data were uploaded to the Biocrates MetIDQ software, where the peak integration and the calibration curves were checked as a pre-processing step, before performing the automatic calculation of the metabolites' concentrations. Subsequently, for each metabolite, the median of the plate-specific medians of the pooled samples was calculated to reset the concentration to the original scale (µM concentrations). For each metabolite, the plate-specific coefficient of variation (CV) was calculated based on the pooled samples. Only metabolites with a CV < 25% on two plates were included in the final data sets.

### 4.7 Fractional protein synthesis rate (FPSR) in selected tissues

Fractional protein synthesis rate (FPSR) is defined as the rate that a labeled amino acid precursor is incorporated into a tissue protein[218]. The FPSR was measured using the flooding dose method[219].

Thirty min before euthanasia, mice were injected i.p. with $^{2}H_5$-ring-phenylalanine ($^{2}H_5$-Phe; 375 mg/g BW; 99.1 atom% $^{2}H$, Euriso-Top GmbH, Saarbrücken, Germany), dissolved in 0.9 % NaCl solution. The mice were euthanized as described in paragraph 4.1 and jejunum, colon, liver, pancreas, M. quadriceps, and M. gastrocnemius were collected, washed in 0.9 % NaCl solution, and snap-frozen in liquid nitrogen. To assess the enrichment of protein-bound $^{2}H_5$-Phe, protein pellets were obtained from splanchnic tissues and M. quadriceps and M. gastrocnemius, as follows: After grinding in liquid nitrogen, 50 mg of tissue were precipitated using 0.2 M perchloric acid ($HClO_4$) and homogenized on ice with a sonication tip (Sonotrode MS 1, Carl Roth, Karlsruhe, Germany) with 30 pulses for 0.5 seconds each and 80 % amplitude. Samples were incubated for 15 min on ice in a sonication bath and centrifuged (3000 x g, 4°C for 10 min) to separate the protein pellet from the supernatant. The pellet was washed with 0.2

M $HClO_4$ and bi-distilled water and centrifuged at 12000 x g and 4 °C for 8 min. Afterward, it was dried under $N_2$ flow at 60 °C and hydrolysed overnight in heating blocks at 110 °C using 1 mL 6 N hydrochloric acid and 10 µL of 16 mg/ml ascorbic acid. The hydrolysed pellet was dried under N2 flow at 60 °C, derivatized with 70 µL of N-methyl-N-tert-butyldimethyl silyltrifluoroacetamide (MTBSTFA) (Acros Organics, Thermo Fisher Scientific GmbH, Geel, Belgium) and 50 µL of acetonitrile and incubated for 15 min in a sonication bath at 30 °C and then for further 30 min at 105 °C in heating blocks. Fifty µL of each sample was mixed with 50 µL of ethyl acetate and transferred to an insert vial for measurements with the gas chromatography-mass spectrometry (GC-MS) system. Plasma was used to assess the enrichment of ²H5-Phe in the free precursor. Twenty-five µl plasma were precipitated using a 3.5-fold amount of acetonitrile and centrifuged at 16.000 x g, 4 °C for 20 min. The supernatant was separated from the pellet and dried at 60 °C under N2 flow. Then, the samples were derivatized with 50 µL of MTBSTFA and 50 µL of acetonitrile and incubated for 15 min in a sonication bath at 30 °C and for further 30 min at 105 °C on heath blocks. Fifty µL of each sample was mixed with 50 µL of ethyl acetate and transferred to an insert vial for the measurements with GCMS. The samples were analysed using a GC-MS-QP2010 Ultra system (Shimadzu, Kyoto, Japan). The calibration of the instrument was different for protein pellet and plasma samples. The enrichments of ²H5-Phe used for the pellet ranged from 0 - 2.5 mole percent excess (MPE) in steps of 0.5 MPE, while for the plasma the ²H5-Phe enrichments ranged 0 - 50 MPE in steps of 10 MPE. The measurements of ²H5-Phe enrichment were performed according to Dänicke et al. (2006)[219] with modifications as the fragments used for natural and enriched abundance of phenylalanine were m/z 234 and 239, respectively. However, for the measurements of the muscle samples the signal of the m/z 239 was too low and the resolution could not be appropriately increased without overloading the system, thus the method was modified after Welle et al. (2006)[220], thus the fragment m/z 235 was used to measure the relative abundance of m/z 239. The abundances of the fragments m/z 234 and 235 were used to calculate the enrichment as the product of 239/235 x 235/234 minus the natural $^2H_5$-Phe abundance in muscles. The GC separation was performed on a Zebron ZB-5HT column (30 m, 0.25 mm inner diameter, 0.25 µm film thickness; Phenomenex, Aschaffenburg, Germany) in split mode with He as the gas carrier. The MS operated in selected ion monitoring mode, with the electron impact ionisation mode set to 70 eV at 200 °C, and the interface temperature set at 260 °C. The split ratio was set to 50 for the pellet and to 10 for the plasma samples. The detector voltage was 0.8 kV for the pellet and 1.4 kV for the plasma. However, adjustments were made if the intensity of the signal was too low or too high. The GC-MS data obtained were analysed

using the software GCMS solution (Shimadzu, Japan). The peak areas were obtained by manual integration and the $^2H_5$-Phe enrichment was calculated as molar percent excess (MPE), according to the following equation:

$$^2H_5 - \text{Phe } enrichment\ [MPE] = \frac{R}{R+1} * 100$$

Where

$$R = \frac{Peak\ area_{Phe(M+5)}}{Peak\ area_{Phe(M+0)}} - \frac{Peak\ area_{Phe(M+5)}}{Peak\ area_{Phe(M+0)}} background$$

Eventually, the FPSR was calculated in percent per day using the following formula[221]:

$$FPSR\ [\frac{\%}{d}] = \frac{(\frac{MPE\ of\ protein - bound\ \ ^2H_5 - \text{Phe}}{MPE\ of\ free\ precursor})}{time} * 100$$

## 4.8 Concentration of free 1- and 3-methyl-histidine (1-MH and 3-MH) in M. quadriceps

The concentrations of free 1-MH and 3-MH in M. quadriceps tissue (30 mg) were determined after homogenization by sonication with an ultrasonic tip (Sonotrode MS 0.5, Carl Roth, Stuttgart, Germany) using 25 pulses during 0.5 s each and 80% amplitude. Samples were then centrifuged at 3.000 × g for 10 min at 4 °C according to Zhao et al (2020)[222]. The supernatant was collected, diluted ten-fold with ultrapure water, and analysed using a reverse-phase HPLC system 1260 Infinity II with the G7129A autosampler, the G7112B binary pump, G7116A multicolumn thermostat and G1321A fluorescence detector (Agilent Technologies, Germany), accordingly to Kuhla et al. (2010) [217], but using a reverse phase column Gemini (250 × 4.6 mm, 5 µm C18 110 Å (Phenomenex, Aschaffenburg, Germany).

## 4.9 Gene expression in M. quadriceps and M. gastrocnemius

Total RNA was extracted from 70 mg M. quadriceps and M. gastrocnemius tissue using TriFast buffer according to the manufacturer's instruction (peqGOLD TriFast; VWR International GmbH, Hannover, Germany). Total RNA was quantified by a nanophotometer (Implen GmbH, Munich, Germany) and the quality was assessed with a Bioanalyzer 2100 and RNA 6000 Nano kit (Agilent Technologies, Waldbronn, Germany). The RNA integrity number ranged between

8.5 and 10. The cDNA was produced from 1 µg purified RNA, with the SensiFAST™ cDNA Synthesis Kit (Bioline, Berlin, Germany) according to the manufacturer's instructions. Primers were made by Integrated DNA Technologies (IDT, Antwerp, Belgium), using pre-designed PrimeTime qPCR Primer Assays for mice. Primers were tested using serial dilutions (1/10, 1/20, 1/50, 1/100, and 1/1000 diluted pooled cDNA), and a final cDNA dilution of 1/20 was selected for the q-RT PCR analyses, as this was the lowest dilution that resulted in sample cycle numbers (Cq) below 30. Primer details are presented in the appendix section (Table S1). Samples were analysed in duplicates in 96 well plates (Roche, Mannheim, Germany) using the LC 96 system (Roche Diagnostics, Mannheim, Germany). Two inter-run calibrators consisting of 10- and 20-fold diluted pooled cDNA, a no-template, and a no-enzyme control were added to each plate. The q-RT PCR was performed using the SensiFAST SYBR No-Rox Mix (Code: 98050, Bioline, Berlin, Germany), according to the manufacturer instructions, with a total volume of 10 µL. Each target gene was analysed under the same conditions: enzyme activation and initial denaturation (95 °C for 30 s); denaturation/annealing repeated 40 cycles (95 °C for 30 s, 60 °C for 20 s); and melt curve analysis from 65 to 98 °C with 1 °C increment every 5 sec. LinRegPCR v 2014.5 was used to obtain the PCR efficiency, and the quantification cycle values (Ramakers et al., 2003). Average PCR efficiency and Cq values are reported in the appendix section (Table S1). The mRNA expression values of target genes were normalized to four stable reference genes: *B2M*, *Polr2a*, *Rplp0*, and *Ppia*. The PCR efficiency and Cq values were then obtained for each sample using LinRegPCR v 2014.5. The normalization of target genes mRNA was performed using the qBASEplus 2.0 software, taking into account amplification efficiencies, inter-run variations, and normalization factors. All data was reported as per the Minimum Information for Publication of Quantitative Real-Time PCR Experiments (MIQE) guidelines[223].

### 4.10 Statistical analyses

The data were analysed using GraphPad Prism (GraphPad Software, version 9.4.1, San Diego, CA, USA). Parametrical continuous dependent variables were analysed using a two-way repeated measurements (RM) ANOVA with a post-hoc Tukey's test. Parametrical independent variables were analysed using a one-way ANOVA with Šidák's multiple comparison test. Non parametrical variables were analysed using the Kruskal-Wallis test with Dunn's multiple comparison test. The presentation of the data and the statistical tests used for data analysis are described in the legends of the tables and figures. Adjusted p-values of $< 0.05$ were considered statistically significant.

# 5 RESULTS

The main findings described in this dissertation have been published and discussed in an original research article[224].

## 5.1 Cholestasis and markers of liver damage in a BDL mouse model

Our findings are in line with previous studies in C57BL/6 mice, as they showed that BDL, but not sham surgery, caused a severe CLD with impressive necrosis and inflammation. The necrotic tissue (marked with an * in Figure 5 upper row) is visible as spots where the tissue architecture is altered and disrupted, appearing almost dissolving; while the inflamed areas are visible as darker immune cells infiltrations in the tissue (marked with an arrow in Figure 5 upper row). Moreover, a progressive beginning fibrosis, visible as collagen fibers stained in red (Figure 5 lower row) was observed from postoperative days 7 to 14 (Figure 5).

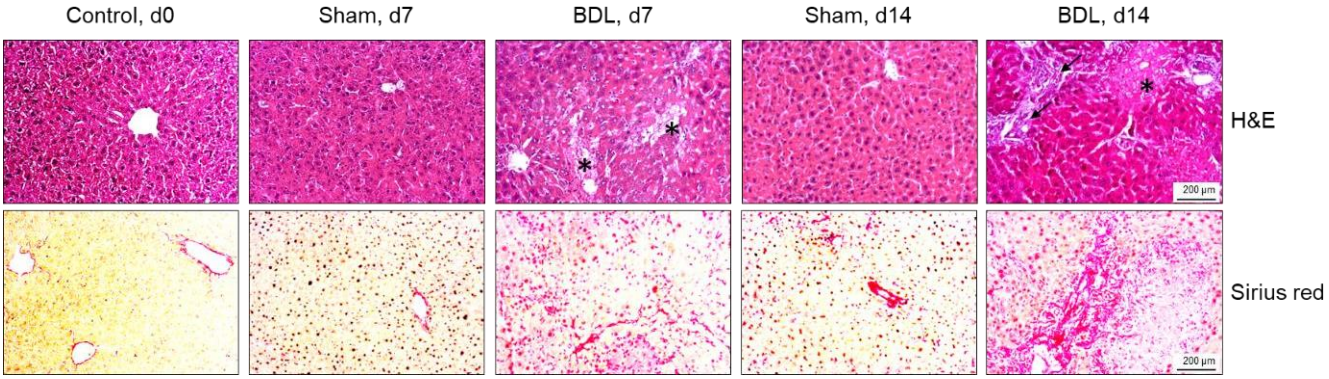


**Figure 5**: H/E and Sirius Red staining of liver tissue sections of mice with BDL and sham surgery. Mice underwent BDL or Sham surgery and were sacrificed on postoperative days 7 (d7) and 14 (d14). Mice without surgery (d0) served as controls. Formalin-fixed paraffin-embedded sections of liver tissue were stained with H&E (upper row) and Sirius red (lower row). Typical pictures for each group (BDL (n=7/10) and Sham (n=9)) and time point (d0, d7 and d14) are shown (original magnification x100). Upper row: asterisks point to necrotic tissue and arrows to areas of inflammation, bile duct proliferation, and fibrosis. Lower row: collagen fibers are coloured red. Figure after Agrifoglio et al. (2025)[224]

Furthermore, CLD was associated with strongly elevated levels of bilirubin as well as ASAT-, ALAT-, and AP-activities in blood plasma (Table 6). In addition, a pancreatic response to cholestasis was also observed in the BDL groups, as shown by the increased lipase activities. However, the albumin levels did not differ significantly between the experimental groups, and PCHE and urea were even increased in at least one of the BDL groups, while blood glucose and TG concentrations after BDL were lower. Moreover, BDL surgery was associated with

increased plasma concentrations of cholesterol and Ca (Table 6), while the levels of uric acid, Na, K, and Mg, and the urinary concentrations of urea and UA (Figure 6), did not differ between the sham and BDL groups. It was also found that plasma levels of individual bile acids showed a significant increase of taurocholic acid, taurochenodeoxycholic acid, and glycocholic acid after BDL surgery, while the concentration of cholic acid was diminished (Table 6).

**Table 6. Concentrations of plasma parameters of mice with BDL or sham surgery and in intact controls**

| **Parameter** [unit] | **d0** (n=34) | **Sham, d7** (n=20) | **BDL, d7** (n=18-20) | **Sham, d14** (n=19) | **BDL, d14** (n=17) |
|---|---|---|---|---|---|
| Bilirubin [µmol/l] | 2.5 ± 0.2 | 1.7 ± 0.2 | 338.5 ± 22.8*** | 1.8 ± 0.2 | 317.7 ± 17*** |
| ASAT [U/l] | 96.9 ± 6.5 | 80.0 ± 9.0 | 1563.6 ± 200.3*** | 73.6 ± 10.0 | 1217.7 ± 163.1*** |
| ALAT [U/l] | 34.7 ± 2.9 | 36.7 ± 5.0 | 809.0 ± 80.2*** | 47.7 ± 13.1 | 594.1 ± 90.7*** |
| PCHE [kU/L] | 3.5 ± 0.1 | 3.2 ± 0.1 | 5.1 ± 0.1*** | 3.1 ± 0.1 | 5.3 ± 0.2*** |
| AP [U/L] | 78.8 ± 2.7 | 55.1 ± 2.3 | 966.2 ± 90.3*** | 60.9 ± 1.5 | 1623.4 ± 101.8*** |
| Lipase [U/l] | 64.7 ± 2.8 | 51.9 ± 3.2 | 208.6 ± 36.7*** | 58.7 ± 3.1 | 449.2 ± 87.3*** |
| Urea [mmol/L] | 9.9 ± 0.2 | 10.1 ± 0.2 | 20.6 ± 3.5* | 10.3 ± 0.3 | 13.1 ± 1.4 |
| Uric acid [mmol/l] | 82.9 ± 14.3 | 156.6 ± 23.1 | 97.2 ± 10.6 | 118.8 ± 24.1 | 91.9 ± 10.2 |
| Albumin [g/L] | 28.1 ± 0.4 | 27.2 ± 0.6 | 29.0 ± 0.7 | 25.8 ± 0.3 | 26.4 ± 0.7 |
| Glucose [mmol/l] | 13.4 ± 0.8 | 15.9 ± 1.3 | 8.2 ± 0.4*** | 14.8 ± 0.9 | 6.9 ± 0.4*** |
| Cholesterol [mmol/l] | 2.2 ± 0.1 | 2.2 ± 0.1 | 17.9 ± 2.3*** | 2.1 ± 0.1 | 17.8 ± 1.9*** |
| TG [mmol/l] | 1.0 ± 0.1 | 1.2 ± 0.1 | 0.8 ± 0.1* | 1.0 ± 0.1 | 0.7 ± 0.1 |
| Ca [mmol/l] | 2.2 ± 0.03 | 2.2 ± 0.04 | 2.7 ± 0.05*** | 2.2 ± 0.03 | 2.7 ± 0.04*** |
| Na [mmol/l] | 154 ± 1.0 | 158.8 ± 7.6 | 179.8 ± 9.7 | 170.4 ± 11 | 195.1 ± 14.3 |
| K [mmol/l] | 4.4 ± 0.1 | 5.1 ± 0.2 | 5.4 ± 0.3 | 4.7 ± 0.3 | 5.7 ±0.3 |
| Mg [mmol/l] | 1.1 ± 0.04 | 1.1 ± 0.06 | 1.3 ± 0.05 | 1.0 ± 0.03 | 1.2 ± 0.03 |
| TCA [µmol/l] | 0.9 ± 0.4 | 0.8 ± 0.1 | 225.5 ± 23.2* | 9.3 ± 5.2 | 203.1 ± 23.7* |
| TCDA [µmol/l] | 0.06 ± 0.02 | 0.05 ± 0.01 | 43.1 ± 5.1* | 0.32 ± 0.16 | 28.3 ± 3.5 |
| GCA [µmol/l] | 0.02 ± 0.00 | 0.03 ± 0.01 | 30.8 ± 7.4* | 0.04 ± 0.01 | 11.2 ± 4.5 |
| CA [µmol/l] | 0.11 ± 0.04 | 0.47 ± 0.08 | 0.084 ± 0.021* | 2.7 ± 2.2 | 0.50 ± 0.14 |

The mice were sacrificed on postoperative days 7 (d7) and 14 (d14). Mice without surgery (d0) served as controls. Data are presented as mean ± SEM. *p<0.05, ***p<0.001; BDL vs. sham-operated mice; One-way ANOVA with Šídák's multiple comparisons test (normally distributed data); Kruskal-Wallis-Test with Dunn's multiple comparisons test (not-normally distributed data). Abbreviations: TCA: taurocholic acid; TCDA: tauroursodeoxycholic acid; GCA: glycocholic acid; CA: cholic acid. Table from Agrifoglio et al. (2025)[224]

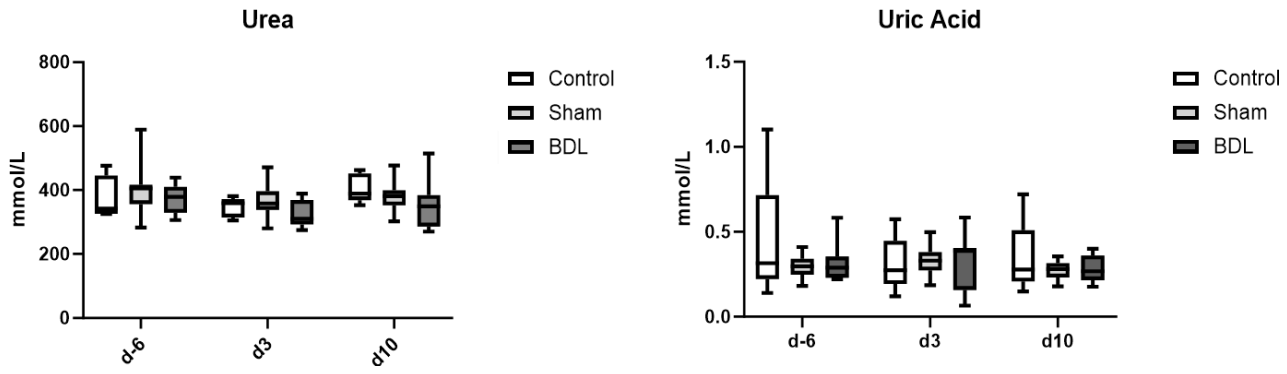


**Figure 6:** Concentrations of urinary N-metabolites of mice with BDL or sham surgery and in intact controls. Urine was collected at pre-operative d-6, and post-operative d3 and d10. The mice were sacrificed on postoperative d10. The control group did not undergo any surgical intervention, whereas the Sham group underwent sham surgery, and the BDL group underwent BDL surgery. Data are shown as box plots (min-max) with median (horizontal line). *$p<0.05$. Two-way RM ANOVA (Tukey's multiple comparisons test). Control n=5; Sham n=11; BDL n=11.

## 5.2 CLD is associated with a catabolic state and an altered protein metabolism

Mice with BDL-induced CLD showed lower feed and water consumption, associated with significant body weight loss during the two-week experimental period (Figure 7 A-C). Specifically, the water intake did not change in the control group. The Sham mice showed a decrease in water intake from d-6 to d3 ($p<0.05$), but the water consumption rose again on d10 when compared to d3 ($p<0.05$) (Figure 7A). The BDL group showed a decrease in water intake. The water consumption on both d3 and d10 was lower when compared to d-6 ($p<0.0001$) (Figure 7A). Water consumption of control and sham mice did not differ. However, the BDL mice showed a significant reduction in water consumption compared to the sham mice at d3 ($p<0.05$) and to both sham and control mice at d10 ($p<0.0001$ and $p<0.05$, respectively) (Figure 7A). The control and sham mice also showed an unchanged food consumption, whereas the BDL mice decreased feed consumption over the experimental period (Figure 7B). There was a difference in feed intake within the BDL group both between d-2 and d3 ($p<0.001$) and between d-2 and d10 ($p<0.001$). Furthermore, the BDL mice showed reduced feed intake compared to sham mice at d3 ($p<0.01$) and to both sham and control mice at d10 ($p<0.0001$ and $p<0.01$, respectively) (Figure 7B). BDL surgery also resulted in a reduced N-BAL (Figure 8A), which reflects the lower feed intake and suggests a loss of total body protein.

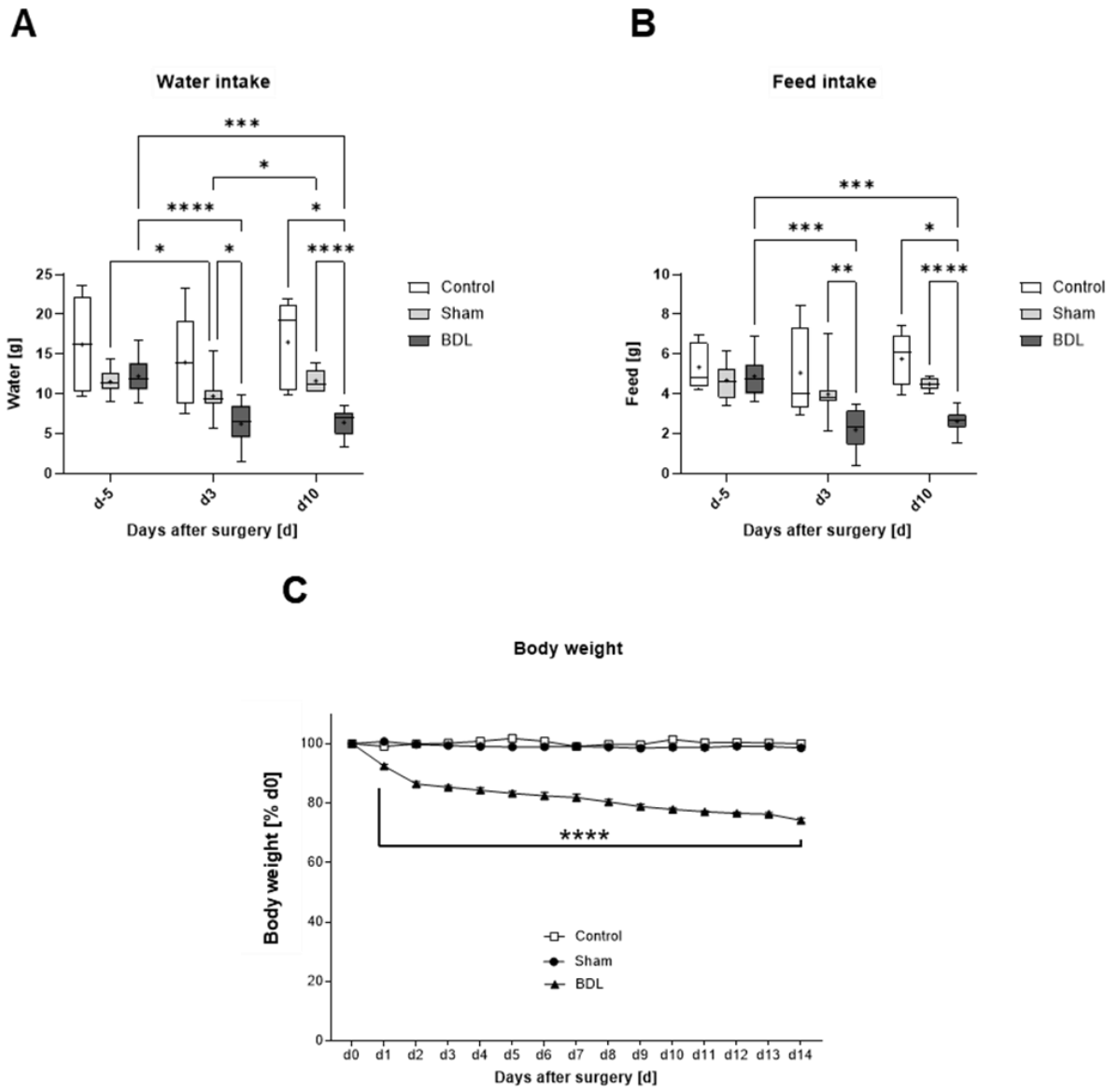


**Figure 7:** Water and feed intake (A-B), body weight (C), N-BAL (D), TEE (E), and FPSR (F) of mice with BDL or sham surgery and in intact controls. TEE was calculated from postoperative d-3 to d10. Data are shown as box plots (min-max) with median (horizontal line) and mean (dot) (A, B) or as median ± interquartile range (C). Numbers of mice (controls-sham-BDL): 5-11-10 (A, B) and 14-19-17 (C). $p<0.05$, $^{**}p<0.01$, $^{***}p<0.001$, $^{****}p<0.0001$. Two-way RM ANOVA with Tukey's multiple comparisons test. In C, for a better overview, only the significant differences between the groups are shown, but not between the time points. Figure modified from Agrifoglio et al. (2025)[224]

The BDL mice (Figure 8A) had a lower N-BAL both at d3 and d10 when compared to d-2 ($p<0.01$ and $p<0.05$, respectively) while no difference in N-BAL was detected in the control (Figure 9A) and sham (Figure 8A) groups. Moreover, the BDL mice have a lower N-BAL than

control mice at d10 ($p<0.05$) (Figure 8A). Furthermore, mice with BDL surgery displayed a lower TEE than the control mice (Figure 8B) ($p<0.05$).

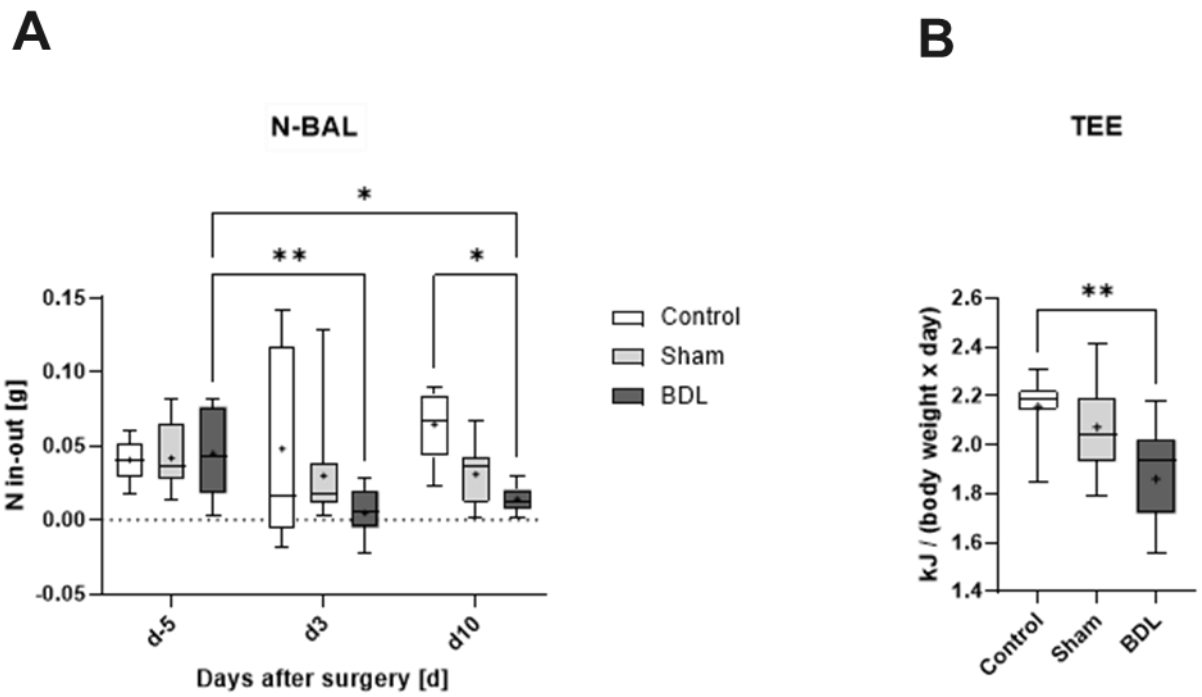


**Figure 8:** N-BAL (A), TEE (B) of mice with BDL and sham surgery TEE was calculated from postoperative d-3 to d10. Data are shown as box plots (min-max) with median (horizontal line) and mean (dot). Numbers of mice (controls-sham-BDL): 5-11-10 (A); 8-11-11 (B). *p<0.05, **p<0.01. Two-way RM ANOVA with Tukey's multiple comparisons test (A) Kruskal-Wallis-Test with Dunn's multiple comparisons test (B). Figure modified from Agrifoglio et al. (2025)[224]

Measurements of FPSR in mice with BDL showed lower values in the liver, M. quadriceps and M. gastrocnemius, while the FPSR in the pancreas remained unaffected (Figure 9). Specifically, the BDL mice showed a decreased liver FPSR at d14 when compared to controls ($p<0.05$), while they exhibited a decreased M. quadriceps FPSR compared to controls both at d7 and d14 ($p<0.01$ and $p<0.001$, respectively) and to sham mice at d7 ($p<0.01$) (Figure 9). Control mice also showed a higher M. gastrocnemius FPSR compared to Sham and BDL at d7 and d14 ($p<0.01$. However, BDL had a lower M. gastrocnemius compared to sham mice both at d7 and 14 (both $p<0.01$) (Figure 9).

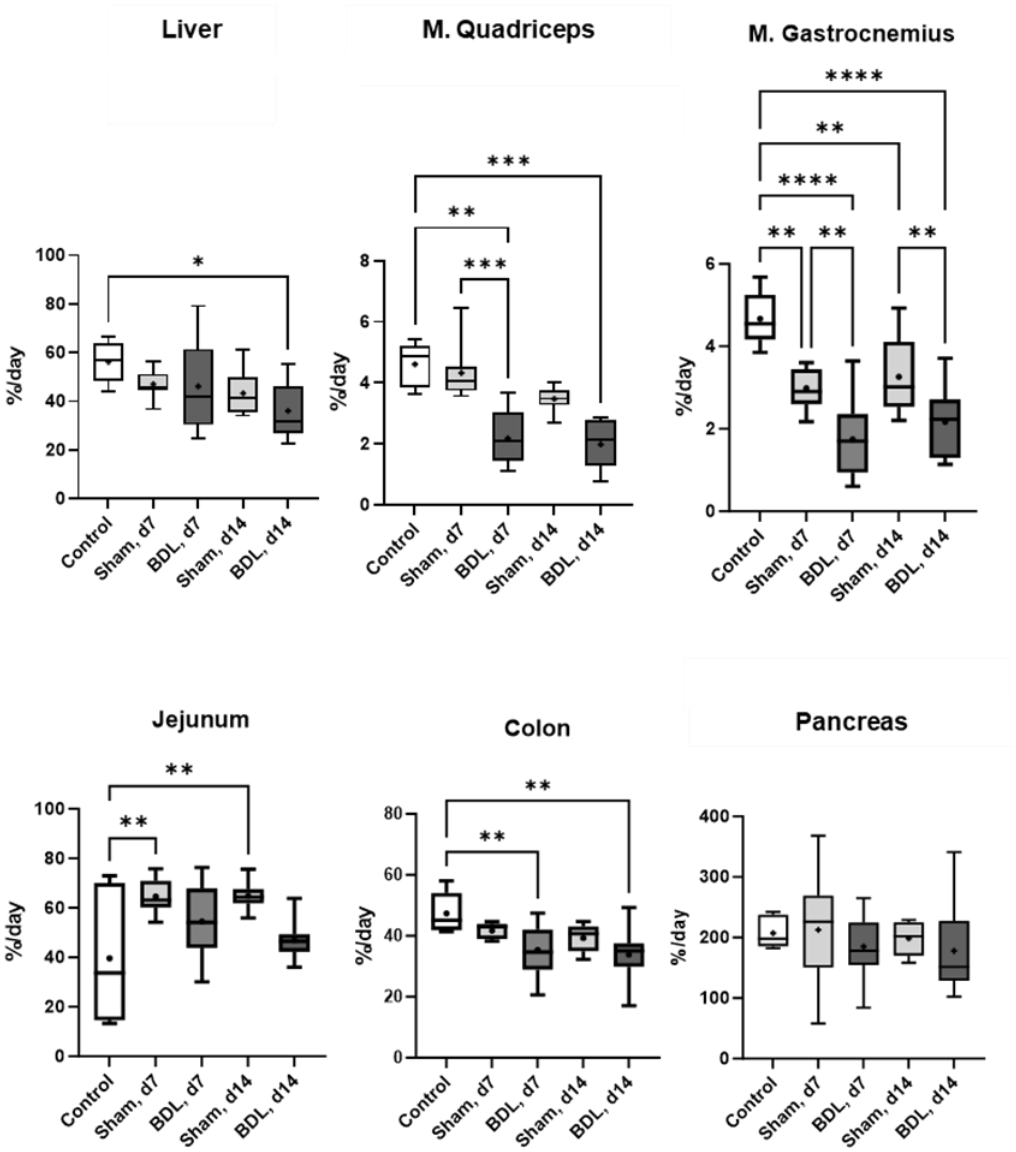


**Figure 9:** FPSR of mice with BDL or sham surgery and in intact controls. The mice were sacrificed at d7 or d14 post-surgery. Data are shown in box plots (min-max) with median (horizontal line) and mean (dot). Numbers of mice (controls-sham-BDL): 5-8-9 (d7); 6-8-9 (d14). *p<0.05, **p<0.01, ***p<0.001, ****p<0.0001. Kruskal-Wallis-Test with Dunn's multiple comparisons test (M. quadriceps); one-way ANOVA with Šídák's multiple comparisons test (liver, colon, M. gastrocnemius, Jejunum, Pancreas). Figure modified from Agrifoglio et al. (2025)[224]

To investigate the protein metabolism in more detail, plasma levels of AAs were determined (Figure 10). Interestingly, only arginine showed a significantly lower concentration in the BDL groups, while levels of ornithine and citrulline, as well as aspartic and glutamic acid, histidine, and phenylalanine, were higher after BDL surgery. Specifically, BDL mice had lower arginine concentration when compared to controls at both d7 and d14 (both $p<0.0001$) and when compared to sham mice at d7 ($p<0.0001$). Vice versa, BDL had higher concentrations of ornithine than controls at d7 ($p<0.01$) and d14 ($p<0.0001$) and sham mice at d7 ($p<0.0001$). BDL mice also showed higher concentrations of citrulline when compared to controls at d14 ($p<0.05$) and to sham mice at d7 ($p<0.05$). The concentration of aspartic acid was also increased in the BDL mice in comparison to controls at both d7 ($p<0.001$) and d14 ($d<0.0001$) and to sham mice at d7 ($p<0.01$). Glutamic acid followed the same pattern, as the BDL had higher concentrations than controls at d7 and d14 ($p<0.05$ and $p<0.001$, respectively) and sham mice ($p<0.01$). Histidine concentration was higher in BDL mice when compared to controls at d14 and sham at d7 ($p<0.01$ and $p<0.05$, respectively). The BDL mice also displayed higher concentrations of phenylalanine compared to controls at both d7 ($p<0.05$) and d14 ($p<0.0001$) and to sham mice at d7 ($p<0.05$). BDL was also associated with strikingly increased plasma levels of taurine compared to controls at both d7 and 14 (both $p<0.01$) and to sham mice at d7 ($p<0.001$) (Figure 10).

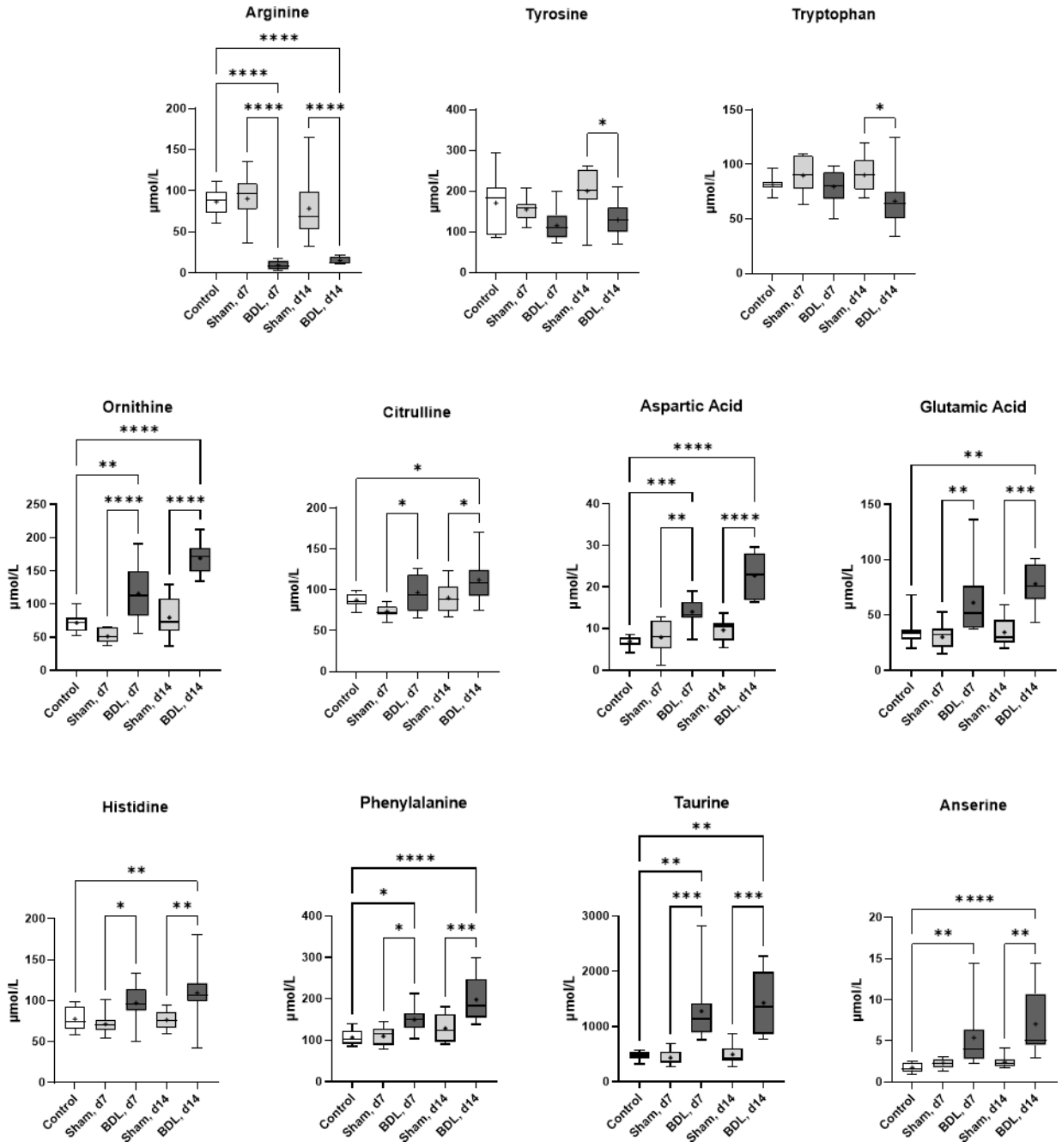


**Figure 10:** Concentrations of plasma free amino acids in mice with BDL or sham surgery and in intact controls. The mice were sacrificed on d0 (controls) and on postoperative days 7 (d7) and 14 (d14). Data are shown as box plots (min-max) with median (horizontal line) and mean (dot). BDL, d14: n=8; all other groups: n≥7; *p<0.05, **p<0.01, ***p<0.001, ****p<0.0001. One-way ANOVA with Šídák's multiple comparisons test (arginine, ornithine, citrulline, aspartic acid, phenylalanine); Kruskal-Wallis-test with Dunn's multiple comparisons test (all others). Figure from Agrifoglio et al. (2025)[224]

Plasma AAs that did not differ in concentration between mice with BDL and sham surgery are included in Table 7. The table also shows that neither the families of essential nor non-essential, branched-chain, ketogenic, or glucogenic AAs displayed differences between these experimental groups.

**Table 7. Concentrations of free amino acids in plasma that did not differ between mice with BDL or sham surgery and in intact controls**

| Amino acid [µmol/L] | Controls d0 (±SEM) (n= 9-10) | Sham d7 (±SEM) (n= 11) | BDL d7 (±SEM) (n= 8-10) | Sham d14 (±SEM) (n= 10) | BDL d14 (±SEM) (n= 7-10) |
|---|---|---|---|---|---|
| Cysteine | 110 (± 4.09) | 110 (± 5.32) | 110 (± 8.41) | 128 (± 6.22) | 112 (± 11.4) |
| Asparagine | 38.5 (± 1.18) | 40.6 (± 3.64) | 55.1 (± 4.81) | 49.0 (± 2.38) | 65.7 (± 3.51) |
| Serine | 135 (± 7.36) | 128 (± 6.19) | 149 (± 10.2) | 152 (± 5.23) | 176 (± 7.72) |
| Glutamine | 632 (± 23.7) | 618 (± 32.7) | 769 (± 50.6) | 711 (± 28.0) | 855 (± 49.1) |
| Glycine | 268 (± 10.47) | 263 (± 16.7) | 275 (± 23.0) | 298 (± 7.97) | 318 (± 21.3) |
| Threonine | 185 (± 4.19) | 166 (± 9.69) | 166 (± 10.1) | 198 (± 8.93) | 200 (± 13.5) |
| Alanine | 505 (± 19.8) | 487 (± 24.8) | 530 (± 40.1) | 594 (± 38.5) | 584 (± 38.5) |
| Anserine | 1.77 (± 0.17) | 2.31 (± 0.16) | 5.39 (± 1.31) | 2.43 (± 0.21) | 7.04 (± 1.33) |
| Tyrosine | 171 (± 20.2) | 155 (± 7.7) | 115 (± 11.4) | 200 (± 17.0) | 121 (± 12.4) |
| Valine | 231 (± 6.22) | 192 (± 6.81) | 177 (± 12.4) | 240 (± 18.0) | 195 (± 14.6) |
| Methionine | 52.4 (± 1.51) | 46.5 (± 2.99) | 51.9 (± 3.70) | 55.7 (± 2.77) | 64.2 (± 3.65) |
| Tryptophane | 81.5 (± 2.09) | 90.0 (± 5.17) | 79.7 (± 4.73) | 90.3 (± 4.93) | 59.9 (± 7.5) |
| Isoleucine | 88.2 (± 3.08) | 76.1 (± 4.12) | 67.0 (± 5.78) | 92.5 (± 8.24) | 69.5 (± 5.73) |
| Leucine | 129 (± 5.73) | 116 (± 7.64) | 117 (± 9.87) | 140 (± 13.2) | 121 (± 8.22) |
| Lysine | 225 (± 7.07) | 187 (± 7.05) | 201 (± 16.0) | 219 (± 16.6) | 237 (± 11.1) |
| Hydroxyproline | 13 (± 1.65) | 24.9 (± 3.93) | 34.4 (± 4.58) | 35.1 (± 4.21) | 39.1 (± 4.81) |
| Proline | 102 (± 10.2) | 147 (± 17.8) | 173 (± 14.7) | 203 (± 18.6) | 228 (± 32.2) |
| Essential AA | 1263 (± 28.3) | 1146 (± 52.0) | 1115 (± 62.7) | 1319 (± 78.3) | 1249 (± 81.6) |
| Non essential AA | 1999 (± 65.1) | 1987 (± 92.6) | 2251 (± 148) | 2379 (± 95.0) | 2558 (± 155) |
| BCAA | 449 (± 13.9) | 384 (± 18.0) | 361 (± 27.4) | 472 (± 38.7) | 385 (± 28.1) |
| Aromatic AA | 437 (± 26.7) | 426 (± 16.5) | 442 (± 24.8) | 496 (± 29.9) | 472 (± 61.3) |

| | | | | | |
|---|---|---|---|---|---|
| Glutamine Family | 856 (± 32.6) | 885 (± 50.8) | 1011 (± 70.0) | 1027 (± 37.2) | 1171 (± 79.7) |
| Arginine Family | 1056 (± 33.0) | 1059 (± 54.8) | 1290 (± 87.7) | 1255 (± 50.0) | 1535 (± 83.7) |
| Ketogenic AA | 355 (± 10.1) | 303 (± 13.8) | 319 (± 23.3) | 359 (± 27.8) | 359 (± 18.4) |
| Glucogenic AA | 908 (± 31.6) | 879 (± 44.5) | 955 (± 71.5) | 1044 (± 49.9) | 1078 (64.3) |

The mice were sacrificed on postoperative days 7 (d7) and 14 (d14). Mice without surgery (d0) served as controls. Data are presented as mean ± SEM. One-way ANOVA with Šídák's multiple comparisons test (normally distributed data); Kruskal-Wallis-Test with Dunn's multiple comparisons test (not-normally distributed data). Abbreviations: BDL: Bile duct ligation surgery group; Sham: Sham surgery group; BCAA: branched chains Aas. Table modified from Agrifoglio et al. (2025)[224]

## 5.3 Sarcopenia and BDL-mediated CLD

The MRI assessment showed that BDL, but not sham surgery, led to a decrease in the volume of the M. quadriceps over the two-week experimental period (Fig. 11A). In fact, the muscle volume of the BDL at d13 mice was lower than the one at d-1 and d6 ($p<0.05$). Furthermore, at d13 the BDL mice had a lower M. quadriceps volume than sham mice ($p<0.05$). Furthermore, the BDL group displayed a lower skeletal muscle-to-body weight ratio both for M. quadriceps and M. gastrocnemius (Figure 11B). Both ratios were lower than the controls and the sham mice at d14 (M. quadriceps, both $p<0.01$; M. gastrocnemius both $p<0.0001$). Noticeably, CLD was also associated with reduced muscle strength, which was already detectable on the second day post-BDL surgery (Figure 11C).

To gain further insights on muscle status, histological stainings of M. quadriceps and M. gastrocnemius were used to assess capillary-to-fiber and nuclei-to-fiber ratio. Only histological photos of M. quadriceps are shown as exemplary histology (Figure 12A). The results show a trend towards a lower capillary-to-fiber and nuclei-to-fiber ratio in the BDL groups compared to sham-operated mice and controls (Figure 12B).

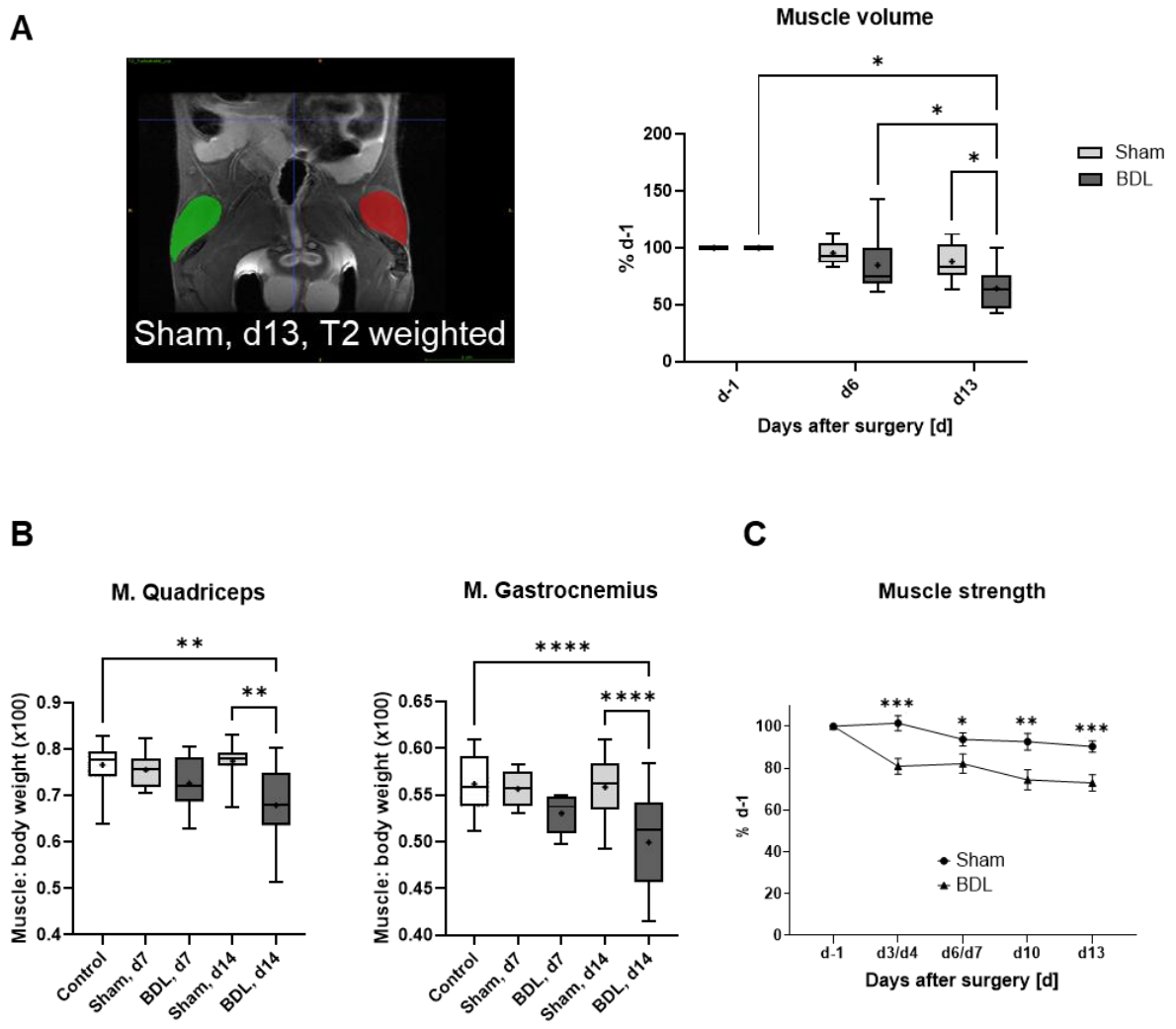


**Figure 11**: Muscle volume (A), muscle-to-body weight ratio (B) and muscle strength (C) are reduced in bile duct-ligated mice. Mice with BDL or sham surgery and untreated controls underwent repeated measurements of muscle volume by MRI (A) and muscle strength using a grip strength meter (C) at the indicated time points. On days 7 and 14 after surgery, mice were sacrificed, and the muscle-to-body weight ratio was determined for the quadriceps and gastrocnemius muscles (B). Data are shown as box plots (min-max) with median (horizontal line) and mean (dot) (sham surgery: n=11, BDL: n=6), * $p<0.05$ (two-way RM ANOVA with Tukey's multiple comparisons test). On the left is an example image of the analysis of the quadriceps muscle volume (coronal view, left (red) and right (green) muscles are marked). Data in (B) are presented as box plots (min-max) with median (horizontal line) and mean (dot); n≥6; **$p<0.01$, ****$p<0.0001$. One-way ANOVA with Šídák's multiple comparisons test (M. quadriceps); Kruskal-Wallis-test with Dunn's multiple comparisons test (M. gastrocnemius). (C) Data are shown as median ± interquartile range (Sham: n=19, BDL: n=18), ** $p<0.01$ (two-way RM ANOVA with Tukey's multiple comparisons test). For a better overview, only the significant differences between the groups are shown, but not between the time points. Figure from Agrifoglio et al., (2025)[224]

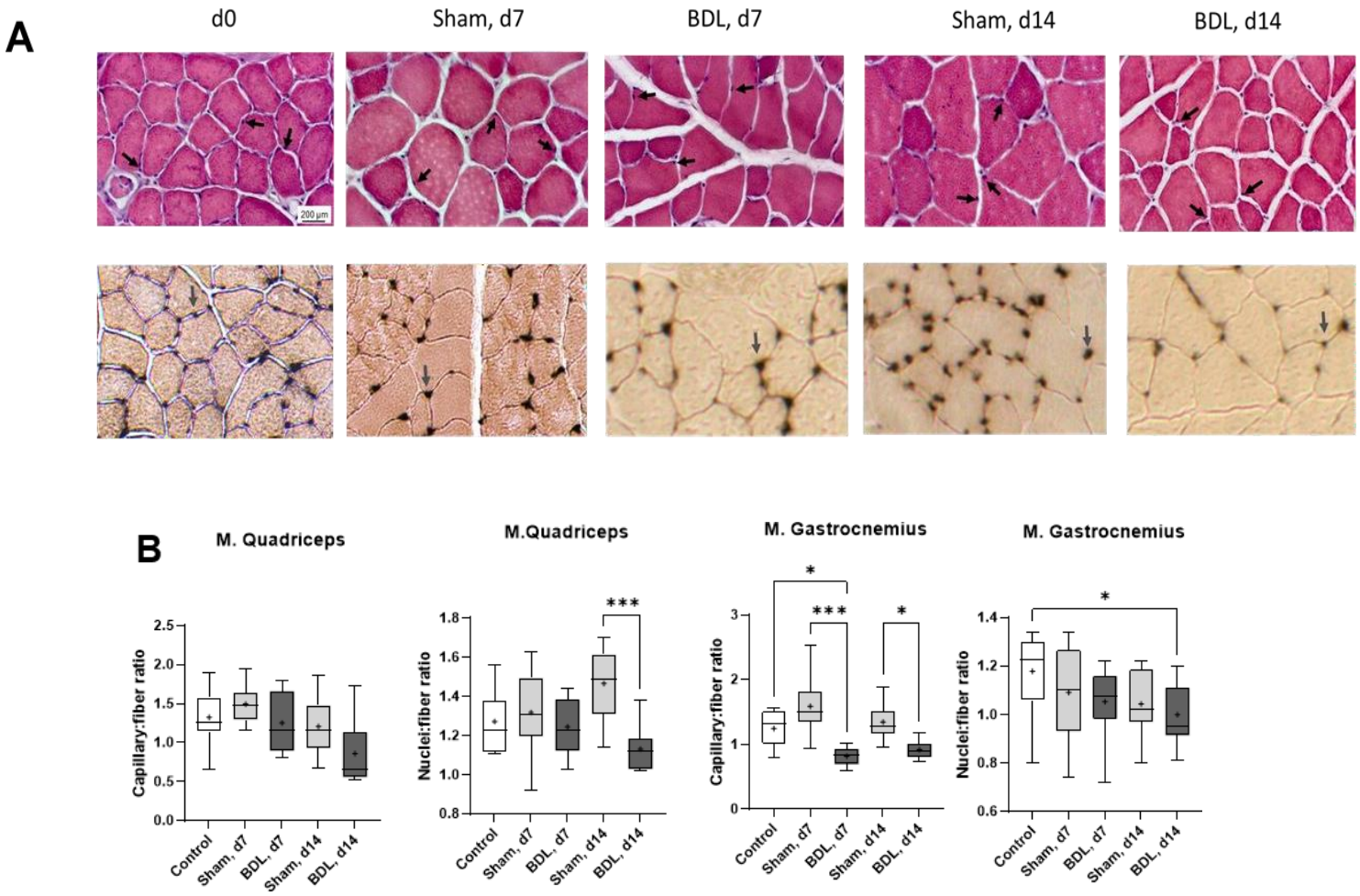


**Figure 12:** Histological findings in M. quadriceps and M. gastrocnemius of mice with BDL and Sham surgery. (A) H&E (upper row) and Ammonium sulfide (lower row) staining of muscle quadriceps tissue sections of mice with BDL and sham surgery. Mice were sacrificed on postoperative d7 d14. Mice without surgery (d0) served as controls. (A) Typical pictures for each group (BDL (n=9/10) and Sham (n=8/9) and time point (d0, d7, and d14) are shown (original magnification x100). Upper row: black arrows point to nuclei. Lower row: grey arrows point to capillaries. Data in (B) are shown as box plots (min-max) with median (horizontal line) and mean (dot); (B): n=8-10; *p<0.05, ***p<0.001. One-way ANOVA with Šídák's multiple comparisons test (Nuclei:fiber ratio M. quadriceps; Kruskal-Wallis-test with Dunn's multiple comparisons test (all others). Figure modified from Agrifoglio et al. (2025)[224]

Additionally, the concentrations of 1-MH were higher in M. quadriceps of mice with BDL than in the sham surgery ($p<0.01$ at d7; $p<0.001$ at d14) and control ($p<0.01$) groups, while levels of 3-MH did not differ between the experimental groups (Figure 13). On the other hand, the measurements of 3-MH and 1-MH in urine revealed that concentrations of 3-MH but not of 1-MH were higher after BDL surgery (Figure 13).

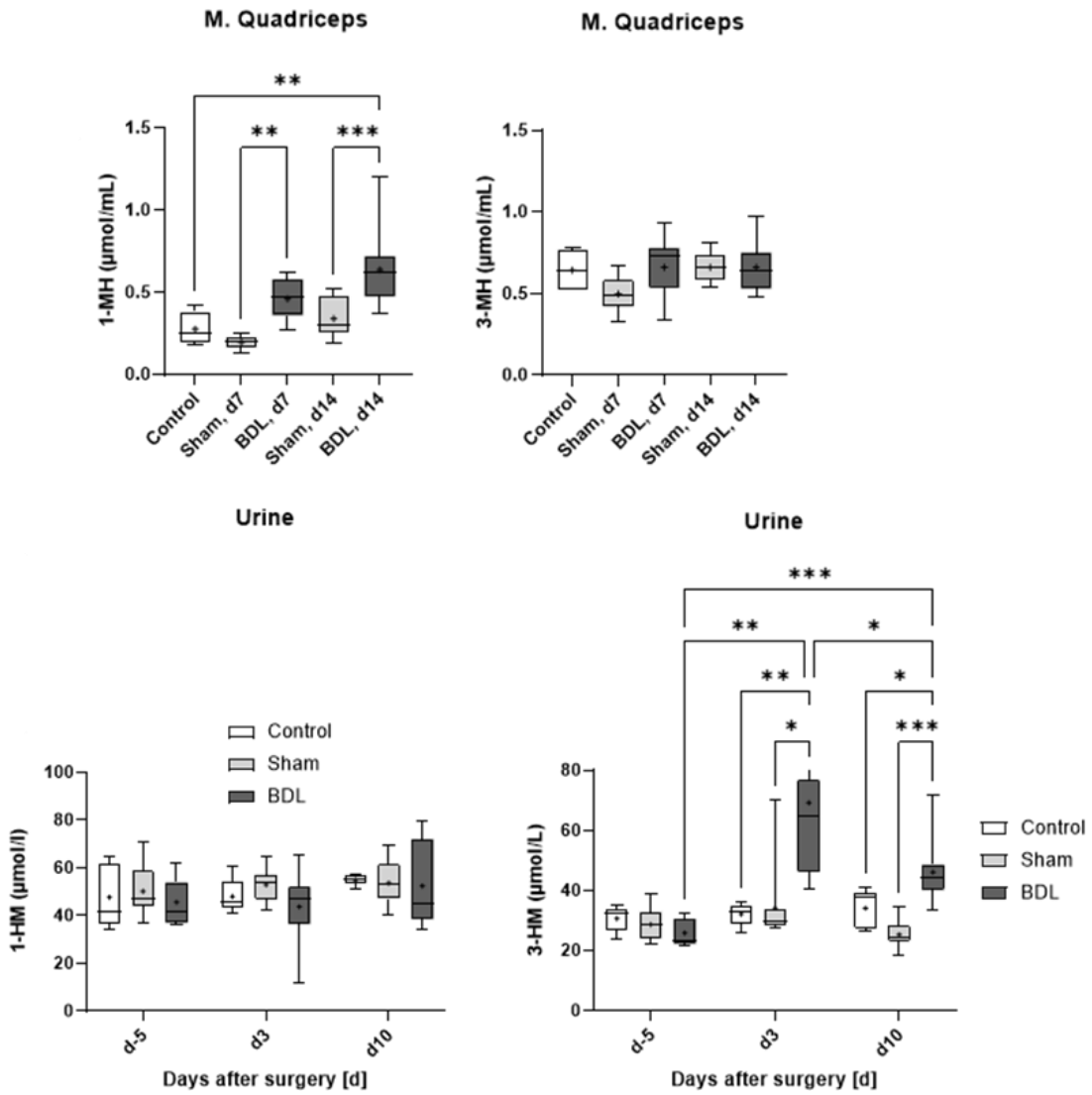


**Figure 13:** Markers of muscle catabolism in muscle lysate and urine in mice with BDL and Sham surgery. Mice were sacrificed on postoperative d7 and d14. Mice without surgery (d0) served as controls. Data are shown as box plots (min-max) with median (horizontal line) and mean (dot); Muscle lysate 1- and 3-MH controls: n=4, other groups: n=9. Urine 1- and 3-MH: controls: n=5; sham group and BDL: n=11. *p<0.05, **p<0.01, ***p<0.001, One-way ANOVA with Šídák's multiple comparisons test (1-MH and 3-MH in muscle lysates); two-way RM ANOVA with Tukey‘s multiple comparisons test (1-MH and 3-MH in urine). Figure modified from Agrifoglio et al. (2025)[224]

To gain mechanistic insights into muscle pathology, we analysed the expression of various genes involved in anabolic and catabolic processes in M. quadriceps and M. gastrocnemius (Figure 14-15). When compared to sham and control groups, the M. quadriceps of mice with BDL had or tended to have higher mRNA levels of genes associated with atrophy and protein

degradation[225] (Tripartite Motif Containing 63 (*Trim63*), Fbox protein32 (*Fbxo32*) and ubiquitin B) and the muscle growth inhibitor myostatin[226]. Specifically, in M. quadriceps (Figure 14) BDL mice had higher expression of *Trim63* than control and sham mice both at d7 and d14 ($p<0.001$). The expression of *Fbxo32* was also enhanced in BDL mice when compared to controls and sham at d7 ($p<0.01$), while BDL displayed higher *Mstn* expression than sham mice at d14 ($p<0.05$). In M. gastrocnemius (Figure 15), the expression of *Trim 63* was higher in BDL mice at d7 compared to the sham ($p<0.01$), while the expression of *Fbxo32* was higher in the BDL group at d14, compared to sham ($p<0.01$). The BDL mice had also higher *Ubb* expression than the control and sham mice both at d7 and d14 ($p<0.01$). However, different expression profiles were observed for genes involved in the action of insulin and insulin-like growth factors (Figure 14-15). While insulin receptor substrate 1 (*IRS-1*) and *IGFBP-5* were downregulated in the BDL mice compared to the other groups, the expression of IGF-1 receptor (*IGF 1R*) and *IGFBP-3* was higher in the BDL groups (d7 and d14 after surgery, respectively). In addition, upregulation of phosphatidylinositol 3-kinase r1 subunit (*Pik3r1*) and *Akt1*, genes involved in the induction of muscle growth[227], was observed in these mice. Specifically, in the M. quadriceps of BDL mice, *Irs-1* was downregulated compared to the control and sham group at d7 ($p<0.0001$ and $p<001$, respectively) and d14 ($p<0.001$ and $p<0.01$, respectively). The BDL mice also showed a lower abundance of *Igfbp-5* compared to both controls and sham mice at d7 and d14 ($p<0.05$). On the other hand, *Igf1r* was upregulated in the M. quadriceps of BDL mice compared to sham mice at d7 ($p<0.01$) and to control and sham groups at d14 ($p<0.0001$ and $p<0.001$ respectively). The BDL mice also had higher expression of *Igfbp-3* than controls and sham mice at d7 and d14 ($p<0.0001$). Expression of *Akt1* was also increased in BDL mice compared to control and sham mice at d7 ($p<0.05$) and to control mice at d14 ($p<0.0001$). The *Pik3r1* expression in the BDL group was also higher than in sham mice at d7 ($p<0.01$) and control and sham mice at d14 ($p<0.01$ and $p<0.05$, respectively). A similar gene expression pattern was found in the gastrocnemius muscle. Indeed, BDL mice had lower *Irs-1* expression in M. gastrocnemius, than controls at d 7 ($p<0.01$) and controls and sham at d14 ($p<0.001$). The abundance of *Igfbp-5* was also downregulated in BDL mice compared to controls and sham at d7 and at d14 ($p<0.0001$). However, the*Igfbp-3* expression was higher in BDL mice compared to sham, both at d7 and d14 ($p<0.01$). The BDL mice also had higher expression of Akt1 than controls and sham at d7 ($p<0.001$ and $p<0.05$, respectively) and at d14 ($p<0.0001$). Expression of *Pik3r1* was also upregulated in BDL mice compared to controls and sham both at d7 and d14 ($p<0.0001$).

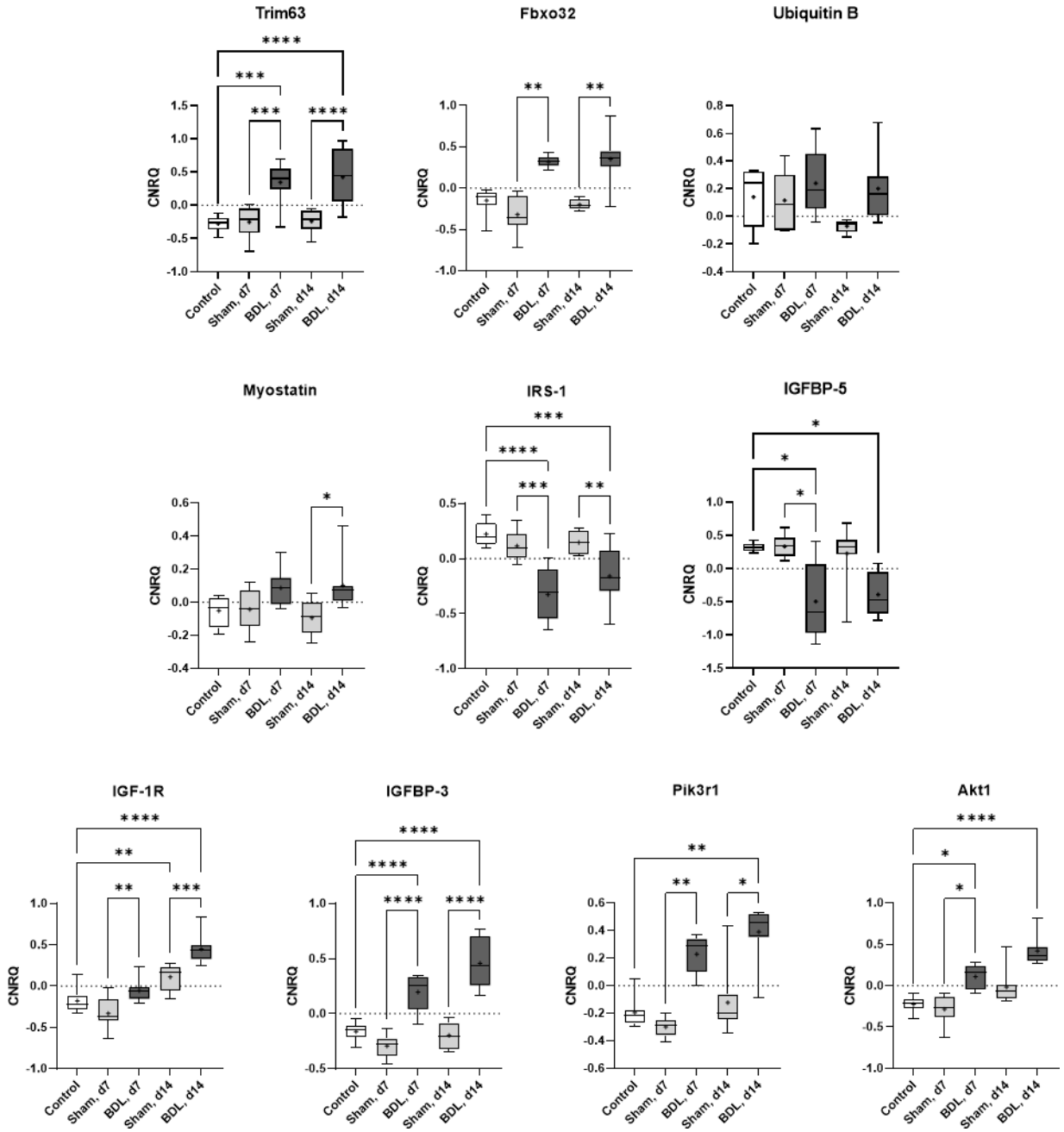


**Figure 14:** Effects of BDL on the expression of catabolic and anabolic genes in the muscle quadriceps. Mice underwent BDL or sham surgery and were sacrificed on postoperative days 7 (d7) and 14 (d14). Mice without surgery served as controls. Gene expression in the quadriceps muscle was quantified by real-time PCR as described in the Methods section. Relative gene expression levels are expressed as CNRQ (calibrated normalized relative quantity) values. Data are shown as box plots (min-max) with median (horizontal line) and mean (dot). n=8 mice per group; *p<0.05, **p<0.01, ***p<0.001, ****p<0.0001. One-way ANOVA with Šídák's multiple comparisons test (Trim63, IRS-1, IGF-1R, and IGFBP-3); Kruskal-Wallis-Test with Dunn's multiple comparisons test (all other genes). Figure from Agrifoglio et al. (2025)[224]

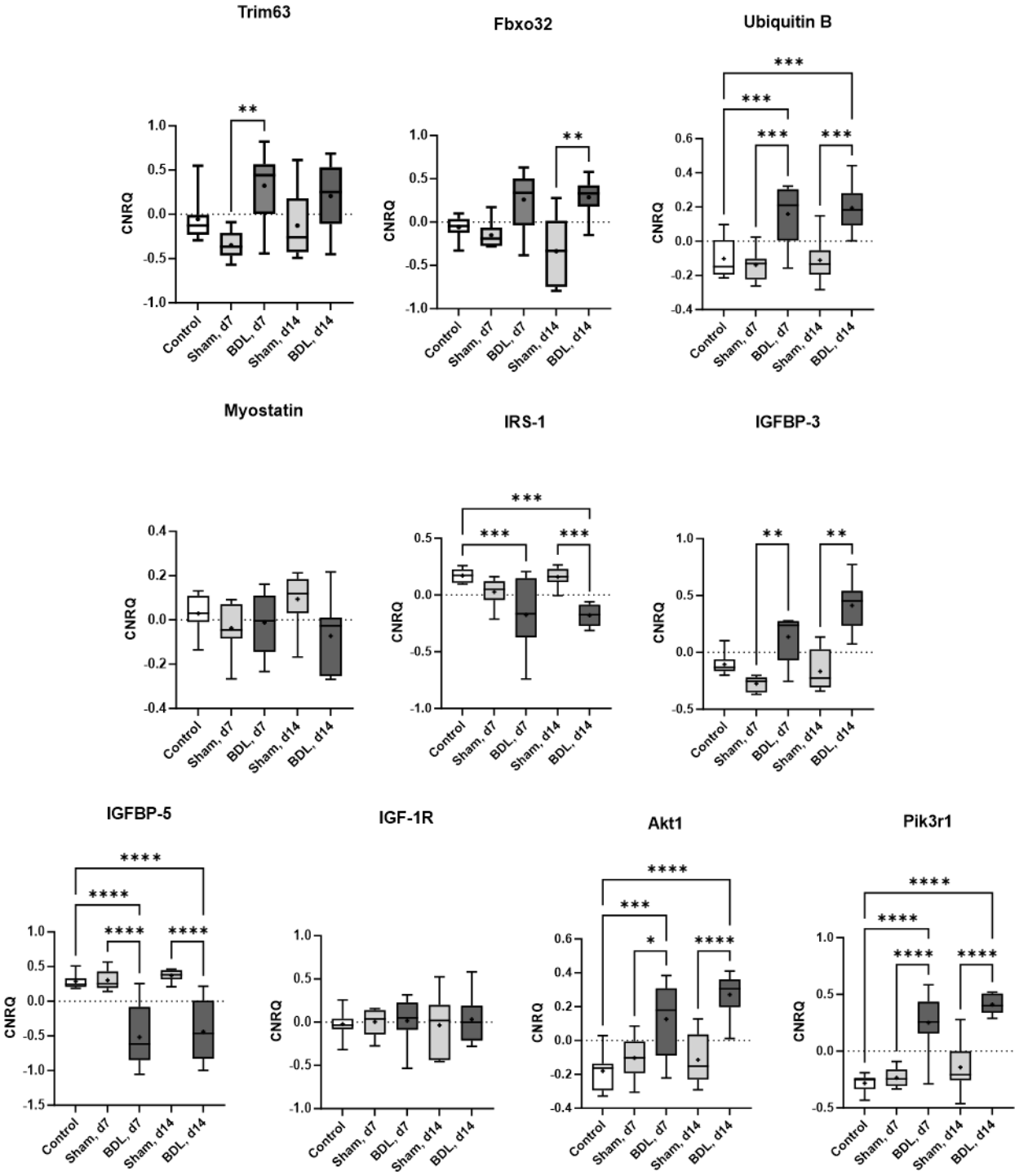


**Figure 15:** Effects of BDL on the expression of catabolic and anabolic genes in the muscle gastrocnemius. Mice underwent BDL or sham surgery and were sacrificed on postoperative days 7 (d7) and 14 (d14). Mice without surgery served as controls. Gene expression in the quadriceps muscle was quantified by real-time PCR. Relative gene expression levels are expressed as CNRQ (calibrated normalized relative quantity) values. Data are shown as box plots (min-max) with median (horizontal line) and mean (dot). n=8 mice per group; *p<0.05, **p<0.01, ***p<0.001, ****p<0.0001. One-way ANOVA with Šídák's multiple comparisons test (Ubiquitin B, Myostatin, IRS-1, IGFBP-5 and Akt1); Kruskal-Wallis-Test with Dunn's multiple comparisons test (all other genes). Figure from Agrifoglio et al. (2025)[224]

## 5.4 Mediators of inflammation, catabolic, and anabolic processes in blood plasma

In mice with BDL higher plasma concentrations of inflammation markers were observed than in intact controls and sham operated mice (Figure 16). Plasma protein concentrations of TNFRI in BDL mice were higher than in controls and sham both at d7 ($p<0.0001$) and d14 ($p<0.001$ and $p<0.0001$, respectively). The levels of TNFRII were also higher in BDL mice than in controls at d7 ($p<0.01$) and in both control and sham mice on d14 ($p<0.01$). Plasma concentrations of IL6-Rα were also raised in BDL mice compared to control and sham mice at d7 ($p<0.05$ and $p<0.01$, respectively) and to sham mice at d14 ($p<0.001$). These results are consistent with a systemic proinflammatory state associated with CLD. Furthermore, the BDL mice also showed higher levels of VEGF (which is involved in vascular growth, but also in liver fibrosis[228]) when compared to both controls and sham at d7 ($p<0.01$ and $p<0.05$, respectively) and at d14 ($p<0.05$). Also, the concentration of the mediator of liver regeneration HGF29 was increased in the plasma of BDL mice when compared to the sham at both d7 and d14 ($p<0.05$). Strikingly, the levels of anabolic hormone IGF-1 and its binding protein IGFBP-1 were also elevated in BDL mice. In fact, BDL mice displayed higher concentrations of IGF-1 than sham mice at d7 ($p<0.05$) as well as higher concentrations of IGFBP-1 than their control and sham counterparts at d7 and d14 ($p<0.001$ and $p<0.05$, respectively for both time points). Interestingly, the BDL mice showed lower myostatin concentration than controls and sham mice both at d7 and d14 ($p<0.001$ and $p<0.05$, respectively for both time points) (Figure 16)). No differences were found for the concentrations of the hepatokines FGF-21, IGFBP-3, EGF-1, and EGFR1 between mice with BDL and sham surgery

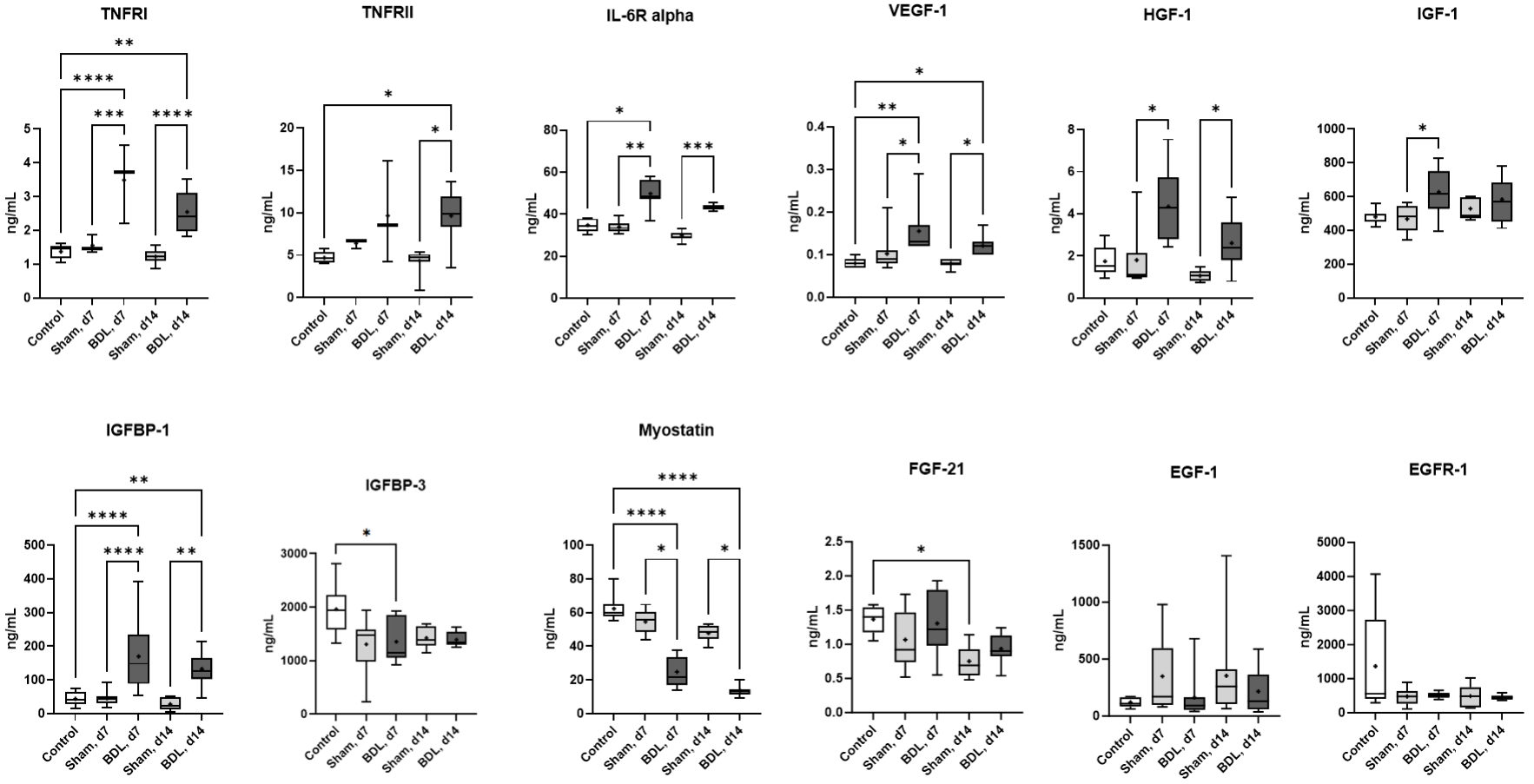


**Figure 16:** Plasma protein concentrations of mediators of inflammation, catabolic, and anabolic processes. Mice with BDL or sham surgery were sacrificed on postoperative days 7 (d7) and 14 (d14). Mice without surgery served as controls. Data are shown as box plots (min-max) with median (horizontal line) and mean (dot). n≥7 mice per group; *p<0.05, **p<0.01, ***p<0.001, ****p<0.0001. One-way ANOVA with Šídák's multiple comparisons test (TNFR1); Kruskal-Wallis-Test with Dunn's multiple comparisons test (all other protein. Figure modified from Agrifoglio et al. (2025)[224]

# 6 DISCUSSION

This study aimed to gain a comprehensive insight into the molecular mechanisms linking malnutrition and sarcopenia in chronic liver disease and specifically to study the development of sarcopenia from the early stages of BDL-induced CLD, hypothesizing that it occurs already in the initial phases of the disease. To serve this purpose, a 14-days experimental murine C57BL/6J BDL model was used. This model allowed the investigation of the development of sarcopenia from the initial course of cholestatic liver damage. It also enabled the identification of alterations in AA patterns, concentrations of molecular markers for inflammation and muscle damage, plasma metabolites associated with liver damage and malnutrition, and molecular pathways in skeletal muscle. The data acquired in this work may serve as a starting point to set up future mechanistic and interventional studies, particularly needed in clinical settings. In fact, patients suffering from end-stage liver disease are often additionally affected by disease-related malnutrition and sarcopenia, which worsen the prognosis and the course of the disease. In this regard, it has been estimated that in German hospitals 1 out of 4 patients suffers from malnutrition, and that this condition is usually associated with longer hospital stays, malignant diseases, and several comorbidities and thus with a high burden[170]. In the case of cirrhotic patients, malnutrition is defined as a protein-caloric subtype and its etiology ranges from a negative nitrogen balance to several gastrointestinal conditions, including fat malabsorption in the case of CLD[184–187]. The prevalence of malnutrition in patients with liver diseases varies from 20% to 90% according to the methods and criteria used for its diagnosis[189].On the other hand, sarcopenia has been estimated to be a comorbidity affecting around 32% of patients with gastrointestinal conditions[173, 178]. The main cause of sarcopenia is an imbalance between protein synthesis and protein breakdown, a condition that is enhanced in LC patients, due to a pro-inflammatory state and accelerated catabolism[182, 183]. Although the prognostic significance of malnutrition and sarcopenia in liver diseases is clear, the diagnosis is difficult. This is due to a lack of validated biomarkers, preventing an early diagnosis. Furthermore, the pathophysiological mechanisms have not yet been fully clarified[229]. Given these premises, this preclinical animal study allowed the investigation and monitoring of malnutrition and sarcopenia over the course of the disease and especially from the very early starting point of liver damage.

## 6.1 Cholestasis and markers of liver damage in a BDL mouse model

This study shows that BDL surgery led to a severe cholestatic liver injury, including necrosis, inflammation, and fibrosis, as shown by the histological findings. While the liver of the control and sham mice did not display any histological alteration, the BDL group showed necrosis and initial fibrosis both at d7 and d14 after surgery, similar to what has been previously shown[124]. In fact, in the case of cholestasis, there is an impaired bile formation or excretion, which causes the accumulation of biliary constituents beyond the limits of the normal cellular architecture of the liver, as the accumulation of BA leads to hepatocyte swelling, and triggers inflammation. This leads to cellular damage and alteration of the hepatic parenchyma[230]. In addition, the BDL mice exhibited several hallmarks of liver damage, such as increased ALAT, AP, and ASAT plasma concentrations as well as higher levels of bilirubin and cholesterol. Increased plasma levels of ALAT, ASAT, and bilirubin were reported before in BDL mice[231], while high plasma AP concentrations are indicators of cholestasis[232]. Furthermore, the BDL mice displayed lower plasma concentrations of TG. This is likely a consequence of cholestasis, as it could be the result of an absorption disorder due to a lack of bile acids in the intestine and reduced micelle formation[233]. BDL mice also feature hypercholesterolemia, which is also associated with cholestatic disorders[234]. Cholesterol plays a major role in cell membrane integrity and function[235] and it is mainly synthetized and stored in the liver, which is responsible of its conversion into bile salts or its excretion via bile[236]. However, in case of biliary obstruction bile acids' intrahepatic concentration increases drastically. The hepatocytes exposed to high concentrations of bile acids go through inflammatory processes and eventually cell death and disruption, with the release of cellular components, including cholesterol[237]. Moreover, it has been shown that the bile acid TCA, whose concentration was elevated in BDL mice plasma, can activate HSCs and thus further contribute to LC progression[238]. However, CLD did not cause general organ failure during the experimental period, as shown by the increased IGF-1 and HGF-1 plasma concentrations in the BDL mice. It has been reported that interlobular cholangiocytes overexpress IGF-1 in response to primary biliary cirrhosis, which was interpreted as an attempt to prevent apoptosis and counteract liver damage[209]. In this regard, the BDL mice also expressed higher concentrations of the bile acid TCDA, which in experimental settings has proved to ameliorate CLD. In fact, administration of TCDA after BDL has improved bile flow, and reduced fibrosis and gene expression of pro-apoptotic markers[239, 240]. Furthermore, the BDL mice exhibited higher concentrations of HGF-1, which is secreted from

peripheral organs such as kidneys and lungs, as well as from Kupffer cells in response to hepatic injury to trigger liver regeneration[241, 242]. Altogether this data suggests that BDL induced progressive liver damage, which however did not result in liver failure over the 14d experimental period.

## 6.2 Malnutrition and metabolic changes as a result of cholestatic liver disease

This murine model of CLD induced via BDL was associated with decreased feed and water intake, as well as with a reduced BW in the BDL mice compared to the Sham group. In principle, lower feed intake and BW could be due to surgical stress. However, the stable BW, feed, and water intake in the Sham group over the time course of the experiments show that these decreases in the BDL group are not related to the surgery itself. Our findings are in line with other studies[128, 231], which also found an association between BDL surgery weight loss and reduced feed intake. In general, reduced dietary intake is crucial in the pathogenesis of malnutrition in liver disease patients. However, there are several mechanisms contributing to malnutrition in liver diseases such as malabsorption, poor dietary intake, increased intestinal protein loss, low protein synthesis, and alterations in substrate utilization. Fat malabsorption is often present in CLD, mostly due to insufficient bile release[187]. As far as inadequate food intake is concerned, it has been shown that there are several factors influencing the appetite and consequent food intake in liver disease. In fact, gastroparesis, ascites, and gut dysmotility are known causes of reduced food intake in liver conditions, which can even be worsened in case of hospitalization and starvation due to endoscopies[243, 244]. Another cause of appetite loss can be attributed to the dysregulation of hunger hormones. Furthermore, the BDL mice displayed a decreased N-BAL, mostly due to a decreased food intake, and TEE, when compared to the Sham operated ones. The TEE is the sum of resting energy expenditure, diet, and activity-induced energy expenditure[168]. The lower TEE can be explained by the lower energy needed to metabolize the smaller amount of ingested food and as a result of the lower energy needed to maintain and move a lighter body[168]. However, the BDL mice showed a TEE reduction of around 20%, which is coherent with the approximately 20% body weight loss on d3 and d10, but not with the 50% decrease in feed intake. Given that resting energy expenditure is the parameter that mostly affects TEE and that muscle energy expenditure is the primary contributor to resting energy expenditure[245], it is plausible that the weight loss of BDL mice is primarily a loss of metabolically active tissue, such as skeletal muscle. Furthermore, while feed and therefore protein intake was reduced by approximately 50% of the intake prior to BDL

surgery, N-BAL was reduced by 87% at d10 when compared to the N-BAL observed in healthy mice before surgery. The lower N-BAL is likely related to a disproportionately greater N loss due to the enhanced protein catabolism associated with inflammation in liver disease[246], as suggested by the increased plasma levels of the pro-inflammatory markers IL-6Rα, TNFRI, and TNFRII in BDL mice. The reduced feed/protein intake and the pro-inflammatory state of the BDL mice are also likely to be major contributors to the reduced rates of protein synthesis in the liver and skeletal muscle, potentially exacerbating the lower N-BAL. These data point to a catabolic state in BDL mice. To gain deeper insights into protein metabolism, analyses of plasma levels of AA were performed. Interestingly, plasma levels of most AA remained constant after BDL. However, BDL mice showed altered concentrations of all the AA related to the urea cycle. Specifically, arginine concentration was lower in BDL mice both at d7 and d14, while ornithine and citrulline concentrations were increased. It has been reported that rats undergoing BDL surgery exhibit low arginine concentrations, due to high circulating levels of arginase[247], which would also explain the increased ornithine levels after surgery. Another possibility is that the low plasma arginine concentration could be due to an enhanced oxidation by Nitric oxide synthase (NOS). NOS oxidizes arginine to produce nitric oxide which is an important signaling molecule with potentially both hepatoprotective and hepatotoxic actions[248–250]. Furthermore, citrulline is a byproduct of NOS reactions which could explain the higher plasma levels of citrulline in BDL mice. However, synthesis of citrulline from ornithine cannot be excluded either, as cannot be excluded a leakage of these two AA from the damaged hepatocytes. The BDL mice also displayed strikingly increased plasma taurine concentrations. This could be caused by an underutilization for bile acids conjugation and a leakage from damaged hepatocytes[251]. The BDL mice also showed an increase in plasma levels of anserine, 1-MH, and histidine, which likely also derived from muscle leakage upon damage. Despite these altered AA patterns, the BDL mice didn't show any alteration in the plasma levels of aromatic and branched-chain amino acids, in contrast to what commonly happens in case of decompensated LC[252]. The BDL mice also showed no difference in the concentrations of essential, non-essential, ketogenic, and glucogenic AA, when compared to controls and sham.

### 6.3 Cholestatic liver disease impairs muscle physiology and leads to sarcopenia

Mice undergoing BDL surgery displayed decreased muscle strength, and muscle volume compared to sham-operated mice, and a lower muscle-to-body weight ratio than sham and controls. These results are in line with other studies, as decreased muscle strength and volume

after BDL surgery have been reported[128, 253]. Moreover, the BDL mice showed reduced FPSR in both M. quadriceps and M. gastrocnemius when compared to both sham and control groups. It is known that one of the main mechanisms of sarcopenia is an imbalance between muscle protein synthesis and muscle protein breakdown[254], thus this data altogether points to a sarcopenic state of the BDL mice. To gain deeper insights into the muscle status of the mice, we assessed the capillary:fiber ratio and the nuclei:fiber ratio in both M. quadriceps and M. gastrocnemius, using ammonium sulfide and H/E staining, respectively. Mice undergoing BDL surgery showed decreased capillary:fiber ratio and nuclei:fiber ratio. Both conditions further highlight a sarcopenic state after BDL. In fact, capillaries play an essential role in supporting metabolic and energetic requirements and maintaining skeletal muscle homeostasis[255], and it has been shown that capillary rarefaction may contribute to a diminished muscle mass and impaired physical function by limiting transcapillary transport of essential AA, nutrients, hormones, and oxygen[256]. On the other hand, the number and spatial distribution of the nuclei in the muscle are essential for muscle size and for securing the cytosolic transport and distribution of proteins within the myonuclear domain[257–259], thus nuclei loss, especially via apoptosis, is a major contributing factor to sarcopenia[260]. In addition, urinary and plasma samples were analysed to find markers of sarcopenia. The BDL mice showed higher urinary 3-MH concentrations than the sham and control groups. In fact, 3-MH is a marker for myofibrillar protein breakdown, coming from actine and myosin degradation[261–264]. The analyses of plasma samples reported in this study showed that BDL mice displayed strikingly high concentrations of taurine and, on the opposite, concerning low circulating levels of arginine. These results point to sarcopenia. Another reason for the increased taurine levels in the circulation of BDL mice could be due to injured muscle tissue, as it is the most abundant free AA in skeletal muscle and it is also essential for muscle contraction[265]. As for the lower circulating levels of arginine, it is important to remember that arginine plays a crucial role in muscle homeostasis. In fact, it not only is an amidine donor for guanidoacetic acid, necessary for creatine synthesis[266], but it also serves as a substrate for nitric oxide synthase to produce nitric oxide, a regulator of several skeletal muscle functions including excitation-contraction coupling, regulation of blood flow, myocyte differentiation, respiration, and glucose homeostasis[267]. Moreover, to investigate the mechanisms leading to sarcopenia, we analysed the mRNA levels in M. quadriceps and M. gastrocnemius. BDL mice overexpress genes associated with muscle atrophy such as *Mstn, Trim-63,* and *Fboxo-32*. Mstn encodes myostatin, a myokine of the TGF-β family that negatively regulates skeletal muscle cell proliferation and differentiation. When myostatin binds to its receptor, it activates pathways that lead to activation of genes negatively associated

with muscle growth such as *Fboxo-32* and *Trim63*[268]. *Fboxo-32* encodes for F-box protein 32, which initiates and maintains proteolysis in skeletal muscle[268], while *Trim63* encodes an E3 ubiquitin ligase which plays a major role in the atrophy of skeletal muscle and is essential for the degradation of myosin heavy chain proteins, myosin light chain, myosin binding protein, and for muscle-type creatine kinase[269]. Interestingly, despite the overexpression of myostatin in skeletal muscle, the circulating levels of the myokine are lower in the BDL mice. This might be consistent with processes of counter-regulation and regeneration after the initial liver injury and the resulting muscle wasting. However, it was also shown that there is a progressive decrease in myostatin levels as cirrhosis progresses[270]. The BDL mice also showed increased expression of genes related to cell growth and proliferation pathways, such as *Pik3r1* and *Akt-1*[271]. This may be compatible with an attempt at counteracting the muscle damage with ongoing, although insufficient, repair processes. Taken together, the gene expression profiles suggest that degenerative processes occur in the skeletal muscles of mice with BDL-induced CLD, which in turn may induce compensatory counter-regulation.

## 6.4 Relationship between inflammation, malnutrition and sarcopenia in cholestatic liver disease

CLD causes inflammation due to the retention of bile caused by cholestasis[26]. The BDL mice showed increased plasma circulation of pro-inflammatory markers such as IL-6Rα, TNFRI, TNFRII and VEGF, meaning that systemic inflammation associated to CLD is present in this model. During cholestasis, cell death is mediated by bile acid-associated death receptors, among which TNFR is highly expressed in the hepatocytes[272]. On the other hand, TNFRII has no death domain[273], but it can collaborate with TNFR in inducing cell death[274, 275]. The high plasma concentrations of IL6R-α in BDL mice indicate inflammation associated to liver damage, as IL6 binds to IL6R-α in the event of liver injury and triggers the acute phase response[276, 277]. Furthermore, IL6R-α was higher in the plasma of BDL mice 7 days after surgery than 14 days after surgery, suggesting that inflammation occurs already in the early stages of the disease. If the liver injury persists, the acute phase response turns into chronic inflammation with massive production of cytokines, which trigger VEGF production by hepatic stellate cells[278]. The BDL mice also displayed increased concentrations of VEGF, which not only stimulates angiogenesis and fibrogenesis but is also positively associated with liver disease severity[228, 279, 280]. The formation of new vessels, which modify the normal liver vascularization, is a process closely related to the progression of fibrosis[278]. This pro-inflammatory status found in the BDL mice

has an effect on both the nutritional status and the muscle metabolism of the BDL mice. In fact, inflammation is known to be one of the pivotal causes of inadequate food intake, as systemic inflammation not only causes an increase of cytokine production but exerts pro-anorectic effects[281]. Pro-inflammatory factors have also been shown to have an effect on the neural system and to be able to alter appetite by involving peripheral sensory neurons as well as neurotransmitters[282]. Inflammation also triggers several brain-induced responses such as fever, anorexia, and taste alterations[283]. Moreover, inflammation is associated with enhanced protein catabolism in liver disease[246], making it a factor that plays a major role in the decreased protein synthesis in both liver and skeletal muscle. This causes an alteration in the nitrogen metabolism, reflected in the diminished N-BAL in the BDL mice. Furthermore, TNF is one of the major contributors to the activation of the ubiquitin-proteasome system, which is responsible for muscle breakdown[284]. Thus, taken altogether, the data suggests that inflammation is an early event caused by BDL surgery and that it plays a crucial role in both CLD-associated malnutrition and sarcopenia.

### 6.5 Conclusions

In summary, this study has shown that a BDL mouse model is associated with cholestatic liver damage over a 14-day observation period (Figure 17), as evidenced by histological hepatic changes and increased enzymatic activities of ALAT, ASAT, and AP, as well as higher blood bilirubin and cholesterol levels. However, the cholestasis did not lead to a generalized organ failure during the experimental period, as shown by the increased IGF-1 and HGF-1 plasma concentrations in the BDL mice, which probably represent a mechanism to counteract the CLD. The BDL mice group developed malnutrition (reflected in the lower BW, N-BAL, and TEE), alteration of the protein and energy metabolism, and inflammation associated with liver injury, as shown by the increased plasma concentrations of inflammatory markers such as IL6R-α, TNFRI, TNFRII, and VEGF. In this model, the inflammation is likely to play a role in the exacerbation of malnutrition, in the N loss, and in enhanced protein catabolism, which is most likely taking place in muscle tissue (Figure 17). In fact, our model shows that BDL is associated with sarcopenia. The sarcopenic state is due to an imbalance between protein synthesis and protein catabolism, which in this mouse model is reflected in the high urinary concentrations of 3-MH, and the lower FPSR in muscle tissue in the BDL mice. The BDL mice also showed several other hallmarks of muscle wasting, such as decreased grip strength, lower muscle volume, capillary:fiber ratio and nuclei:fiber ratio, as well as the overexpression of genes

associated with muscle atrophy and catabolism in M. quadriceps and M. gastrocnemius. The simultaneous overexpression of genes associated with sarcopenia, muscle growth, and cell proliferation indicates a further attempt of the tissue to limit the damage with ongoing repair processes, similar to what happens in the liver. The high concentrations of circulating conjugated bile acids further exacerbate the condition, as they not only trigger further inflammations but also induce muscle atrophy. In addition, the altered circulating concentrations of amino acids such as arginine and taurine show how liver damage, malnutrition, inflammation, and muscle damage are processes tightly intertwined. In fact, the early development of sarcopenia after BDL (which takes place in the initial phases of the CLD, right after liver damage and not only after a latency period in which malnutrition first develops) is a multicausal process featuring reduced protein synthesis, increased muscle protein breakdown, low arginine levels (possibly related to nitrosative stress), a systemic pro-inflammatory and catabolic state.

Altogether, the comprehensive data collected in this study lay the foundations to further set up mechanistic and interventional studies focused on the deeper molecular mechanisms regulating the liver-muscle axis and taking into account the metabolic alterations described in this work.

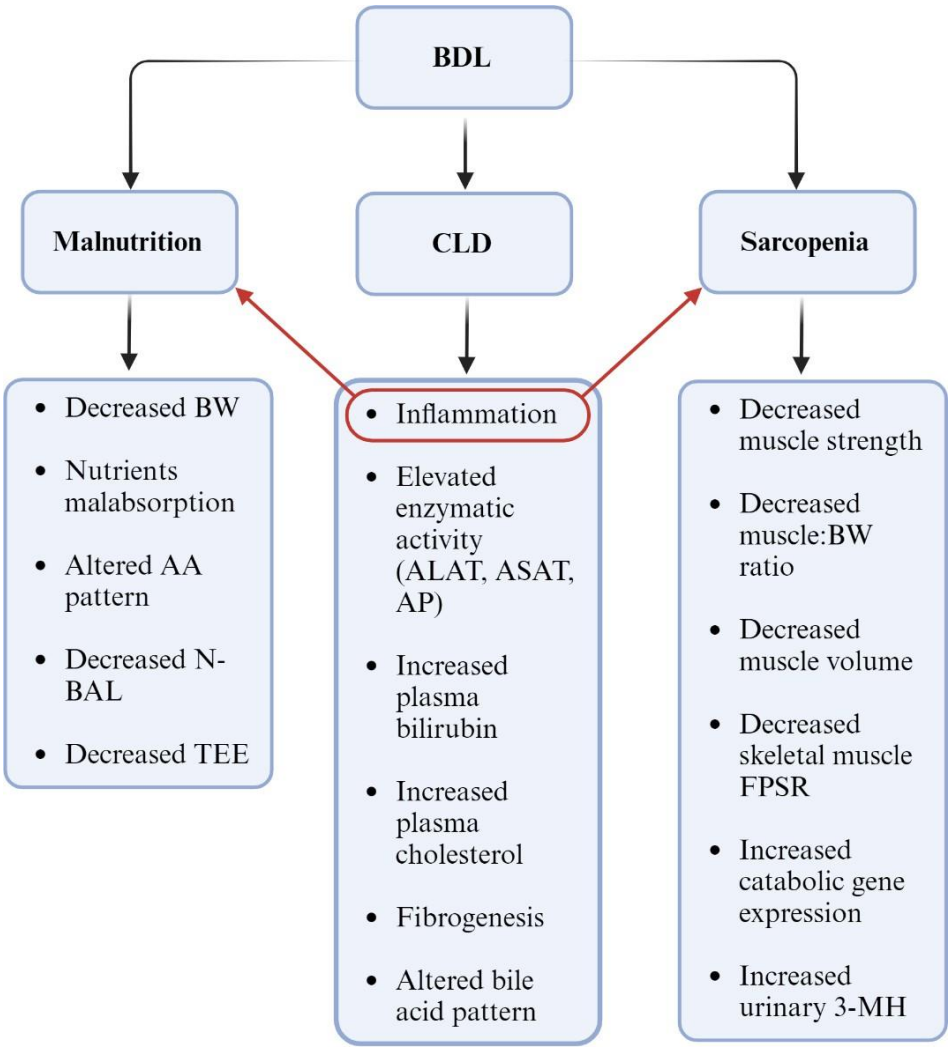


**Figure 17**. Main findings of the study. This 14-days murine model of CLD induced via BDL surgery is associated with cholestatic liver damage, malnutrition, and sarcopenia. In this model, the inflammation is likely to play a role in the exacerbation of malnutrition, in the N loss, and in enhanced protein catabolism, which is most likely taking place in muscle tissue. Abbreviations: BDL: bile duct ligation; CLD: cholestatic liver disease; BW: body weight; AA: amino acids, N-BAL: nitrogen balance; TEE: total energz expenditure; ALAT: alanine aminotransferase; ASAT: aspartate aminotransferase; FPSR: fractional protein synthesis rate; 3-MH: 3-methyl histidine

# 7 REFERENCES


1. Malandro, M. S., and Kilberg, M. S., "Molecular biology of mammalian amino acid transporters," *Annual review of biochemistry*, V. 65, 1996, pp. 305–336.
2. Liu, X., Wang, H., Liang, X., and Roberts, M. S., "Hepatic Metabolism in Liver Health and Disease," *Liver Pathophysiology*, Elsevier, 2017, pp. 391–400.
3. Barmore, W., Azad, F., and Stone, W. L., "StatPearls: Physiology, Urea Cycle," Treasure Island (FL), 2024.
4. Busetto, L., "Visceral obesity and the metabolic syndrome: effects of weight loss," *Nutrition, metabolism, and cardiovascular diseases : NMCD*, V. 11, No. 3, 2001, pp. 195–204.
5. Browning, J. D., and Horton, J. D., "Molecular mediators of hepatic steatosis and liver injury," *The Journal of clinical investigation*, V. 114, No. 2, 2004, pp. 147–152.
6. Pyper, S. R., Viswakarma, N., Yu, S., and Reddy, J. K., "PPARalpha: energy combustion, hypolipidemia, inflammation and cancer," *Nuclear receptor signaling*, V. 8, 2010, e002.
7. Dentin, R., Girard, J., and Postic, C., "Carbohydrate responsive element binding protein (ChREBP) and sterol regulatory element binding protein-1c (SREBP-1c): two key regulators of glucose metabolism and lipid synthesis in liver," *Biochimie*, V. 87, No. 1, 2005, pp. 81–86.
8. Mithieux, G., "Brain, liver, intestine: a triumvirate to coordinate insulin sensitivity of endogenous glucose production," *Diabetes & metabolism*, 36 Suppl 3, 2010, S50-3.
9. Daly, M. E., Vale, C., Walker, M., Littlefield, A., Alberti, K. G., and Mathers, J. C., "Acute effects on insulin sensitivity and diurnal metabolic profiles of a high-sucrose compared with a high-starch diet," *The American journal of clinical nutrition*, V. 67, No. 6, 1998, pp. 1186–1196.
10. Chiang, J. Y. L., and Ferrell, J. M., "Bile Acid Metabolism in Liver Pathobiology," *Gene expression*, V. 18, No. 2, 2018, pp. 71–87.
11. Ridlon, J. M., Kang, D.-J., and Hylemon, P. B., "Bile salt biotransformations by human intestinal bacteria," *Journal of lipid research*, V. 47, No. 2, 2006, pp. 241–259.
12. Rehm, J., Mathers, C., Popova, S., Thavorncharoensap, M., Teerawattananon, Y., and Patra, J., "Global burden of disease and injury and economic cost attributable to alcohol use and alcohol-use disorders," *Lancet (London, England)*, V. 373, No. 9682, 2009, pp. 2223–2233.
13. Mokdad, A. A., Lopez, A. D., Shahraz, S., Lozano, R., Mokdad, A. H., Stanaway, J., Murray, C. J. L., and Naghavi, M., "Liver cirrhosis mortality in 187 countries between 1980 and 2010: a systematic analysis," *BMC Medicine*, V. 12, 2014.
14. Teli, M. R., Day, C. P., Burt, A. D., Bennett, M. K., and James, O. F., "Determinants of progression to cirrhosis or fibrosis in pure alcoholic fatty liver," *Lancet (London, England)*, V. 346, No. 8981, 1995, pp. 987–990.
15. Hernández-Évole, H., Jiménez-Esquivel, N., Pose, E., and Bataller, R., "Alcohol-associated liver disease: Epidemiology and management," *Annals of hepatology*, V. 29, No. 1, 2024, p. 101162.
16. Gao, B., and Bataller, R., "Alcoholic liver disease: pathogenesis and new therapeutic targets," *Gastroenterology*, V. 141, No. 5, 2011, pp. 1572–1585.

17. Pose, E., Pera, G., Torán, P., Gratacós-Ginès, J., Avitabile, E., Expósito, C., Díaz, A., Graupera, I., Rubio, A. B., Ginès, P., Fabrellas, N., and Caballeria, L., "Interaction between metabolic syndrome and alcohol consumption, risk factors of liver fibrosis: A population-based study," *Liver international : official journal of the International Association for the Study of the Liver*, V. 41, No. 7, 2021, pp. 1556–1564.
18. Boyle, M., Masson, S., and Anstee, Q. M., "The bidirectional impacts of alcohol consumption and the metabolic syndrome: Cofactors for progressive fatty liver disease," *Journal of hepatology*, V. 68, No. 2, 2018, pp. 251–267.
19. Eslam, M., Sanyal, A. J., and George, J., "MAFLD: A Consensus-Driven Proposed Nomenclature for Metabolic Associated Fatty Liver Disease," *Gastroenterology*, V. 158, No. 7, 2020, 1999-2014.e1.
20. Eslam, M., Newsome, P. N., Sarin, S. K., Anstee, Q. M., Targher, G., Romero-Gomez, M., Zelber-Sagi, S., Wai-Sun Wong, V., Dufour, J.-F., Schattenberg, J. M., Kawaguchi, T., Arrese, M., Valenti, L., Shiha, G., Tiribelli, C., Yki-Järvinen, H., Fan, J.-G., Grønbæk, H., Yilmaz, Y., Cortez-Pinto, H., Oliveira, C. P., Bedossa, P., Adams, L. A., Zheng, M.-H., Fouad, Y., Chan, W.-K., Mendez-Sanchez, N., Ahn, S. H., Castera, L., Bugianesi, E., Ratziu, V., and George, J., "A new definition for metabolic dysfunction-associated fatty liver disease: An international expert consensus statement," *Journal of hepatology*, V. 73, No. 1, 2020, pp. 202–209.
21. Chan, W.-K., Chuah, K.-H., Rajaram, R. B., Lim, L.-L., Ratnasingam, J., and Vethakkan, S. R., "Metabolic Dysfunction-Associated Steatotic Liver Disease (MASLD): A State-of-the-Art Review," *Journal of obesity & metabolic syndrome*, V. 32, No. 3, 2023, pp. 197–213.
22. Le, M. H., Yeo, Y. H., Li, X., Li, J., Zou, B., Wu, Y., Ye, Q., Huang, D. Q., Zhao, C., Zhang, J., Liu, C., Chang, N., Xing, F., Yan, S., Wan, Z. H., Tang, N. S. Y., Mayumi, M., Liu, X., Liu, C., Rui, F., Yang, H., Yang, Y., Jin, R., Le, R. H. X., Xu, Y., Le, D. M., Barnett, S., Stave, C. D., Cheung, R., Zhu, Q., and Nguyen, M. H., "2019 Global NAFLD Prevalence: A Systematic Review and Meta-analysis," *Clinical gastroenterology and hepatology : the official clinical practice journal of the American Gastroenterological Association*, V. 20, No. 12, 2022, 2809-2817.e28.
23. Dulai, P. S., Singh, S., Patel, J., Soni, M., Prokop, L. J., Younossi, Z., Sebastiani, G., Ekstedt, M., Hagstrom, H., Nasr, P., Stal, P., Wong, V. W.-S., Kechagias, S., Hultcrantz, R., and Loomba, R., "Increased risk of mortality by fibrosis stage in nonalcoholic fatty liver disease: Systematic review and meta-analysis," *Hepatology (Baltimore, Md.)*, V. 65, No. 5, 2017, pp. 1557–1565.
24. Lai, L.-L., Wan Yusoff, W. N. I., Vethakkan, S. R., Nik Mustapha, N. R., Mahadeva, S., and Chan, W.-K., "Screening for non-alcoholic fatty liver disease in patients with type 2 diabetes mellitus using transient elastography," *Journal of gastroenterology and hepatology*, V. 34, No. 8, 2019, pp. 1396–1403.
25. Boyer, J. L., "Bile formation and secretion," *Comprehensive Physiology*, V. 3, No. 3, 2013, pp. 1035–1078.
26. Wang, H., Vohra, B. P. S., Zhang, Y., and Heuckeroth, R. O., "Transcriptional profiling after bile duct ligation identifies PAI-1 as a contributor to cholestatic injury in mice," *Hepatology (Baltimore, Md.)*, V. 42, No. 5, 2005, pp. 1099–1108.

27. Lindor, K. D., Gershwin, M. E., Poupon, R., Kaplan, M., Bergasa, N. V., and Heathcote, E. J., "Primary biliary cirrhosis," *Hepatology (Baltimore, Md.)*, V. 50, No. 1, 2009, pp. 291–308.
28. Younossi, Z. M., Bernstein, D., Shiffman, M. L., Kwo, P., Kim, W. R., Kowdley, K. V., and Jacobson, I. M., "Diagnosis and Management of Primary Biliary Cholangitis," *The American journal of gastroenterology*, V. 114, No. 1, 2019, pp. 48–63.
29. Lazaridis, K. N., and LaRusso, N. F., "Primary Sclerosing Cholangitis," *The New England journal of medicine*, V. 375, No. 12, 2016, pp. 1161–1170.
30. Boonstra, K., Weersma, R. K., van Erpecum, K. J., Rauws, E. A., Spanier, B. W. M., Poen, A. C., van Nieuwkerk, K. M., Drenth, J. P., Witteman, B. J., Tuynman, H. A., Naber, A. H., Kingma, P. J., van Buuren, H. R., van Hoek, B., Vleggaar, F. P., van Geloven, N., Beuers, U., and Ponsioen, C. Y., "Population-based epidemiology, malignancy risk, and outcome of primary sclerosing cholangitis," *Hepatology (Baltimore, Md.)*, V. 58, No. 6, 2013, pp. 2045–2055.
31. Locke, G. R., Therneau, T. M., Ludwig, J., Dickson, E. R., and Lindor, K. D., "Time course of histological progression in primary biliary cirrhosis," *Hepatology (Baltimore, Md.)*, V. 23, No. 1, 1996, pp. 52–56.
32. Prince, M., Chetwynd, A., Newman, W., Metcalf, J. V., and James, O. F. W., "Survival and symptom progression in a geographically based cohort of patients with primary biliary cirrhosis: follow-up for up to 28 years," *Gastroenterology*, V. 123, No. 4, 2002, pp. 1044–1051.
33. Carbone, M., Mells, G. F., Pells, G., Dawwas, M. F., Newton, J. L., Heneghan, M. A., Neuberger, J. M., Day, D. B., Ducker, S. J., Sandford, R. N., Alexander, G. J., and Jones, D. E. J., "Sex and age are determinants of the clinical phenotype of primary biliary cirrhosis and response to ursodeoxycholic acid," *Gastroenterology*, V. 144, No. 3, 2013, 560-569.e7; quiz e13-4.
34. Porayko, M. K., Wiesner, R. H., LaRusso, N. F., Ludwig, J., MacCarty, R. L., Steiner, B. L., Twomey, C. K., and Zinsmeister, A. R., "Patients with asymptomatic primary sclerosing cholangitis frequently have progressive disease," *Gastroenterology*, V. 98, No. 6, 1990, pp. 1594–1602.
35. Kaplan, G. G., Laupland, K. B., Butzner, D., Urbanski, S. J., and Lee, S. S., "The burden of large and small duct primary sclerosing cholangitis in adults and children: a population-based analysis," *The American journal of gastroenterology*, V. 102, No. 5, 2007, pp. 1042–1049.
36. Tischendorf, J. J. W., Hecker, H., Krüger, M., Manns, M. P., and Meier, P. N., "Characterization, outcome, and prognosis in 273 patients with primary sclerosing cholangitis: A single center study," *The American journal of gastroenterology*, V. 102, No. 1, 2007, pp. 107–114.
37. Hasegawa, S., Yoneda, M., Kurita, Y., Nogami, A., Honda, Y., Hosono, K., and Nakajima, A., "Cholestatic Liver Disease: Current Treatment Strategies and New Therapeutic Agents," *Drugs*, V. 81, No. 10, 2021, pp. 1181–1192.
38. Triantos, C. K., Koukias, N. M., Nikolopoulou, V. N., and Burroughs, A. K., "Meta-analysis: ursodeoxycholic acid for primary sclerosing cholangitis," *Alimentary pharmacology & therapeutics*, V. 34, No. 8, 2011, pp. 901–910.

39. Kim, H. Y., and Jang, J. W., "Sarcopenia in the prognosis of cirrhosis: Going beyond the MELD score," *World Journal of Gastroenterology : WJG*, V. 21, No. 25, 2015, pp. 7637–7647.
40. Tirnitz-Parker, J. E. E., ed., "Hepatocellular Carcinoma," Exon Publications, Australia, 2019, 165 pp.
41. "The global, regional, and national burden of cirrhosis by cause in 195 countries and territories, 1990-2017: a systematic analysis for the Global Burden of Disease Study 2017," *The lancet. Gastroenterology & hepatology*, V. 5, No. 3, 2020, pp. 245–266.
42. Asrani, S. K., Devarbhavi, H., Eaton, J., and Kamath, P. S., "Burden of liver diseases in the world," *Journal of hepatology*, V. 70, No. 1, 2019, pp. 151–171.
43. Schattenberg, J. M., Galle, P. R., and Schuchmann, M., "Apoptosis in liver disease," *Liver international : official journal of the International Association for the Study of the Liver*, V. 26, No. 8, 2006, pp. 904–911.
44. Baik, S. J., Kim, T. H., Yoo, K., Moon, I. H., Choi, J. Y., Chung, K. W., and Song, D. E., "Decreased S100B expression in chronic liver diseases," *The Korean Journal of Internal Medicine*, V. 32, No. 2, 2016, pp. 269–276.
45. Yang, J., Zhang, L., Yu, C., Yang, X.-F., and Wang, H., "Monocyte and macrophage differentiation: circulation inflammatory monocyte as biomarker for inflammatory diseases," *Biomarker research*, V. 2, No. 1, 2014, p. 1.
46. Kisseleva, T., and Brenner, D. A., "Mechanisms of fibrogenesis," *Experimental biology and medicine (Maywood, N.J.)*, V. 233, No. 2, 2008, pp. 109–122.
47. Iwaisako, K., Jiang, C., Zhang, M., Cong, M., Moore-Morris, T. J., Park, T. J., Liu, X., Xu, J., Wang, P., Paik, Y.-H., Meng, F., Asagiri, M., Murray, L. A., Hofmann, A. F., Iida, T., Glass, C. K., Brenner, D. A., and Kisseleva, T., "Origin of myofibroblasts in the fibrotic liver in mice," *Proceedings of the National Academy of Sciences of the United States of America*, V. 111, No. 32, 2014, E3297-305.
48. Nishio, T., Hu, R., Koyama, Y., Liang, S., Rosenthal, S. B., Yamamoto, G., Karin, D., Baglieri, J., Ma, H.-Y., Xu, J., Liu, X., Dhar, D., Iwaisako, K., Taura, K., Brenner, D. A., and Kisseleva, T., "Activated hepatic stellate cells and portal fibroblasts contribute to cholestatic liver fibrosis in MDR2 knockout mice," *Journal of hepatology*, V. 71, No. 3, 2019, pp. 573–585.
49. Bataller, R., and Brenner, D. A., "Liver fibrosis," *The Journal of clinical investigation*, V. 115, No. 2, 2005, pp. 209–218.
50. Fallowfield, J. A., Mizuno, M., Kendall, T. J., Constandinou, C. M., Benyon, R. C., Duffield, J. S., and Iredale, J. P., "Scar-associated macrophages are a major source of hepatic matrix metalloproteinase-13 and facilitate the resolution of murine hepatic fibrosis," *Journal of immunology (Baltimore, Md. : 1950)*, V. 178, No. 8, 2007, pp. 5288–5295.
51. Zhu, C., Kim, K., Wang, X., Bartolome, A., Salomao, M., Dongiovanni, P., Meroni, M., Graham, M. J., Yates, K. P., Diehl, A. M., Schwabe, R. F., Tabas, I., Valenti, L., Lavine, J. E., and Pajvani, U. B., "Hepatocyte Notch activation induces liver fibrosis in nonalcoholic steatohepatitis," *Science translational medicine*, V. 10, No. 468, 2018.
52. Wang, X., Zheng, Z., Caviglia, J. M., Corey, K. E., Herfel, T. M., Cai, B., Masia, R., Chung, R. T., Lefkowitch, J. H., Schwabe, R. F., and Tabas, I., "Hepatocyte

TAZ/WWTR1 Promotes Inflammation and Fibrosis in Nonalcoholic Steatohepatitis," *Cell metabolism*, V. 24, No. 6, 2016, pp. 848–862.
53. Lan, T., Kisseleva, T., and Brenner, D. A., "Deficiency of NOX1 or NOX4 Prevents Liver Inflammation and Fibrosis in Mice through Inhibition of Hepatic Stellate Cell Activation," *PloS one*, V. 10, No. 7, 2015, e0129743.
54. Xie, G., Karaca, G., Swiderska-Syn, M., Michelotti, G. A., Krüger, L., Chen, Y., Premont, R. T., Choi, S. S., and Diehl, A. M., "Cross-talk between Notch and Hedgehog regulates hepatic stellate cell fate in mice," *Hepatology (Baltimore, Md.)*, V. 58, No. 5, 2013, pp. 1801–1813.
55. Lee, Y.-S., Kim, S. Y., Ko, E., Lee, J.-H., Yi, H.-S., Yoo, Y. J., Je, J., Suh, S. J., Jung, Y. K., Kim, J. H., Seo, Y. S., Yim, H. J., Jeong, W.-I., Yeon, J. E., Um, S. H., and Byun, K. S., "Exosomes derived from palmitic acid-treated hepatocytes induce fibrotic activation of hepatic stellate cells," *Scientific reports*, V. 7, No. 1, 2017, p. 3710.
56. Di Rosa, M., and Malaguarnera, L., "Genetic variants in candidate genes influencing NAFLD progression," *Journal of molecular medicine (Berlin, Germany)*, V. 90, No. 2, 2012, pp. 105–118.
57. Kim, J. Y., Garcia-Carbonell, R., Yamachika, S., Zhao, P., Dhar, D., Loomba, R., Kaufman, R. J., Saltiel, A. R., and Karin, M., "ER Stress Drives Lipogenesis and Steatohepatitis via Caspase-2 Activation of S1P," *Cell*, V. 175, No. 1, 2018, 133-145.e15.
58. Musso, G., Gambino, R., Durazzo, M., Biroli, G., Carello, M., Fagà, E., Pacini, G., Michieli, F. de, Rabbione, L., Premoli, A., Cassader, M., and Pagano, G., "Adipokines in NASH: postprandial lipid metabolism as a link between adiponectin and liver disease," *Hepatology (Baltimore, Md.)*, V. 42, No. 5, 2005, pp. 1175–1183.
59. Malaguarnera, M., Di Rosa, M., Nicoletti, F., and Malaguarnera, L., "Molecular mechanisms involved in NAFLD progression," *Journal of molecular medicine (Berlin, Germany)*, V. 87, No. 7, 2009, pp. 679–695.
60. Maricic, I., Marrero, I., Eguchi, A., Nakamura, R., Johnson, C. D., Dasgupta, S., Hernandez, C. D., Nguyen, P. S., Swafford, A. D., Knight, R., Feldstein, A. E., Loomba, R., and Kumar, V., "Differential Activation of Hepatic Invariant NKT Cell Subsets Plays a Key Role in Progression of Nonalcoholic Steatohepatitis," *Journal of immunology (Baltimore, Md. : 1950)*, V. 201, No. 10, 2018, pp. 3017–3035.
61. Moon, Y.-A., "The SCAP/SREBP Pathway: A Mediator of Hepatic Steatosis," *Endocrinology and Metabolism*, V. 32, No. 1, 2017, pp. 6–10.
62. O'Shea, R. S., Dasarathy, S., and McCullough, A. J., "Alcoholic liver disease," *Hepatology (Baltimore, Md.)*, V. 51, No. 1, 2010, pp. 307–328.
63. Lucey, M. R., Mathurin, P., and Morgan, T. R., "Alcoholic hepatitis," *The New England journal of medicine*, V. 360, No. 26, 2009, pp. 2758–2769.
64. Albillos, A., Lario, M., and Álvarez-Mon, M., "Cirrhosis-associated immune dysfunction: distinctive features and clinical relevance," *Journal of hepatology*, V. 61, No. 6, 2014, pp. 1385–1396.
65. Tritto, G., Bechlis, Z., Stadlbauer, V., Davies, N., Francés, R., Shah, N., Mookerjee, R. P., Such, J., and Jalan, R., "Evidence of neutrophil functional defect despite inflammation in stable cirrhosis," *Journal of hepatology*, V. 55, No. 3, 2011, pp. 574–581.

66. Albillos, A., La Hera Ad, A. d., Reyes, E., Monserrat, J., Muñoz, L., Nieto, M., Prieto, A., Sanz, E., and Alvarez-Mon, M., "Tumour necrosis factor-alpha expression by activated monocytes and altered T-cell homeostasis in ascitic alcoholic cirrhosis: amelioration with norfloxacin," *Journal of hepatology*, V. 40, No. 4, 2004, pp. 624–631.
67. Lemmers, A., Moreno, C., Gustot, T., Maréchal, R., Degré, D., Demetter, P., Nadai, P. de, Geerts, A., Quertinmont, E., Vercruysse, V., Le Moine, O., and Devière, J., "The interleukin-17 pathway is involved in human alcoholic liver disease," *Hepatology (Baltimore, Md.)*, V. 49, No. 2, 2009, pp. 646–657.
68. Sun, H. Q., Zhang, J. Y., Zhang, H., Zou, Z. S., Wang, F. S., and Jia, J. H., "Increased Th17 cells contribute to disease progression in patients with HBV-associated liver cirrhosis," *Journal of viral hepatitis*, V. 19, No. 6, 2012, pp. 396–403.
69. Tilg, H., Wilmer, A., Vogel, W., Herold, M., Nölchen, B., Judmaier, G., and Huber, C., "Serum levels of cytokines in chronic liver diseases," *Gastroenterology*, V. 103, No. 1, 1992, pp. 264–274.
70. Lee, F. Y., Lu, R. H., Tsai, Y. T., Lin, H. C., Hou, M. C., Li, C. P., Liao, T. M., Lin, L. F., Wang, S. S., and Lee, S. D., "Plasma interleukin-6 levels in patients with cirrhosis. Relationship to endotoxemia, tumor necrosis factor-alpha, and hyperdynamic circulation," *Scandinavian journal of gastroenterology*, V. 31, No. 5, 1996, pp. 500–505.
71. Koyama, Y., Wang, P., Liang, S., Iwaisako, K., Liu, X., Xu, J., Zhang, M., Sun, M., Cong, M., Karin, D., Taura, K., Benner, C., Heinz, S., Bera, T., Brenner, D. A., and Kisseleva, T., "Mesothelin/mucin 16 signaling in activated portal fibroblasts regulates cholestatic liver fibrosis," *The Journal of clinical investigation*, V. 127, No. 4, 2017, pp. 1254–1270.
72. Brinkmann, V., Reichard, U., Goosmann, C., Fauler, B., Uhlemann, Y., Weiss, D. S., Weinrauch, Y., and Zychlinsky, A., "Neutrophil extracellular traps kill bacteria," *Science (New York, N.Y.)*, V. 303, No. 5663, 2004, pp. 1532–1535.
73. Meier, A., Chien, J., Hobohm, L., Patras, K. A., Nizet, V., and Corriden, R., "Inhibition of Human Neutrophil Extracellular Trap (NET) Production by Propofol and Lipid Emulsion," *Frontiers in pharmacology*, V. 10, 2019, p. 323.
74. Diaz-Soto, M. P., and Garcia-Tsao, G., "Management of varices and variceal hemorrhage in liver cirrhosis: a recent update," *Therapeutic advances in gastroenterology*, V. 15, 2022, 17562848221101712.
75. Ginés, P., Quintero, E., Arroyo, V., Terés, J., Bruguera, M., Rimola, A., Caballería, J., Rodés, J., and Rozman, C., "Compensated cirrhosis: natural history and prognostic factors," *Hepatology (Baltimore, Md.)*, V. 7, No. 1, 1987, pp. 122–128.
76. Pellicoro, A., Ramachandran, P., Iredale, J. P., and Fallowfield, J. A., "Liver fibrosis and repair: immune regulation of wound healing in a solid organ," *Nature reviews. Immunology*, V. 14, No. 3, 2014, pp. 181–194.
77. Pellicoro, A., Aucott, R. L., Ramachandran, P., Robson, A. J., Fallowfield, J. A., Snowdon, V. K., Hartland, S. N., Vernon, M., Duffield, J. S., Benyon, R. C., Forbes, S. J., and Iredale, J. P., "Elastin accumulation is regulated at the level of degradation by macrophage metalloelastase (MMP-12) during experimental liver fibrosis," *Hepatology (Baltimore, Md.)*, V. 55, No. 6, 2012, pp. 1965–1975.

78. Mallat, A., and Lotersztajn, S., “Reversion of hepatic stellate cell to a quiescent phenotype: From myth to reality?,” *Journal of hepatology*, V. 59, No. 2, 2013, pp. 383–386.
79. Troeger, J. S., Mederacke, I., Gwak, G.-Y., Dapito, D. H., Mu, X., Hsu, C. C., Pradere, J.-P., Friedman, R. A., and Schwabe, R. F., “Deactivation of hepatic stellate cells during liver fibrosis resolution in mice,” *Gastroenterology*, V. 143, No. 4, 2012, 1073-83.e22.
80. Ellis, E. L., and Mann, D. A., “Clinical evidence for the regression of liver fibrosis,” *Journal of hepatology*, V. 56, No. 5, 2012, pp. 1171–1180.
81. Groszmann, R. J., and Wongcharatrawee, S., “The hepatic venous pressure gradient: anything worth doing should be done right,” *Hepatology (Baltimore, Md.)*, V. 39, No. 2, 2004, pp. 280–282.
82. Salerno, F., Cammà, C., Enea, M., Rössle, M., and Wong, F., “Transjugular intrahepatic portosystemic shunt for refractory ascites: a meta-analysis of individual patient data,” *Gastroenterology*, V. 133, No. 3, 2007, pp. 825–834.
83. Kovalak, M., Lake, J., Mattek, N., Eisen, G., Lieberman, D., and Zaman, A., “Endoscopic screening for varices in cirrhotic patients: data from a national endoscopic database,” *Gastrointestinal endoscopy*, V. 65, No. 1, 2007, pp. 82–88.
84. D'Amico, G., and Franchis, R. de, “Upper digestive bleeding in cirrhosis. Post-therapeutic outcome and prognostic indicators,” *Hepatology (Baltimore, Md.)*, V. 38, No. 3, 2003, pp. 599–612.
85. Nusrat, S., Khan, M. S., Fazili, J., and Madhoun, M. F., “Cirrhosis and its complications: evidence based treatment,” *World Journal of Gastroenterology : WJG*, V. 20, No. 18, 2014, pp. 5442–5460.
86. Simonetto, D. A., Gines, P., and Kamath, P. S., “Hepatorenal syndrome: pathophysiology, diagnosis, and management,” *BMJ (Clinical research ed.)*, V. 370, 2020, m2687.
87. Valerio, C., Theocharidou, E., Davenport, A., and Agarwal, B., “Human albumin solution for patients with cirrhosis and acute on chronic liver failure: Beyond simple volume expansion,” *World Journal of Hepatology*, V. 8, No. 7, 2016, pp. 345–354.
88. Egerod Israelsen, M., Gluud, L. L., and Krag, A., “Acute kidney injury and hepatorenal syndrome in cirrhosis,” *Journal of gastroenterology and hepatology*, V. 30, No. 2, 2015, pp. 236–243.
89. Bosoi, C. R., and Rose, C. F., “Identifying the direct effects of ammonia on the brain,” *Metabolic brain disease*, V. 24, No. 1, 2009, pp. 95–102.
90. Amodio, P., Bemeur, C., Butterworth, R., Cordoba, J., Kato, A., Montagnese, S., Uribe, M., Vilstrup, H., and Morgan, M. Y., “The nutritional management of hepatic encephalopathy in patients with cirrhosis: International Society for Hepatic Encephalopathy and Nitrogen Metabolism Consensus,” *Hepatology (Baltimore, Md.)*, V. 58, No. 1, 2013, pp. 325–336.
91. Ferenci, P., Herneth, A., and Steindl, P., “Newer approaches to therapy of hepatic encephalopathy,” *Seminars in liver disease*, V. 16, No. 3, 1996, pp. 329–338.
92. Jiang, Q., Jiang, X.-H., Zheng, M.-H., Jiang, L.-M., Chen, Y.-P., and Wang, L., “Rifaximin versus nonabsorbable disaccharides in the management of hepatic encephalopathy: a meta-analysis,” *European journal of gastroenterology & hepatology*, V. 20, No. 11, 2008, pp. 1064–1070.

93. Sharma, B. C., Sharma, P., Agrawal, A., and Sarin, S. K., "Secondary prophylaxis of hepatic encephalopathy: an open-label randomized controlled trial of lactulose versus placebo," *Gastroenterology*, V. 137, No. 3, 2009, 885-91, 891.e1.
94. Trautwein, C., Friedman, S. L., Schuppan, D., and Pinzani, M., "Hepatic fibrosis: Concept to treatment," *Journal of hepatology*, V. 62, 1 Suppl, 2015, S15-24.
95. "EASL Clinical Practice Guidelines for the management of patients with decompensated cirrhosis," *Journal of hepatology*, V. 69, No. 2, 2018, pp. 406–460.
96. Liu, Y., Meyer, C., Xu, C., Weng, H., Hellerbrand, C., Dijke, P. ten, and Dooley, S., "Animal models of chronic liver diseases," *American journal of physiology. Gastrointestinal and liver physiology*, V. 304, No. 5, 2013, G449-68.
97. Tsukamoto, H., Matsuoka, M., and French, S. W., "Experimental models of hepatic fibrosis: a review," *Seminars in liver disease*, V. 10, No. 1, 1990, pp. 56–65.
98. Tsuchida, T., Lee, Y. A., Fujiwara, N., Ybanez, M., Allen, B., Martins, S., Fiel, M. I., Goossens, N., Chou, H.-I., Hoshida, Y., and Friedman, S. L., "A simple diet- and chemical-induced murine NASH model with rapid progression of steatohepatitis, fibrosis and liver cancer," *Journal of hepatology*, V. 69, No. 2, 2018, pp. 385–395.
99. Bubnov, R. V., Drahulian, M. V., Buchek, P. V., and Gulko, T. P., "High regenerative capacity of the liver and irreversible injury of male reproductive system in carbon tetrachloride-induced liver fibrosis rat model," *The EPMA journal*, V. 9, No. 1, 2018, pp. 59–75.
100. He, Q., Zhang, F., Shu, J., Li, S., Liang, Z., Du, M., Liu, X., Liu, T., Li, M., Yin, X., Pan, Q., Lu, F., Wang, L., and Wang, L., "Immunocompromised rabbit model of chronic HEV reveals liver fibrosis and distinct efficacy of different vaccination strategies," *Hepatology (Baltimore, Md.)*, V. 76, No. 3, 2022, pp. 788–802.
101. Panasevich, M. R., Meers, G. M., Linden, M. A., Booth, F. W., Perfield, J. W., Fritsche, K. L., Wankhade, U. D., Chintapalli, S. V., Shankar, K., Ibdah, J. A., and Rector, R. S., "High-fat, high-fructose, high-cholesterol feeding causes severe NASH and cecal microbiota dysbiosis in juvenile Ossabaw swine," *American journal of physiology. Endocrinology and metabolism*, V. 314, No. 1, 2018, E78-E92.
102. Matsuo, M., Murata, S., Hasegawa, S., Hatada, Y., Ohtsuka, M., and Taniguchi, H., "Novel liver fibrosis model in Macaca fascicularis induced by thioacetamide," *Scientific reports*, V. 10, No. 1, 2020, p. 2450.
103. Wu, S.-Y., Yang, W.-Y., Cheng, C.-C., Hsiao, M.-C., Tsai, S.-L., Lin, H.-K., Lin, K.-H., and Yuh, C.-H., "Low Molecular Weight Fucoidan Prevents Radiation-Induced Fibrosis and Secondary Tumors in a Zebrafish Model," *Cancers*, V. 12, No. 6, 2020.
104. Seok, J., Warren, H. S., Cuenca, A. G., Mindrinos, M. N., Baker, H. V., Xu, W., Richards, D. R., McDonald-Smith, G. P., Gao, H., Hennessy, L., Finnerty, C. C., López, C. M., Honari, S., Moore, E. E., Minei, J. P., Cuschieri, J., Bankey, P. E., Johnson, J. L., Sperry, J., Nathens, A. B., Billiar, T. R., West, M. A., Jeschke, M. G., Klein, M. B., Gamelli, R. L., Gibran, N. S., Brownstein, B. H., Miller-Graziano, C., Calvano, S. E., Mason, P. H., Cobb, J. P., Rahme, L. G., Lowry, S. F., Maier, R. V., Moldawer, L. L., Herndon, D. N., Davis, R. W., Xiao, W., Tompkins, R. G., Abouhamze, A., Balis, U. G. J., Camp, D. G., De, A. K., Harbrecht, B. G., Hayden, D. L., Kaushal, A., O'Keefe, G. E., Kotz, K. T., Qian, W., Schoenfeld, D. A., Shapiro, M. B., Silver, G. M., Smith, R. D.,

Storey, J. D., Tibshirani, R., Toner, M., Wilhelmy, J., Wispelwey, B., and Wong, W. H., "Genomic responses in mouse models poorly mimic human inflammatory diseases," *Proceedings of the National Academy of Sciences of the United States of America*, V. 110, No. 9, 2013, pp. 3507–3512.

105. Hefler, J., Marfil-Garza, B. A., Pawlick, R. L., Freed, D. H., Karvellas, C. J., Bigam, D. L., and Shapiro, A. M. J., "Preclinical models of acute liver failure: a comprehensive review," *PeerJ*, V. 9, 2021.
106. Abrantes, J., van der Loo, W., Le Pendu, J., and Esteves, P. J., "Rabbit haemorrhagic disease (RHD) and rabbit haemorrhagic disease virus (RHDV): a review," *Veterinary research*, V. 43, No. 1, 2012, p. 12.
107. Ezran, C., Karanewsky, C. J., Pendleton, J. L., Sholtz, A., Krasnow, M. R., Willick, J., Razafindrakoto, A., Zohdy, S., Albertelli, M. A., and Krasnow, M. A., "The Mouse Lemur, a Genetic Model Organism for Primate Biology, Behavior, and Health," *Genetics*, V. 206, No. 2, 2017, pp. 651–664.
108. Glenny, E. M., Coleman, M. F., Giles, E. D., Wellberg, E. A., and Hursting, S. D., "Designing Relevant Preclinical Rodent Models for Studying Links Between Nutrition, Obesity, Metabolism, and Cancer," *Annual review of nutrition*, V. 41, 2021, pp. 253–282.
109. Ravichandra, A., and Schwabe, R. F., "Mouse Models of Liver Fibrosis," *Methods in molecular biology (Clifton, N.J.)*, V. 2299, 2021, pp. 339–356.
110. Yanguas, S. C., Cogliati, B., Willebrords, J., Maes, M., Colle, I., van den Bossche, B., Oliveira, C. P. M. S. de, Andraus, W., Alves, V. A. F., Leclercq, I., and Vinken, M., "Experimental models of liver fibrosis," *Archives of toxicology*, V. 90, No. 5, 2016, pp. 1025–1048.
111. Starkel, P., and Leclercq, I. A., "Animal models for the study of hepatic fibrosis," *Best practice & research. Clinical gastroenterology*, V. 25, No. 2, 2011, pp. 319–333.
112. Wu, J., and Norton, P. A., "Animal models of liver fibrosis," *Scandinavian journal of gastroenterology*, V. 31, No. 12, 1996, pp. 1137–1143.
113. Domenicali, M., Caraceni, P., Giannone, F., Baldassarre, M., Lucchetti, G., Quarta, C., Patti, C., Catani, L., Nanni, C., Lemoli, R. M., and Bernardi, M., "A novel model of CCl4-induced cirrhosis with ascites in the mouse," *Journal of hepatology*, V. 51, No. 6, 2009, pp. 991–999.
114. Zimmermann, T., Müller, A., Machnik, G., Franke, H., Schubert, H., and Dargel, R., "Biochemical and morphological studies on production and regression of experimental liver cirrhosis induced by thioacetamide in Uje: WIST rats," *Zeitschrift fur Versuchstierkunde*, V. 30, 5-6, 1987, pp. 165–180.
115. Lamas-Paz, A., Hao, F., Nelson, L. J., Vázquez, M. T., Canals, S., Del Gómez Moral, M., Martínez-Naves, E., Nevzorova, Y. A., and Cubero, F. J., "Alcoholic liver disease: Utility of animal models," *World Journal of Gastroenterology : WJG*, V. 24, No. 45, 2018, pp. 5063–5075.
116. Brandon-Warner, E., Schrum, L. W., Schmidt, C. M., and McKillop, I. H., "Rodent models of alcoholic liver disease: of mice and men," *Alcohol (Fayetteville, N.Y.)*, V. 46, No. 8, 2012, pp. 715–725.
117. D'Souza El-Guindy, N. B., Kovacs, E. J., Witte, P. de, Spies, C., Littleton, J. M., Villiers, W. J. S. de, Lott, A. J., Plackett, T. P., Lanzke, N., and Meadows, G. G.,

"Laboratory models available to study alcohol-induced organ damage and immune variations: choosing the appropriate model," *Alcoholism, clinical and experimental research*, V. 34, No. 9, 2010, pp. 1489–1511.
118. Wiernsperger, N., "Hepatic function and the cardiometabolic syndrome," *Diabetes, Metabolic Syndrome and Obesity: Targets and Therapy*, V. 6, 2013, pp. 379–388.
119. Stephenson, K., Kennedy, L., Hargrove, L., Demieville, J., Thomson, J., Alpini, G., and Francis, H., "Updates on Dietary Models of Nonalcoholic Fatty Liver Disease: Current Studies and Insights," *Gene expression*, V. 18, No. 1, 2018, pp. 5–17.
120. Hao, F., Cubero, F. J., Ramadori, P., Liao, L., Haas, U., Lambertz, D., Sonntag, R., Bangen, J.-M., Gassler, N., Hoss, M., Streetz, K. L., Reissing, J., Zimmermann, H. W., Trautwein, C., Liedtke, C., and Nevzorova, Y. A., "Inhibition of Caspase-8 does not protect from alcohol-induced liver apoptosis but alleviates alcoholic hepatic steatosis in mice," *Cell death & disease*, V. 8, No. 10, 2017, e3152.
121. Tsukamoto, H., French, S. W., Benson, N., Delgado, G., Rao, G. A., Larkin, E. C., and Largman, C., "Severe and progressive steatosis and focal necrosis in rat liver induced by continuous intragastric infusion of ethanol and low fat diet," *Hepatology (Baltimore, Md.)*, V. 5, No. 2, 1985, pp. 224–232.
122. Cameron, G. R., and Oakley, C. L., "Ligation of the common bile duct," *J. Pathol.*, V. 35, No. 5, 1932, pp. 769–798.
123. Abshagen, K., König, M., Hoppe, A., Müller, I., Ebert, M., Weng, H., Holzhütter, H.-G., Zanger, U. M., Bode, J., Vollmar, B., Thomas, M., and Dooley, S., "Pathobiochemical signatures of cholestatic liver disease in bile duct ligated mice," *BMC systems biology*, V. 9, 2015, p. 83.
124. Tag, C. G., Sauer-Lehnen, S., Weiskirchen, S., Borkham-Kamphorst, E., Tolba, R. H., Tacke, F., and Weiskirchen, R., "Bile duct ligation in mice: induction of inflammatory liver injury and fibrosis by obstructive cholestasis," *Journal of visualized experiments : JoVE*, No. 96, 2015.
125. van Campenhout, S., van Vlierberghe, H., and Devisscher, L., "Common Bile Duct Ligation as Model for Secondary Biliary Cirrhosis," *Methods in molecular biology (Clifton, N.J.)*, V. 1981, 2019, pp. 237–247.
126. Kountouras, J., Billing, B. H., and Scheuer, P. J., "Prolonged bile duct obstruction: a new experimental model for cirrhosis in the rat," *British journal of experimental pathology*, V. 65, No. 3, 1984, pp. 305–311.
127. Popov, Y., Sverdlov, D. Y., Bhaskar, K. R., Sharma, A. K., Millonig, G., Patsenker, E., Krahenbuhl, S., Krahenbuhl, L., and Schuppan, D., "Macrophage-mediated phagocytosis of apoptotic cholangiocytes contributes to reversal of experimental biliary fibrosis," *American journal of physiology. Gastrointestinal and liver physiology*, V. 298, No. 3, 2010, G323-34.
128. Bosoi, C. R., Oliveira, M. M., Ochoa-Sanchez, R., Tremblay, M., Have, G. A. ten, Deutz, N. E., Rose, C. F., and Bemeur, C., "The bile duct ligated rat: A relevant model to study muscle mass loss in cirrhosis," *Metabolic brain disease*, V. 32, No. 2, 2017, pp. 513–518.
129. Giusto, M., Barberi, L., Di Sario, F., Rizzuto, E., Nicoletti, C., Ascenzi, F., Renzi, A., Caporaso, N., D'Argenio, G., Gaudio, E., Musarò, A., and Merli, M., "Skeletal muscle

myopenia in mice model of bile duct ligation and carbon tetrachloride-induced liver cirrhosis," *Physiological reports*, V. 5, No. 7, 2017.
130. Joyeux, H., Joyeux, A., Raoux, P., Brissac, C., Blanc, F., and Solassol, C., "Troubles métaboliques de l'anhépatie expérimentale et nutrition parentérale," *Annales de l'anesthesiologie francaise*, V. 18, No. 11, 1977, pp. 939–947.
131. Yamaguchi, Y., Bollinger, R. R., DeFaria, E., Landis, B., and Quarfordt, S., "A simplified single stage total hepatectomy in the rat with maintenance of gastrointestinal absorptive function," *Hepatology (Baltimore, Md.)*, V. 9, No. 1, 1989, pp. 69–74.
132. Nyberg, S. L., Shirabe, K., Peshwa, M. V., Sielaff, T. D., Crotty, P. L., Mann, H. J., Remmel, R. P., Payne, W. D., Hu, W. S., and Cerra, F. B., "Extracorporeal application of a gel-entrapment, bioartificial liver: demonstration of drug metabolism and other biochemical functions," *Cell transplantation*, V. 2, No. 6, 1993, pp. 441–452.
133. Frühauf, N. R., Oldhafer, K. J., Westermann, S., Sotiropoulos, G. C., and Kaiser, G. M., "Acute hepatic failure in swine: hepatectomy versus vascular occlusion," *Journal of investigative surgery : the official journal of the Academy of Surgical Research*, V. 17, No. 3, 2004, pp. 163–171.
134. Arkadopoulos, N., Chen, S. C., Khalili, T. M., Detry, O., Hewitt, W. R., Lilja, H., Kamachi, H., Petrovic, L., Mullon, C. J., Demetriou, A. A., and Rozga, J., "Transplantation of hepatocytes for prevention of intracranial hypertension in pigs with ischemic liver failure," *Cell transplantation*, V. 7, No. 4, 1998, pp. 357–363.
135. Filipponi, F., Boggi, U., Meacci, L., Burchielli, S., Vistoli, F., Bellini, R., Prota, C., Colizzi, L., Kusmic, C., Campani, D., Gneri, C., Trivella, M. G., and Mosca, F., "A new technique for total hepatectomy in the pig for testing liver support devices," *Surgery*, V. 125, No. 4, 1999, pp. 448–455.
136. Rozga, J., Jeppsson, B., Bengmark, S., and Demetriou, A. A., "A simple two-stage technique of total hepatectomy in the rat," *The Journal of surgical research*, V. 52, No. 1, 1992, pp. 46–49.
137. Guglielmi, A., Ruzzenente, A., Conci, S., Valdegamberi, A., and Iacono, C., "How much remnant is enough in liver resection?," *Digestive surgery*, V. 29, No. 1, 2012, pp. 6–17.
138. Meyer, C., Dostou, J. M., Welle, S. L., and Gerich, J. E., "Role of human liver, kidney, and skeletal muscle in postprandial glucose homeostasis," *American journal of physiology. Endocrinology and metabolism*, V. 282, No. 2, 2002, E419-27.
139. Zheng, D., MacLean, P. S., Pohnert, S. C., Knight, J. B., Olson, A. L., Winder, W. W., and Dohm, G. L., "Regulation of muscle GLUT-4 transcription by AMP-activated protein kinase," *Journal of applied physiology (Bethesda, Md. : 1985)*, V. 91, No. 3, 2001, pp. 1073–1083.
140. Stoppani, J., Hildebrandt, A. L., Sakamoto, K., Cameron-Smith, D., Goodyear, L. J., and Neufer, P. D., "AMP-activated protein kinase activates transcription of the UCP3 and HKII genes in rat skeletal muscle," *American journal of physiology. Endocrinology and metabolism*, V. 283, No. 6, 2002, E1239-48.
141. Scott, W., Stevens, J., and Binder-Macleod, S. A., "Human skeletal muscle fiber type classifications," *Physical therapy*, V. 81, No. 11, 2001, pp. 1810–1816.

142. Argilés, J. M., Campos, N., Lopez-Pedrosa, J. M., Rueda, R., and Rodriguez-Mañas, L., “Skeletal Muscle Regulates Metabolism via Interorgan Crosstalk: Roles in Health and Disease,” *Journal of the American Medical Directors Association*, V. 17, No. 9, 2016, pp. 789–796.
143. Matsakas, A., and Patel, K., “Skeletal muscle fibre plasticity in response to selected environmental and physiological stimuli,” *Histology and histopathology*, V. 24, No. 5, 2009, pp. 611–629.
144. Perriello, G., Nurjhan, N., Stumvoll, M., Bucci, A., Welle, S., Dailey, G., Bier, D. M., Toft, I., Jenssen, T. G., and Gerich, J. E., “Regulation of gluconeogenesis by glutamine in normal postabsorptive humans,” *The American journal of physiology*, V. 272, 3 Pt 1, 1997, E437-45.
145. Breen, L., and Phillips, S. M., “Skeletal muscle protein metabolism in the elderly: Interventions to counteract the 'anabolic resistance' of ageing,” *Nutrition & metabolism*, V. 8, 2011, p. 68.
146. Yoshida, T., and Delafontaine, P., “Mechanisms of IGF-1-Mediated Regulation of Skeletal Muscle Hypertrophy and Atrophy,” *Cells*, V. 9, No. 9, 2020.
147. García, P. S., Cabbabe, A., Kambadur, R., Nicholas, G., and Csete, M., “Brief-reports: elevated myostatin levels in patients with liver disease: a potential contributor to skeletal muscle wasting,” *Anesthesia and analgesia*, V. 111, No. 3, 2010, pp. 707–709.
148. Qiu, J., Tsien, C., Thapalaya, S., Narayanan, A., Weihl, C. C., Ching, J. K., Eghtesad, B., Singh, K., Fu, X., Dubyak, G., McDonald, C., Almasan, A., Hazen, S. L., Naga Prasad, S. V., and Dasarathy, S., “Hyperammonemia-mediated autophagy in skeletal muscle contributes to sarcopenia of cirrhosis,” *American journal of physiology. Endocrinology and metabolism*, V. 303, No. 8, 2012, E983-93.
149. Han, H. Q., Zhou, X., Mitch, W. E., and Goldberg, A. L., “Myostatin/activin pathway antagonism: molecular basis and therapeutic potential,” *The international journal of biochemistry & cell biology*, V. 45, No. 10, 2013, pp. 2333–2347.
150. Egerman, M. A., and Glass, D. J., “Signaling pathways controlling skeletal muscle mass,” *Critical reviews in biochemistry and molecular biology*, V. 49, No. 1, 2014, pp. 59–68.
151. Wing, S. S., Lecker, S. H., and Jagoe, R. T., “Proteolysis in illness-associated skeletal muscle atrophy: from pathways to networks,” *Critical reviews in clinical laboratory sciences*, V. 48, No. 2, 2011, pp. 49–70.
152. Sandri, M., Lin, J., Handschin, C., Yang, W., Arany, Z. P., Lecker, S. H., Goldberg, A. L., and Spiegelman, B. M., “PGC-1alpha protects skeletal muscle from atrophy by suppressing FoxO3 action and atrophy-specific gene transcription,” *Proceedings of the National Academy of Sciences of the United States of America*, V. 103, No. 44, 2006, pp. 16260–16265.
153. Da Silva Rosa, S. C., Nayak, N., Caymo, A. M., and Gordon, J. W., “Mechanisms of muscle insulin resistance and the cross-talk with liver and adipose tissue,” *Physiological reports*, V. 8, No. 19, 2020, e14607.
154. Kawaguchi, T., Taniguchi, E., Itou, M., Sakata, M., Sumie, S., and Sata, M., “Insulin resistance and chronic liver disease,” *World Journal of Hepatology*, V. 3, No. 5, 2011, pp. 99–107.

155. Kim, H.-J., Higashimori, T., Park, S.-Y., Choi, H., Dong, J., Kim, Y.-J., Noh, H.-L., Cho, Y.-R., Cline, G., Kim, Y.-B., and Kim, J. K., "Differential effects of interleukin-6 and -10 on skeletal muscle and liver insulin action in vivo," *Diabetes*, V. 53, No. 4, 2004, pp. 1060–1067.
156. Muñoz-Cánoves, P., Scheele, C., Pedersen, B. K., and Serrano, A. L., "Interleukin-6 myokine signaling in skeletal muscle: a double-edged sword?," *The FEBS journal*, V. 280, No. 17, 2013, pp. 4131–4148.
157. Banzet, S., Koulmann, N., Simler, N., Sanchez, H., Chapot, R., Serrurier, B., Peinnequin, A., and Bigard, X., "Control of gluconeogenic genes during intense/prolonged exercise: hormone-independent effect of muscle-derived IL-6 on hepatic tissue and PEPCK mRNA," *Journal of applied physiology (Bethesda, Md. : 1985)*, V. 107, No. 6, 2009, pp. 1830–1839.
158. Febbraio, M. A., Ott, P., Nielsen, H. B., Steensberg, A., Keller, C., Krustrup, P., Secher, N. H., and Pedersen, B. K., "Hepatosplanchnic clearance of interleukin-6 in humans during exercise," *American journal of physiology. Endocrinology and metabolism*, V. 285, No. 2, 2003, E397-402.
159. Nardelli, S., Gioia, S., Faccioli, J., Riggio, O., and Ridola, L., "Sarcopenia and cognitive impairment in liver cirrhosis: A viewpoint on the clinical impact of minimal hepatic encephalopathy," *World Journal of Gastroenterology : WJG*, V. 25, No. 35, 2019, pp. 5257–5265.
160. Da Zhou, Shi, Y., Zhang, D., Zuo, J., Zeng, C., Mamtawla, G., Huang, L., Gao, X., Zhang, L., and Wang, X., "Liver-secreted FGF21 induces sarcopenia by inhibiting satellite cell myogenesis via klotho beta in decompensated cirrhosis," *Redox biology*, V. 76, 2024, p. 103333.
161. Delogu, W., Caligiuri, A., Provenzano, A., Rosso, C., Bugianesi, E., Coratti, A., Macias-Barragan, J., Galastri, S., Di Maira, G., and Marra, F., "Myostatin regulates the fibrogenic phenotype of hepatic stellate cells via c-jun N-terminal kinase activation," *Digestive and liver disease : official journal of the Italian Society of Gastroenterology and the Italian Association for the Study of the Liver*, V. 51, No. 10, 2019, pp. 1400–1408.
162. Ponziani, F. R., Picca, A., Marzetti, E., Calvani, R., Conta, G., Del Chierico, F., Capuani, G., Faccia, M., Fianchi, F., Funaro, B., Josè Coelho-Junior, H., Petito, V., Rinninella, E., Paroni Sterbini, F., Reddel, S., Vernocchi, P., Cristina Mele, M., Miccheli, A., Putignani, L., Sanguinetti, M., Pompili, M., and Gasbarrini, A., "Characterization of the gut-liver-muscle axis in cirrhotic patients with sarcopenia," *Liver international : official journal of the International Association for the Study of the Liver*, V. 41, No. 6, 2021, pp. 1320–1334.
163. Heinrich, P. C., Müller, M., and Graeve, L., "Löffler/Petrides Biochemie und Pathobiochemie," Springer Berlin Heidelberg, Berlin, Heidelberg, 2014.
164. Voet, D., and Voet, J. G., "Biochemie," 1. korr. Nachdr. der 1. Aufl. 1992, VCH, Weinheim, 1994 [erschienen] 1996, 1237 pp.
165. Pang, G., Xie, J., Chen, Q., and Hu, Z., "Energy intake, metabolic homeostasis, and human health," *Food Science and Human Wellness*, V. 3, 3-4, 2014, pp. 89–103.

166. Javed, F., He, Q., Davidson, L. E., Thornton, J. C., Albu, J., Boxt, L., Krasnow, N., Elia, M., Kang, P., Heshka, S., and Gallagher, D., "Brain and high metabolic rate organ mass: contributions to resting energy expenditure beyond fat-free mass," *The American journal of clinical nutrition*, V. 91, No. 4, 2010, pp. 907–912.
167. National Academies of Sciences, Engineering, and Medicine, Health and Medicine Division, Food and Nutrition Board, Committee on the Dietary Reference Intakes for Energy. Dietary Reference Intakes for Energy. Washington (DC): National Academies Press (US), and 2023 Jan 17. 4, Factors Affecting Energy Expenditure and Requirements. Available from: https://www.ncbi.nlm.nih.gov/books/NBK591031/#.
168. Westerterp, K. R., "Control of energy expenditure in humans," *European journal of clinical nutrition*, V. 71, No. 3, 2017, pp. 340–344.
169. www.who.int/features/qa/malnutrition/en.
170. Pirlich, M., Schütz, T., Norman, K., Gastell, S., Lübke, H. J., Bischoff, S. C., Bolder, U., Frieling, T., Güldenzoph, H., Hahn, K., Jauch, K.-W., Schindler, K., Stein, J., Volkert, D., Weimann, A., Werner, H., Wolf, C., Zürcher, G., Bauer, P., and Lochs, H., "The German hospital malnutrition study," *Clinical nutrition (Edinburgh, Scotland)*, V. 25, No. 4, 2006, pp. 563–572.
171. Jensen, G. L., Cederholm, T., Correia, M. I. T. D., Gonzalez, M. C., Fukushima, R., Higashiguchi, T., Baptista, G. A. de, Barazzoni, R., Blaauw, R., Coats, A. J. S., Crivelli, A., Evans, D. C., Gramlich, L., Fuchs-Tarlovsky, V., Keller, H., Llido, L., Malone, A., Mogensen, K. M., Morley, J. E., Muscaritoli, M., Nyulasi, I., Pirlich, M., Pisprasert, V., van der Schueren, M. de, Siltharm, S., Singer, P., Tappenden, K. A., Velasco, N., Waitzberg, D. L., Yamwong, P., Yu, J., Compher, C., and van Gossum, A., "GLIM Criteria for the Diagnosis of Malnutrition: A Consensus Report From the Global Clinical Nutrition Community," *JPEN. Journal of Parenteral and Enteral Nutrition*, V. 43, No. 1, 2019, pp. 32–40.
172. Cederholm, T., Barazzoni, R., Austin, P., Ballmer, P., Biolo, G., Bischoff, S. C., Compher, C., Correia, I., Higashiguchi, T., Holst, M., Jensen, G. L., Malone, A., Muscaritoli, M., Nyulasi, I., Pirlich, M., Rothenberg, E., Schindler, K., Schneider, S. M., van der Schueren, M. A. E. de, Sieber, C., Valentini, L., Yu, J. C., van Gossum, A., and Singer, P., "ESPEN guidelines on definitions and terminology of clinical nutrition," *Clinical nutrition (Edinburgh, Scotland)*, V. 36, No. 1, 2017, pp. 49–64.
173. Cruz-Jentoft, A. J., Bahat, G., Bauer, J., Boirie, Y., Bruyère, O., Cederholm, T., Cooper, C., Landi, F., Rolland, Y., Sayer, A. A., Schneider, S. M., Sieber, C. C., Topinkova, E., Vandewoude, M., Visser, M., and Zamboni, M., "Sarcopenia: revised European consensus on definition and diagnosis," *Age and ageing*, V. 48, No. 1, 2019, pp. 16–31.
174. Sayer, A. A., Syddall, H. E., Gilbody, H. J., Dennison, E. M., and Cooper, C., "Does sarcopenia originate in early life? Findings from the Hertfordshire cohort study," *The journals of gerontology. Series A, Biological sciences and medical sciences*, V. 59, No. 9, 2004, M930-4.
175. Dodds, R. M., Syddall, H. E., Cooper, R., Benzeval, M., Deary, I. J., Dennison, E. M., Der, G., Gale, C. R., Inskip, H. M., Jagger, C., Kirkwood, T. B., Lawlor, D. A., Robinson, S. M., Starr, J. M., Steptoe, A., Tilling, K., Kuh, D., Cooper, C., and Sayer, A. A., "Grip

strength across the life course: normative data from twelve British studies," *PloS one*, V. 9, No. 12, 2014, e113637.
176. Sayer, A. A., Syddall, H., Martin, H., Patel, H., Baylis, D., and Cooper, C., "The developmental origins of sarcopenia," *The journal of nutrition, health & aging*, V. 12, No. 7, 2008, pp. 427–432.
177. Mijnarends, D. M., Luiking, Y. C., Halfens, R. J. G., Evers, S. M. A. A., Lenaerts, E. L. A., Verlaan, S., Wallace, M., Schols, J. M. G. A., and Meijers, J. M. M., "Muscle, Health and Costs: A Glance at their Relationship," *The journal of nutrition, health & aging*, V. 22, No. 7, 2018, pp. 766–773.
178. Onishi, S., Shiraki, M., Nishimura, K., Hanai, T., Moriwaki, H., and Shimizu, M., "Prevalence of Sarcopenia and Its Relationship with Nutritional State and Quality of Life in Patients with Digestive Diseases," *Journal of nutritional science and vitaminology*, V. 64, No. 6, 2018, pp. 445–453.
179. Leong, D. P., Teo, K. K., Rangarajan, S., Lopez-Jaramillo, P., Avezum, A., Orlandini, A., Seron, P., Ahmed, S. H., Rosengren, A., Kelishadi, R., Rahman, O., Swaminathan, S., Iqbal, R., Gupta, R., Lear, S. A., Oguz, A., Yusoff, K., Zatonska, K., Chifamba, J., Igumbor, E., Mohan, V., Anjana, R. M., Gu, H., Li, W., and Yusuf, S., "Prognostic value of grip strength: findings from the Prospective Urban Rural Epidemiology (PURE) study," *Lancet (London, England)*, V. 386, No. 9990, 2015, pp. 266–273.
180. Jones, C. J., Rikli, R. E., and Beam, W. C., "A 30-s chair-stand test as a measure of lower body strength in community-residing older adults," *Research quarterly for exercise and sport*, V. 70, No. 2, 1999, pp. 113–119.
181. Beaudart, C., McCloskey, E., Bruyère, O., Cesari, M., Rolland, Y., Rizzoli, R., Araujo de Carvalho, I., Amuthavalli Thiyagarajan, J., Bautmans, I., Bertière, M.-C., Brandi, M. L., Al-Daghri, N. M., Burlet, N., Cavalier, E., Cerreta, F., Cherubini, A., Fielding, R., Gielen, E., Landi, F., Petermans, J., Reginster, J.-Y., Visser, M., Kanis, J., and Cooper, C., "Sarcopenia in daily practice: assessment and management," *BMC geriatrics*, V. 16, No. 1, 2016, p. 170.
182. Mijnarends, D. M., Koster, A., Schols, J. M. G. A., Meijers, J. M. M., Halfens, R. J. G., Gudnason, V., Eiriksdottir, G., Siggeirsdottir, K., Sigurdsson, S., Jónsson, P. V., Meirelles, O., and Harris, T., "Physical activity and incidence of sarcopenia: the population-based AGES-Reykjavik Study," *Age and ageing*, V. 45, No. 5, 2016, pp. 614–620.
183. Periyalwar, P., and Dasarathy, S., "Malnutrition in cirrhosis: contribution and consequences of sarcopenia on metabolic and clinical responses," *Clinics in liver disease*, V. 16, No. 1, 2012, pp. 95–131.
184. Plauth, M., and Schütz, E.-T., "Cachexia in liver cirrhosis," *International journal of cardiology*, V. 85, No. 1, 2002, pp. 83–87.
185. Aqel, B. A., Scolapio, J. S., Dickson, R. C., Burton, D. D., and Bouras, E. P., "Contribution of ascites to impaired gastric function and nutritional intake in patients with cirrhosis and ascites," *Clinical gastroenterology and hepatology : the official clinical practice journal of the American Gastroenterological Association*, V. 3, No. 11, 2005, pp. 1095–1100.

186. Gunnarsdottir, S. A., Sadik, R., Shev, S., Simrén, M., Sjövall, H., Stotzer, P. O., Abrahamsson, H., Olsson, R., and Björnsson, E. S., "Small intestinal motility disturbances and bacterial overgrowth in patients with liver cirrhosis and portal hypertension," *The American journal of gastroenterology*, V. 98, No. 6, 2003, pp. 1362–1370.
187. Send, S. R., "Nutritional Management of Cholestasis," *Clinical Liver Disease*, V. 15, No. 1, 2020, pp. 9–12.
188. Phillips, J. R., Angulo, P., Petterson, T., and Lindor, K. D., "Fat-soluble vitamin levels in patients with primary biliary cirrhosis," *The American journal of gastroenterology*, V. 96, No. 9, 2001, pp. 2745–2750.
189. Cheung, K., Lee, S. S., and Raman, M., "Prevalence and mechanisms of malnutrition in patients with advanced liver disease, and nutrition management strategies," *Clinical gastroenterology and hepatology : the official clinical practice journal of the American Gastroenterological Association*, V. 10, No. 2, 2012, pp. 117–125.
190. Ghufran, A., "Nutrition in Chronic Liver Disease: A Point-of-Care Review," *Nutrition in clinical practice : official publication of the American Society for Parenteral and Enteral Nutrition*, V. 35, No. 2, 2020, pp. 211–217.
191. "EASL Clinical Practice Guidelines on nutrition in chronic liver disease," *Journal of hepatology*, V. 70, No. 1, 2019, pp. 172–193.
192. Meyer, F., and Valentini, L., "Disease-Related Malnutrition and Sarcopenia as Determinants of Clinical Outcome," *Visceral medicine*, V. 35, No. 5, 2019, pp. 282–291.
193. Glass, C., Hipskind, P., Tsien, C., Malin, S. K., Kasumov, T., Shah, S. N., Kirwan, J. P., and Dasarathy, S., "Sarcopenia and a physiologically low respiratory quotient in patients with cirrhosis: a prospective controlled study," *Journal of applied physiology (Bethesda, Md. : 1985)*, V. 114, No. 5, 2013, pp. 559–565.
194. Nosadini, R., Avogaro, A., Mollo, F., Marescotti, C., Tiengo, A., Duner, E., Merkel, C., Gatta, A., Zuin, R., and Kreutzenberg, S. de, "Carbohydrate and lipid metabolism in cirrhosis. Evidence that hepatic uptake of gluconeogenic precursors and of free fatty acids depends on effective hepatic flow," *The Journal of clinical endocrinology and metabolism*, V. 58, No. 6, 1984, pp. 1125–1132.
195. Glass, C., Hipskind, P., Cole, D., Lopez, R., and Dasarathy, S., "Handheld calorimeter is a valid instrument to quantify resting energy expenditure in hospitalized cirrhotic patients: a prospective study," *Nutrition in clinical practice : official publication of the American Society for Parenteral and Enteral Nutrition*, V. 27, No. 5, 2012, pp. 677–688.
196. Tsien, C. D., McCullough, A. J., and Dasarathy, S., "Late evening snack: exploiting a period of anabolic opportunity in cirrhosis," *Journal of gastroenterology and hepatology*, V. 27, No. 3, 2012, pp. 430–441.
197. Owen, O. E., Reichle, F. A., Mozzoli, M. A., Kreulen, T., Patel, M. S., Elfenbein, I. B., Golsorkhi, M., Chang, K. H., Rao, N. S., Sue, H. S., and Boden, G., "Hepatic, gut, and renal substrate flux rates in patients with hepatic cirrhosis," *The Journal of clinical investigation*, V. 68, No. 1, 1981, pp. 240–252.
198. Landau, B. R., Schumann, W. C., Chandramouli, V., Magnusson, I., Kumaran, K., and Wahren, J., "14C-labeled propionate metabolism in vivo and estimates of hepatic

gluconeogenesis relative to Krebs cycle flux," *The American journal of physiology*, V. 265, 4 Pt 1, 1993, E636-47.

199. Dasarathy, S., and Hatzoglou, M., "Hyperammonemia and proteostasis in cirrhosis," *Current opinion in clinical nutrition and metabolic care*, V. 21, No. 1, 2018, pp. 30–36.

200. Davuluri, G., Allawy, A., Thapaliya, S., Rennison, J. H., Singh, D., Kumar, A., Sandlers, Y., van Wagoner, D. R., Flask, C. A., Hoppel, C., Kasumov, T., and Dasarathy, S., "Hyperammonaemia-induced skeletal muscle mitochondrial dysfunction results in cataplerosis and oxidative stress," *The Journal of physiology*, V. 594, No. 24, 2016, pp. 7341–7360.

201. Holecek, M., Kandar, R., Sispera, L., and Kovarik, M., "Acute hyperammonemia activates branched-chain amino acid catabolism and decreases their extracellular concentrations: different sensitivity of red and white muscle," *Amino acids*, V. 40, No. 2, 2011, pp. 575–584.

202. Dam, G., Ott, P., Aagaard, N. K., and Vilstrup, H., "Branched-chain amino acids and muscle ammonia detoxification in cirrhosis," *Metabolic brain disease*, V. 28, No. 2, 2013, pp. 217–220.

203. Qiu, J., Thapaliya, S., Runkana, A., Yang, Y., Tsien, C., Mohan, M. L., Narayanan, A., Eghtesad, B., Mozdziak, P. E., McDonald, C., Stark, G. R., Welle, S., Naga Prasad, S. V., and Dasarathy, S., "Hyperammonemia in cirrhosis induces transcriptional regulation of myostatin by an NF-κB-mediated mechanism," *Proceedings of the National Academy of Sciences of the United States of America*, V. 110, No. 45, 2013, pp. 18162–18167.

204. Davuluri, G., Krokowski, D., Guan, B.-J., Kumar, A., Thapaliya, S., Singh, D., Hatzoglou, M., and Dasarathy, S., "Metabolic adaptation of skeletal muscle to hyperammonemia drives the beneficial effects of l-leucine in cirrhosis," *Journal of hepatology*, V. 65, No. 5, 2016, pp. 929–937.

205. La Garza, R. G. de, Morales-Garza, L. A., Martin-Estal, I., and Castilla-Cortazar, I., "Insulin-Like Growth Factor-1 Deficiency and Cirrhosis Establishment," *Journal of clinical medicine research*, V. 9, No. 4, 2017, pp. 233–247.

206. Schiaffino, S., Dyar, K. A., Ciciliot, S., Blaauw, B., and Sandri, M., "Mechanisms regulating skeletal muscle growth and atrophy," *The FEBS journal*, V. 280, No. 17, 2013, pp. 4294–4314.

207. Retamales, A., Zuloaga, R., Valenzuela, C. A., Gallardo-Escarate, C., Molina, A., and Valdés, J. A., "Insulin-like growth factor-1 suppresses the Myostatin signaling pathway during myogenic differentiation," *Biochemical and biophysical research communications*, V. 464, No. 2, 2015, pp. 596–602.

208. Adamek, A., and Kasprzak, A., "Insulin-Like Growth Factor (IGF) System in Liver Diseases," *International journal of molecular sciences*, V. 19, No. 5, 2018.

209. Onori, P., Alvaro, D., Floreani, A. R., Mancino, M. G., Franchitto, A., Guido, M., Carpino, G., Santis, A. de, Angelico, M., Attili, A. F., and Gaudio, E., "Activation of the IGF1 system characterizes cholangiocyte survival during progression of primary biliary cirrhosis," *The journal of histochemistry and cytochemistry : official journal of the Histochemistry Society*, V. 55, No. 4, 2007, pp. 327–334.

210. Ehlers, L., Netz, L. A. W., Reiner, J., Berlin, P., Bannert, K., Bastian, M., Zechner, D., Lamprecht, G., and Jaster, R., "Effects of Bile Duct Ligation and Ghrelin Treatment on

the Colonic Barrier and Microbiome of Mice," *Pharmacology*, V. 107, 11-12, 2022, pp. 564–573.
211. Guidotti, S., Meijer, H. A. J., and van Dijk, G., "Validity of the doubly labeled water method for estimating CO2 production in mice under different nutritional conditions," *American journal of physiology. Endocrinology and metabolism*, V. 305, No. 3, 2013, E317-24.
212. Junghans, P., Görs, S., Langhammer, M., and Metges, C. C., "Breath water-based doubly labelled water method for the noninvasive determination of CO2 production and energy expenditure in mice," *Isotopes in environmental and health studies*, V. 54, No. 6, 2018, pp. 561–572.
213. Lifson, N., "Theory of use of the turnover rates of body water for measuring energy and material balance," *Journal of theoretical biology*, V. 12, No. 1, 1966, pp. 46–74.
214. Blaxter KL, editor. Energy metabolism, : Proceedings of the 3rd symposium held at Troon, Scotland, May 1964. European Association for Animal Production. Publication, no. 11. London, New York: Academic Press, and 1965, eds.
215. Brack, A. S., Bildsoe, H., and Hughes, S. M., "Evidence that satellite cell decrement contributes to preferential decline in nuclear number from large fibres during murine age-related muscle atrophy," *Journal of cell science*, V. 118, Pt 20, 2005, pp. 4813–4821.
216. Marzetti, E., Privitera, G., Simili, V., Wohlgemuth, S. E., Aulisa, L., Pahor, M., and Leeuwenburgh, C., "Multiple pathways to the same end: mechanisms of myonuclear apoptosis in sarcopenia of aging," *TheScientificWorldJournal*, V. 10, 2010, pp. 340–349.
217. Kuhla, B., Kucia, M., Görs, S., Albrecht, D., Langhammer, M., Kuhla, S., and Metges, C. C., "Effect of a high-protein diet on food intake and liver metabolism during pregnancy, lactation and after weaning in mice," *Proteomics*, V. 10, No. 14, 2010, pp. 2573–2588.
218. Cross, K. M., Granados, J. Z., Have, G. A. M. ten, Thaden, J. J., Engelen, M. P. K. J., Lightfoot, J. T., and Deutz, N. E. P., "Protein fractional synthesis rates within tissues of high- and low-active mice," *PloS one*, V. 15, No. 11, 2020.
219. Dänicke, S., Goyarts, T., Döll, S., Grove, N., Spolders, M., and Flachowsky, G., "Effects of the Fusarium toxin deoxynivalenol on tissue protein synthesis in pigs," *Toxicology letters*, V. 165, No. 3, 2006, pp. 297–311.
220. Welle, S., Bhatt, K., and Pinkert, C. A., "Myofibrillar protein synthesis in myostatin-deficient mice," *American journal of physiology. Endocrinology and metabolism*, V. 290, No. 3, 2006, E409-15.
221. Marini, J. C., and Didelija, I. C., "Arginine depletion by arginine deiminase does not affect whole protein metabolism or muscle fractional protein synthesis rate in mice," *PloS one*, V. 10, No. 3, 2015, e0119801.
222. Zhao, Y., Albrecht, E., Sciascia, Q. L., Li, Z., Görs, S., Schregel, J., Metges, C. C., and Maak, S., "Effects of Oral Glutamine Supplementation on Early Postnatal Muscle Morphology in Low and Normal Birth Weight Piglets," *Animals : an open access journal from MDPI*, V. 10, No. 11, 2020.
223. Bustin, S. A., Benes, V., Garson, J. A., Hellemans, J., Huggett, J., Kubista, M., Mueller, R., Nolan, T., Pfaffl, M. W., Shipley, G. L., Vandesompele, J., and Wittwer, C.

T., “The MIQE guidelines: minimum information for publication of quantitative real-time PCR experiments,” *Clinical chemistry*, V. 55, No. 4, 2009, pp. 611–622.
224. Agrifoglio, O., Görs, S., Sciascia, Q., Li, Z., Albrecht, E., Achilles, S., Statz, M., Bastian, M., Lindner, T., Gauß, K. F., Rohde, S., Rischmüller, K., Berlin, P., Lamprecht, G., Jaster, R., Metges, C. C., and Ehlers, L., “Changes in Protein Metabolism and Early Development of Sarcopenia in Mice With Cholestatic Liver Disease,” *Journal of cachexia, sarcopenia and muscle*, V. 16, No. 1, 2025, e13737.
225. Byrne, C. A., McNeil, A. T., Koh, T. J., Brunskill, A. F., and Fantuzzi, G., “Expression of genes in the skeletal muscle of individuals with cachexia/sarcopenia: A systematic review,” *PloS one*, V. 14, No. 9, 2019, e0222345.
226. Baig, M. H., Ahmad, K., Moon, J. S., Park, S.-Y., Ho Lim, J., Chun, H. J., Qadri, A. F., Hwang, Y. C., Jan, A. T., Ahmad, S. S., Ali, S., Shaikh, S., Lee, E. J., and Choi, I., “Myostatin and its Regulation: A Comprehensive Review of Myostatin Inhibiting Strategies,” *Frontiers in physiology*, V. 13, 2022, p. 876078.
227. Glass, D. J., “PI3 kinase regulation of skeletal muscle hypertrophy and atrophy,” *Current topics in microbiology and immunology*, V. 346, 2010, pp. 267–278.
228. Bocca, C., Novo, E., Miglietta, A., and Parola, M., “Angiogenesis and Fibrogenesis in Chronic Liver Diseases,” *Cellular and molecular gastroenterology and hepatology*, V. 1, No. 5, 2015, pp. 477–488.
229. Ebadi, M., Bhanji, R. A., Mazurak, V. C., and Montano-Loza, A. J., “Sarcopenia in cirrhosis: from pathogenesis to interventions,” *Journal of gastroenterology*, V. 54, No. 10, 2019, pp. 845–859.
230. Onofrio, F. Q., and Hirschfield, G. M., “The Pathophysiology of Cholestasis and Its Relevance to Clinical Practice,” *Clinical Liver Disease*, V. 15, No. 3, 2020, pp. 110–114.
231. O'Brien, A., China, L., Massey, K. A., Nicolaou, A., Winstanley, A., Newson, J., Hobbs, A., Audzevich, T., and Gilroy, D. W., “Bile duct-ligated mice exhibit multiple phenotypic similarities to acute decompensation patients despite histological differences,” *Liver international : official journal of the International Association for the Study of the Liver*, V. 36, No. 6, 2016, pp. 837–846.
232. Kaplan, M. M., and Righetti, A., “Induction of rat liver alkaline phosphatase: the mechanism of the serum elevation in bile duct obstruction,” *The Journal of clinical investigation*, V. 49, No. 3, 1970, pp. 508–516.
233. Li, T., and Apte, U., “Bile Acid Metabolism and Signaling in Cholestasis, Inflammation, and Cancer,” *Advances in pharmacology (San Diego, Calif.)*, V. 74, 2015, pp. 263–302.
234. Nemes, K., Åberg, F., Gylling, H., and Isoniemi, H., “Cholesterol metabolism in cholestatic liver disease and liver transplantation: From molecular mechanisms to clinical implications,” *World Journal of Hepatology*, V. 8, No. 22, 2016, pp. 924–932.
235. Maxfield, F. R., and van Meer, G., “Cholesterol, the central lipid of mammalian cells,” *Current opinion in cell biology*, V. 22, No. 4, 2010, pp. 422–429.
236. Russell, D. W., “The enzymes, regulation, and genetics of bile acid synthesis,” *Annual review of biochemistry*, V. 72, 2003, pp. 137–174.
237. Perez, M.-J., and Briz, O., “Bile-acid-induced cell injury and protection,” *World Journal of Gastroenterology : WJG*, V. 15, No. 14, 2009, pp. 1677–1689.

238. Liu, Z., Zhang, Z., Huang, M., Sun, X., Liu, B., Guo, Q., Chang, Q., and Duan, Z., "Taurocholic acid is an active promoting factor, not just a biomarker of progression of liver cirrhosis: evidence from a human metabolomic study and in vitro experiments," *BMC gastroenterology*, V. 18, No. 1, 2018, p. 112.
239. Paridaens, A., Raevens, S., Devisscher, L., Bogaerts, E., Verhelst, X., Hoorens, A., van Vlierberghe, H., van Grunsven, L. A., Geerts, A., and Colle, I., "Modulation of the Unfolded Protein Response by Tauroursodeoxycholic Acid Counteracts Apoptotic Cell Death and Fibrosis in a Mouse Model for Secondary Biliary Liver Fibrosis," *International journal of molecular sciences*, V. 18, No. 1, 2017.
240. Baiocchi, L., Alpini, G., Glaser, S., Angelico, M., Alvaro, D., Francis, H., Marzioni, M., Phinizy, J. L., Barbaro, B., and LeSage, G., "Taurohyodeoxycholate- and tauroursodeoxycholate-induced hypercholeresis is augmented in bile duct ligated rats," *Journal of hepatology*, V. 38, No. 2, 2003, pp. 136–147.
241. Kinoshita, T., Hirao, S., Matsumoto, K., and Nakamura, T., "Possible endocrine control by hepatocyte growth factor of liver regeneration after partial hepatectomy," *Biochemical and biophysical research communications*, V. 177, No. 1, 1991, pp. 330–335.
242. Ishiki, Y., Ohnishi, H., Muto, Y., Matsumoto, K., and Nakamura, T., "Direct evidence that hepatocyte growth factor is a hepatotrophic factor for liver regeneration and has a potent antihepatitis effect in vivo," *Hepatology (Baltimore, Md.)*, V. 16, No. 5, 1992, pp. 1227–1235.
243. Thuluvath, P. J., and Triger, D. R., "Autonomic neuropathy and chronic liver disease," *The Quarterly journal of medicine*, V. 72, No. 268, 1989, pp. 737–747.
244. Quigley, E. M., "Gastrointestinal dysfunction in liver disease and portal hypertension. Gut-liver interactions revisited," *Digestive diseases and sciences*, V. 41, No. 3, 1996, pp. 557–561.
245. Wolfe, R. R., "The underappreciated role of muscle in health and disease," *The American journal of clinical nutrition*, V. 84, No. 3, 2006, pp. 475–482.
246. Gangitano, E., Gnessi, L., and Merli, M., "Protein Catabolism and the Dysregulation of Energy Intake-Related Hormones May Play a Major Role in the Worsening of Malnutrition in Hospitalized Cirrhotic Patients," *Livers*, V. 2, No. 3, 2022, pp. 158–170.
247. Houdijk, A. P., Teerlink, T., Visser, J. J., van Lambalgen, A. A., and van Leeuwen, P. A., "Arginine deficiency in bile duct-ligated rats after surgery: the role of plasma arginase and gut endotoxin restriction," *Gastroenterology*, V. 113, No. 4, 1997, pp. 1375–1383.
248. Li, J., and Billiar, T. R., "Nitric Oxide. IV. Determinants of nitric oxide protection and toxicity in liver," *The American journal of physiology*, V. 276, No. 5, 1999, G1069-73.
249. Iwakiri, Y., and Kim, M. Y., "Nitric oxide in liver diseases," *Trends in pharmacological sciences*, V. 36, No. 8, 2015, pp. 524–536.
250. Tateya, S., Rizzo, N. O., Handa, P., Cheng, A. M., Morgan-Stevenson, V., Daum, G., Clowes, A. W., Morton, G. J., Schwartz, M. W., and Kim, F., "Endothelial NO/cGMP/VASP signaling attenuates Kupffer cell activation and hepatic insulin resistance induced by high-fat feeding," *Diabetes*, V. 60, No. 11, 2011, pp. 2792–2801.
251. Houdijk, A. P. J., Oosterling, S. J., Siroen, M. P. C., Jong, S. de, Richir, M., Rijssenbeek, A. L., Teerlink, T., and van Leeuwen, P. A. M., "Hypertaurinemia in bile

duct-ligated rats after surgery: the effect of gut endotoxin restriction on organ fluxes and oxidative status," *JPEN. Journal of Parenteral and Enteral Nutrition*, V. 30, No. 3, 2006, pp. 186–193.

252. Meyer, F., Bannert, K., Wiese, M., Esau, S., Sautter, L. F., Ehlers, L., Aghdassi, A. A., Metges, C. C., Garbe, L.-A., Jaster, R., Lerch, M. M., Lamprecht, G., and Valentini, L., "Molecular Mechanism Contributing to Malnutrition and Sarcopenia in Patients with Liver Cirrhosis," *International journal of molecular sciences*, V. 21, No. 15, 2020.
253. Kurosawa, T., Goto, M., Kaji, N., Aikiyo, S., Mihara, T., Ikemoto-Uezumi, M., Toyoda, M., Kanazawa, N., Nakazawa, T., Hori, M., and Uezumi, A., "Liver fibrosis-induced muscle atrophy is mediated by elevated levels of circulating TNFα," *Cell death & disease*, V. 12, No. 1, 2021, p. 11.
254. Wilkes, E. A., Selby, A. L., Atherton, P. J., Patel, R., Rankin, D., Smith, K., and Rennie, M. J., "Blunting of insulin inhibition of proteolysis in legs of older subjects may contribute to age-related sarcopenia," *The American journal of clinical nutrition*, V. 90, No. 5, 2009, pp. 1343–1350.
255. Poole, D. C., Kano, Y., Koga, S., and Musch, T. I., "August Krogh: Muscle capillary function and oxygen delivery," *Comparative biochemistry and physiology. Part A, Molecular & integrative physiology*, V. 253, 2021, p. 110852.
256. Prior, S. J., Ryan, A. S., Blumenthal, J. B., Watson, J. M., Katzel, L. I., and Goldberg, A. P., "Sarcopenia Is Associated With Lower Skeletal Muscle Capillarization and Exercise Capacity in Older Adults," *The journals of gerontology. Series A, Biological sciences and medical sciences*, V. 71, No. 8, 2016, pp. 1096–1101.
257. Cramer, A. A. W., Prasad, V., Eftestøl, E., Song, T., Hansson, K.-A., Dugdale, H. F., Sadayappan, S., Ochala, J., Gundersen, K., and Millay, D. P., "Nuclear numbers in syncytial muscle fibers promote size but limit the development of larger myonuclear domains," *Nature communications*, V. 11, No. 1, 2020, p. 6287.
258. Hall, Z. W., and Ralston, E., "Nuclear domains in muscle cells," *Cell*, V. 59, No. 5, 1989, pp. 771–772.
259. Pavlath, G. K., Rich, K., Webster, S. G., and Blau, H. M., "Localization of muscle gene products in nuclear domains," *Nature*, V. 337, No. 6207, 1989, pp. 570–573.
260. Alway, S. E., and Siu, P. M., "Nuclear apoptosis contributes to sarcopenia," *Exercise and sport sciences reviews*, V. 36, No. 2, 2008, pp. 51–57.
261. Elia, M., Carter, A., Bacon, S., Winearls, C. G., and Smith, R., "Clinical usefulness of urinary 3-methylhistidine excretion in indicating muscle protein breakdown," *British medical journal (Clinical research ed.)*, V. 282, No. 6261, 1981, pp. 351–354.
262. Young, V. R., and Munro, H. N., "Ntau-methylhistidine (3-methylhistidine) and muscle protein turnover: an overview," *Federation proceedings*, V. 37, No. 9, 1978, pp. 2291–2300.
263. Bates, P. C., Grimble, G. K., Sparrow, M. P., and Millward, D. J., "Myofibrillar protein turnover. Synthesis of protein-bound 3-methylhistidine, actin, myosin heavy chain and aldolase in rat skeletal muscle in the fed and starved states," *The Biochemical journal*, V. 214, No. 2, 1983, pp. 593–605.
264. Nishizawa, N., Shimbo, M., Hareyama, S., and Funabiki, R., "Fractional catabolic rates of myosin and actin estimated by urinary excretion of Ntau-methylhistidine: the

effect of dietary protein level on catabolic rates under conditions of restricted food intake," *The British journal of nutrition*, V. 37, No. 3, 1977, pp. 345–353.
265. Warskulat, U., Flögel, U., Jacoby, C., Hartwig, H.-G., Thewissen, M., Merx, M. W., Molojavyi, A., Heller-Stilb, B., Schrader, J., and Häussinger, D., "Taurine transporter knockout depletes muscle taurine levels and results in severe skeletal muscle impairment but leaves cardiac function uncompromised," *FASEB journal : official publication of the Federation of American Societies for Experimental Biology*, V. 18, No. 3, 2004, pp. 577–579.
266. Barbul, A., "Arginine: biochemistry, physiology, and therapeutic implications," *JPEN. Journal of Parenteral and Enteral Nutrition*, V. 10, No. 2, 1986, pp. 227–238.
267. Stamler, J. S., and Meissner, G., "Physiology of nitric oxide in skeletal muscle," *Physiological reviews*, V. 81, No. 1, 2001, pp. 209–237.
268. Gumucio, J. P., and Mendias, C. L., "Atrogin-1, MuRF-1, and sarcopenia," *Endocrine*, V. 43, No. 1, 2013, pp. 12–21.
269. Peris-Moreno, D., Taillandier, D., and Polge, C., "MuRF1/TRIM63, Master Regulator of Muscle Mass," *International journal of molecular sciences*, V. 21, No. 18, 2020.
270. Ruiz-Margáin, A., Pohlmann, A., Lanzerath, S., Langheinrich, M., Campos-Murguía, A., Román-Calleja, B. M., Schierwagen, R., Klein, S., Uschner, F. E., Brol, M. J., Torre-Delgadillo, A., Flores-García, N. C., Praktiknjo, M., Macías Rodríguez, R. U., and Trebicka, J., "Myostatin is associated with the presence and development of acute-on-chronic liver failure," *JHEP reports : innovation in hepatology*, V. 5, No. 8, 2023, p. 100761.
271. Schiaffino, S., and Mammucari, C., "Regulation of skeletal muscle growth by the IGF1-Akt/PKB pathway: insights from genetic models," *Skeletal muscle*, V. 1, No. 1, 2011, p. 4.
272. Higuchi, H., and Gores, G. J., "Bile acid regulation of hepatic physiology: IV. Bile acids and death receptors," *American journal of physiology. Gastrointestinal and liver physiology*, V. 284, No. 5, 2003, G734-8.
273. Tiegs, G., and Horst, A. K., "TNF in the liver: targeting a central player in inflammation," *Seminars in immunopathology*, V. 44, No. 4, 2022, pp. 445–459.
274. Küsters, S., Tiegs, G., Alexopoulou, L., Pasparakis, M., Douni, E., Künstle, G., Bluethmann, H., Wendel, A., Pfizenmaier, K., Kollias, G., and Grell, M., "In vivo evidence for a functional role of both tumor necrosis factor (TNF) receptors and transmembrane TNF in experimental hepatitis," *European journal of immunology*, V. 27, No. 11, 1997, pp. 2870–2875.
275. Schümann, J., Mühlen, K., Kiemer, A. K., Vollmar, A. M., and Tiegs, G., "Parenchymal, but not leukocyte, TNF receptor 2 mediates T cell-dependent hepatitis in mice," *Journal of immunology (Baltimore, Md. : 1950)*, V. 170, No. 4, 2003, pp. 2129–2137.
276. Hunter, C. A., and Jones, S. A., "IL-6 as a keystone cytokine in health and disease," *Nature immunology*, V. 16, No. 5, 2015, pp. 448–457.
277. Johnson, D. E., O'Keefe, R. A., and Grandis, J. R., "Targeting the IL-6/JAK/STAT3 signalling axis in cancer," *Nature reviews. Clinical oncology*, V. 15, No. 4, 2018, pp. 234–248.

278. Bautz, F., Rafii, S., Kanz, L., and Möhle, R., "Expression and secretion of vascular endothelial growth factor-A by cytokine-stimulated hematopoietic progenitor cells. Possible role in the hematopoietic microenvironment," *Experimental hematology*, V. 28, No. 6, 2000, pp. 700–706.
279. Elpek, G. Ö., "Angiogenesis and liver fibrosis," *World Journal of Hepatology*, V. 7, No. 3, 2015, pp. 377–391.
280. Fernández, M., Semela, D., Bruix, J., Colle, I., Pinzani, M., and Bosch, J., "Angiogenesis in liver disease," *Journal of hepatology*, V. 50, No. 3, 2009, pp. 604–620.
281. Dirchwolf, M., and Ruf, A. E., "Role of systemic inflammation in cirrhosis: From pathogenesis to prognosis," *World Journal of Hepatology*, V. 7, No. 16, 2015, pp. 1974–1981.
282. Gautron, L., and Layé, S., "Neurobiology of inflammation-associated anorexia," *Frontiers in neuroscience*, V. 3, 2009, p. 59.
283. Nilsson, A., Wilhelms, D. B., Mirrasekhian, E., Jaarola, M., Blomqvist, A., and Engblom, D., "Inflammation-induced anorexia and fever are elicited by distinct prostaglandin dependent mechanisms, whereas conditioned taste aversion is prostaglandin independent," *Brain, behavior, and immunity*, V. 61, 2017, pp. 236–243.
284. Bilodeau, P. A., Coyne, E. S., and Wing, S. S., "The ubiquitin proteasome system in atrophying skeletal muscle: roles and regulation," *American journal of physiology. Cell physiology*, V. 311, No. 3, 2016, C392-403.

# 8 APPENDIX

## 8.1 Abbreviations

| | |
|---|---|
| **µL** | Microliter |
| **µM** | Micromolar |
| **µm** | Micrometre |
| **1-MH** | 3-methyl-histidine |
| **2H5-Phe** | 2H5-ring-phenylalanine |
| **3-MH** | 1-methyl-histidine |
| **AA** | Amino acid |
| **ADP** | Adenosine diphosphate |
| **AEE** | Activity-induced energy expenditure |
| **Akt1** | AKT Serine/Threonine Kinase 1 |
| **ALAT** | Alanine aminotransferase |
| **AP** | Alkaline phosphatase |
| **ASAT** | Aspartate aminotransferase |
| **ATP** | Adenosine triphosphate |
| **B2M** | Beta-2-Microglobulin |
| **BCAA** | Branched chain amino acids |
| **BDL** | Bile duct ligation |
| **BW** | Body weight |
| **Ca** | Calcium |
| **CA** | Cholic acid |
| **cDNA** | Complementary DNA |
| **CK** | Creatinkinase |
| **CLD** | Cholestatic liver disease |
| **Cq** | Cycle numbers |
| **CV** | Coefficient of variation |
| **CYP7A1** | Cholesterol 7alpha-hydroxylase |
| **DAMP** | damage-associated molecular patterns |
| **DEE** | Diet-induced energy expenditure |
| **DNA** | deoxyribonucleic acid |
| **DNA** | Deoxyribonucleic acid |
| **ECM** | Extra cellular matrix |
| **EGF** | Epithelial growth factor |
| **EGFR** | Epithelial growth factor receptor |
| **eIF2** | eukaryotic initiation factor 2 |
| **ELISA** | Enzyme-linked immunosorbent assay |
| **FA** | Fatty acids |
| **Fbxo32** | F-Box Protein 32 |
| **FFM** | Free fat mass |
| **FGF-21** | Fibroblast growth factor 21 |
| **Fox0** | Forkhead box 0 proteins |
| **FPSR** | Fractional protein synthesis rate |

| | |
|---|---|
| **G** | Gram |
| **G6P** | Glucose 6 phosphate |
| **GCA** | Glycocholic acid |
| **GC-MS** | Gas chromatography mass spectrometry |
| **GDF-8** | Growth differentiation factor 8 |
| **H/E** | Haematoxylin/Eosin |
| **HGF** | Hepatocyte growth factor |
| **HPLC** | High pressure liquid chromatography |
| **HSC** | Hepatic stellate cells |
| **IGF-1** | Insulin-like growth factor-1 |
| **Igf1r** | Insulin Like Growth Factor 1 Receptor |
| **Igfbp3** | Insulin Like Growth Factor Binding Protein 3 |
| **Igfbp5** | Insulin Like Growth Factor Binding Protein 5 |
| **IGFBP-x** | Insulin-like growth factor binding protein-x |
| **IL-x** | Interleukin-x |
| **INF- γ** | Interferon-γ |
| **Irs1** | Insulin Receptor Substrate 1 |
| **Kg** | Kilograms |
| **Kg** | Kilogram |
| **LC** | Liver cirrhosis |
| **LC** | Liquid chromatography |
| **MC** | Metabolic cage |
| **Mg** | Milligram |
| **Mg** | Magnesium |
| **Min** | Minute |
| **MIQE** | Minimum Information for Publication of Quantitative Real-Time PCR Experiments |
| **mL** | Millilitre |
| **MPE** | Mole percent excess |
| **MRI** | Magnetic resonance imaging |
| **mRNA** | Messenger ribonucleic acid |
| **MS** | Mass spectrometry |
| **Mstn** | Myostatin |
| **MTBSTFA** | N-methyl-N-(tert-butyldimethylsilyl)trifluoroacetamide |
| **mTOR** | Mammalian target of rapamycin |
| **MuRF1** | Muscle RING-finger protein-1 |
| **N** | Nitrogen |
| **Na** | Sodium |
| **NADPH** | Nicotinamide adenine dinucleotide phosphate |
| **NAFLD** | Non-alcoholic fatty liver disease |
| **NASH** | Non-alcoholic steatohepatitis |
| **N-BAL** | Nitrogen balance |
| **NEFA** | Non-esterified fatty acids |
| **NK** | Natural killer cells |
| **NKT** | T-killer cells |
| **PAMP** | pathogen-associated molecular pattern |

| | |
|---|---|
| **PBC** | Primary biliary cholangitis |
| **PCHE** | Pseudo-cholinesterase |
| **PF** | portal fibroblasts |
| **Pik3r1** | Phosphoinositide-3-Kinase Regulatory Subunit 1 |
| **Polr2a** | RNA Polymerase II Subunit A |
| **Ppia** | Peptidylprolyl Isomerase A |
| **PSC** | primary sclerosing cholangitis |
| **q-RT PCR** | Quantitative real time polymerase chain reaction |
| **REE** | Resting energy expenditure |
| **RNA** | Ribonucleic acid |
| **Rplp0** | Ribosomal Protein Lateral Stalk Subunit P0 |
| **SIRS** | systemic inflammatory response syndrome |
| **SREBP** | sterol regulator binding protein |
| **TCA** | Taurocholic acid |
| **TCDA** | Tauroursodeoxycholic acid |
| **TEE** | Total energy expenditure |
| **TG** | Triglycerides |
| **TGFβ** | Transforming Growth Factor β |
| **TGR5** | Takeda G protein-coupled receptor 5 |
| **TierSchG** | Tierschutzgesetz |
| **TNF** | Tumour necrosis factor |
| **TNFR-x** | Tumour necrosis factor receptor-x |
| **Trim63** | Tripartite Motif Containing 63 |
| **UA** | Uric Acid |
| **UBB** | Ubiquitin B |
| **UDCA** | ursodeoxycholic acid |
| **VEGF** | Vascular endothelial growth |

## 8.2 Table content

## 8.3 Figure content

## 8.4 Materials and methods

| Product | Manufacturer | Catalog number |
|---|---|---|
| 0.2 µm sterilized NALGENE® 4 mm nylon syringe filter | Thermo Scientific, Fisher Scientific GmbH, Schwerte, Germany | 10353291 |
| 0.2 tubes | Eppendorf AG, Hamburg, Germany | 951010006 |
| 0.5 mL tubes | Sarstedt AG und Co.KG, Nürmbrecht, Germany | 72.699 |
| 0.9% NaCl | Merck KGaA, Darmstadt, Germany | 3957.1 |
| 1 mL syringes | B BRAUN Melsungen, Germany | 9161406 |
| 1.5 mL tubes | Sarstedt AG und Co.KG Nürmbrecht, Germany | 72.690.001 |
| 15 mL tubes | Sigma-Aldrich | CLS430055 |
| 2 mL tubes | Eppendorf AG, Hamburg, Germany | 0030120094 |
| $^{2}H_{2}O$ (99.8 atom% $^{2}H$) | Chemotrade, Leipzig, Germany | 116A73 |
| $^{2}H_{5}$-ring-phenylalanine | Euriso-Top GmbH, Saarbrücken, Germany | IND625P-GMPB041A |
| 5-0 polyester suture thread | Ethicon, Norderstedt, Germany | 1721373 |
| 6-0 prolene suture thread | Catgut, Markneukirchen, Germany | 17403100 |
| 7 Tesla MRI machine | Bruker Biospin GmbH, Ettlingen, Germany | BioSpec 70/30 und 94/30 \| Bruker |
| 70% ethanol (absolute ethanol diluted in distilled water) | WALTER CMP GmbH & Co KG | 603-002-00-5 |
| 96% ethanol | WALTER CMP GmbH & Co KG | 603-002-00-5 |
| Absolute ethanol | WALTER CMP GmbH & Co KG | 603-002-00-5 |
| ABX Pentra 400 Clinical Chemistry Analyser | Horiba medical, Montpellier, France | RAB125IEN |
| ABX Pentra CK NAC CP | Horiba medical, Montpellier, France | A11A01632 |
| Acetic Acid | J.T.Baker, Schwerte, Germany | 6052 |
| Allantoin standard | Sigma Aldrich | A-7878 |
| Bioanalyzer 2100 | Agilent Technologies, Waldbronn, Germany | G2939BA |
| Biocrates MetIDQ software | BIOCRATES LifeSciences AG, Innsbruck, Austria | - |
| BIO-GS3 grip strength meter | Bioseb, Vitrolles, France | BIO-GS3 |

| | | |
|---|---|---|
| Cell^F imaging software | OSIS, Münster, Germany | - |
| Creatine standard | Chemapol GmbH Frankfurt, Germany | 91705 |
| Creatinine standard | Chemapol GmbH Frankfurt, Germany | 91703 |
| Cryostat microtome CM3050 S | Leica, Bensheim, Germany | 210137 |
| Elemental analyser | Thermo-Fisher Scientific GmbH, Waltham, MA, USA | 11206100 |
| Eosin | Medite GmbH | 13017-0100 |
| Filter Tips (0.1-1000 µL) | Eppendorf AG, Hamburg, Germany | 0030078691 |
| Freezer (-20 °C) | Phillipp Kirsch GmbH Offenburg, Germany | Froster-Labex®-95 |
| Freezer (-80 °C) | SANYO Electric Co., Ltd., Japan | MDF-U73V |
| G1311C 1260 quaternary pump | Agilent Technologies, Waldbronn, Germany | G7111B |
| G1312A binary pump | Agilent Technologies, Waldbronn Germany | DE63060036 |
| G1316A thermostated column compartment | Agilent Technologies, Waldbronn Germany | DE63071068 |
| G1321A fluorescence detector | Agilent Technologies, Waldbronn Germany | DE60557927 |
| G1362A 1260 refractive index detector | Agilent Technologies, Waldbronn, Germany | G7162A |
| G1379B degasser | Agilent Technologies, Waldbronn Germany | JP82008681 |
| G7112B binary pump | Agilent Technologies, Germany | DEAGO01783 |
| G7116A multicolumn thermostat | Agilent Technologies, Germany | DEAEM02800 |
| G7129A autosampler | Agilent Technologies, Germany | DEAEQ11354 |
| Gas bench | GasBench II, Finnigan, Bremen, Germany | 111 83 42 |
| Gas isotope ratio mass spectrometer | DELTA Plus XL, Thermo Quest, Bremen, Germany | IQLAAEGAATFABHMZZZ |
| GCMS solution software | Shimadzu, Japan | - |
| GC-MS-QP2010 Ultra | Shimadzu, Kyoto, Japan | 20525076083 |
| GDF-8/Myostatin Quantikine ELISA kit | R&D Systems Inc., Minneapolis, USA | DGDF80 |
| GraphPad Software, version 9.4.1 | San Diego, CA, USA | - |
| $H_2{}^{18}O$ (97 atom% $^{18}O$) | Eurisotop, Paris, France | OLM-240-10G |
| $H_2SO_4$ | Honeywell Charlotte, North Carolina, USA | 30743 |
| $HClO_4$ | Merck Chemicals GmbH Darmstadt, Germany | 1005190510 |

| | | |
|---|---|---|
| Heating block | Techne, Cole-Parmer®, Staffordshire, UK | 10325804 |
| Haematoxylin | Medite GmbH | |
| Hippuric acid standard | Berlin Chemie, Menarini | 71796 |
| HP ChemStation software | Agilent Technologies, Waldbronn, Germany | - |
| ITK-Snap software (version 3.8.0) | PICSL, University of Pennsylvania, USA | - |
| Ketamine 550mg/10mL | Ratiopharm GmbH | 7538814 |
| LC 96 system | Roche Diagnostics, Mannheim, Germany | 5815916001 |
| LC Open Lab software | Agilent Technologies, Waldbronn, Germany | - |
| Luminex 100/200 | Luminex Corporate, Austin, USA | APX10031 |
| Metabolic cages | TECNIPLAST GmbH, Hohenpeißenberg, Germany | 01-814-25 |
| Metamizol | Ratiopharm GmbH, Ulm, Germany | 3530394 |
| Microcentrifuge | Thermo-Fisher Scientific GmbH, Waltham, MA, USA | 10196832 |
| Microscope cover slips | Paul Marienfeld GmbH&Co.KG | 107222 |
| Microscope slides | Paul Marienfeld GmbH&Co.KG | 810000 |
| Mikrovette® 500 LH (Lithium heparin) | Sarstedt AG und Co.KG Nürmbrecht, Germany | 20. 1345 |
| mouse IGFBP-1; DuoSet Quantikine ELISA kit | R&D Systems Inc., Minneapolis, USA | DY1588-05 |
| mouse IGFBP-3; DuoSet Quantikine ELISA kit | R&D Systems Inc., Minneapolis, USA | MGB300 |
| mouse IGF-I ELISA kit | Mediagnost, Reutlingen, Germany | E25 |
| MTBSTFA | Acros Organics, Thermo Fisher Scientific GmbH, Geel, Belgium | TS-48927 |
| MxP® Quant 500 kit | BIOCRATES LifeSciences AG, Innsbruck, Austria | 21094.12 |
| Nanophotometer | Implen GmbH, Munich, Germany | P300 |
| NEFA-HR (2) Assay | Fujifilm Wako Chemicals Europe GmbH, Neuss, Germany | 91797 |
| Pipette tips (1-1000 µL) | Sarstedt AG und Co.KG, Nürmbrecht, Germany | 70.762.010 |
| reverse phase column Gemini (250 × 4.6 mm, 5 µm C18 110 Å | Phenomenex, Aschaffenburg, Germany | 00G-4435-E0 |

| | | |
|---|---|---|
| Rezex RCM monosaccharide column (300 × 7.8 mm) | Phenomenex Inc., Aschaffenburg, Germany | 00H-0130-K0 |
| RNA 6000 Nano kit | Agilent Technologies, Waldbronn, Germany | NC1783726 |
| SensiFAST SYBR No-Rox Mix | Bioline, Berlin, Germany | BIO-98005 |
| SensiFAST™ cDNA Synthesis Kit | Bioline, Berlin, Germany | BIO-65054 |
| Sirius red | Sigma-Aldrich | 8185575 |
| Sonotrode MS 1 | Carl Roth, Karlsruhe, Germany | 9106601 |
| Synergi 4µm Hydro-RP 80 Å column (250 × 4.6 mm) | Phenomenex Inc., Aschaffenburg, Germany | 00G-4375-E0 |
| the G1315D diode array detector (210 nm or 230 nm) | Agilent Technologies, Waldbronn, Germany | G7115A |
| Tissue cassette | Simport Scientific Inc. | M499 |
| TriFast buffer | peqGOLD TriFast; VWR International GmbH, Hannover, Germany | 30-2010P |
| Universal Centrifuge | Thermo-Fisher Scientific GmbH, Waltham, MA, USA | 10196832 |
| Urea standard | Merck Chemicals GmbH, Darmstadt, Germany | 108487 |
| Uric acid standard | Merck Chemicals GmbH, Darmstadt, Germany | 229K17724817 |
| xPONENT® 3.1-Software | Luminex Corporate, Austin, USA | - |
| Xylazine | MEDISTAR Arzneimittelvertrieb GmbH | 7099786 |
| Xylene | J.T.Baker | 8118.1 |
| Zebron ZB-5HT column (30 m, 0.25 mm inner diameter, 0.25 µm film thickness | Phenomenex, Aschaffenburg, Germany | Zebron ZB-5HT |

### 8.4.1 Table S1. PCR primers, PCR efficiencies and Cq values for each primer

| **IGF-1 signalling genes** | | | | | | |
|---|---|---|---|---|---|---|
| **Gene Name** | **Gene Abbreviation** | **PrimeTime qPCR Primer Assay** | **Sequence F/R** | **Tissue** | **PCR Efficiency** | **Quantification cycle value (Cq)** |
| Insulin Like Growth Factor 1 Receptor | Igf1r | Mm.PT.58.11619137 | 5‘-GCCTACCTCAATGCCAACA-3‘ | *M. gastrocnemius* | 2.03 | 28 |
| | | | 5‘-TCTCGTAGATGTCTCGTGTCA-3‘ | *M. quadriceps* | 2.03 | 29 |
| Insulin Like Growth Factor Binding Protein 3 | Igfbp3 | Mm.PT.58.6744601 | 5‘-CATCTGAAGTTCCTCAATGTGC-3‘ | *M. gastrocnemius* | 2.13 | 28 |
| | | | 5‘-CCATACTTGTCCACACACCA-3‘ | *M. quadriceps* | 2.16 | 28 |
| Insulin Like Growth Factor Binding Protein 5 | Igfbp5 | Mm.PT.58.11593699 | 5‘-GTACCTGCCCAACTGTGAC-3‘ | *M. gastrocnemius* | 2.11 | 25 |
| | | | 5‘-GCTTCATTCCGTACTTGTCCA-3‘ | *M. quadriceps* | 2.16 | 25 |
| Insulin Receptor Substrate 1 | Irs1 | Mm.PT.58.43919344 | 5`-CCAGCATCAGCTTCCAGAA-3‘ | *M. gastrocnemius* | 2.06 | 26 |
| | | | 5‘-TGTGAATTGTGAAATAGTTCGAGTC-3‘ | *M. quadriceps* | 2.02 | 27 |
| **Myokine genes** | | | | | | |
| **Gene Name** | **Gene Abbreviation** | **PrimeTime qPCR Primer Assay** | **Sequence F/R** | **Tissue** | **PCR Efficiency** | **Quantification cycle value (Cq)** |
| Myostatin | MSTN | Mm.PT.58.13573446 | 5‘-GCCATGATCTTGCTGTAACCT-3‘ | *M. gastrocnemius* | 2.13 | 26 |
| | | | 5‘-CAGTCAAGCCCAAAGTCTCT-3‘ | *M. quadriceps* | 2.11 | 26 |
| **Proteolysis genes** | | | | | | |
| **Gene Name** | **Gene Abbreviation** | **PrimeTime qPCR Primer Assay** | **Sequence F/R** | **Tissue** | **PCR Efficiency** | **Quantification cycle value (Cq)** |
| F-Box Protein 32 | Fbxo32 | Mm.PT.58.7025875 | 5‘-TGAATAGCATCCAGATCAGCA-3‘ | *M. gastrocnemius* | 2.06 | 24 |
| | | | 5‘-GATGTTCAGTTGTAAGCACACAG-3‘ | *M. quadriceps* | 2.04 | 25 |
| Tripartite Motif Containing 63 | Trim63 | Mm.PT.58.32840172 | 5‘-GCTACCTTCCTCTCAAGTGC-3‘ | *M. gastrocnemius* | 2.01 | 24 |
| | | | 5‘-CCTCTGCTATGTGTTCTAAGTCC-3‘ | *M. quadriceps* | 1.99 | 24 |
| Ubiquitin B | UBB | Mm.PT.58.29038744 | 5‘-CCAGTGGGCAGTGATGG-3‘ | *M. gastrocnemius* | 1.98 | 20 |
| | | | 5‘-GCTTACCATGCAACAAAACCT-3‘ | *M. quadriceps* | 2.01 | 20 |
| **Protein synthesis genes** | | | | | | |
| **Gene Name** | **Gene Abbreviation** | **PrimeTime qPCR Primer Assay** | **Sequence F/R** | **Tissue** | **PCR Efficiency** | **Quantification cycle value (Cq)** |
| AKT Serine/Threonine Kinase 1 | Akt1 | Mm.PT.58.8333433 | 5‘-GACGTAGCCATTGTGAAGGAG-3‘ | *M.gastrocnemius* | 2.20 | 28 |
| | | | 5‘-GCCGTTCCTTGTAGCCAAT-3‘ | *M.quadriceps* | 2.12 | 28 |

| | | | | | | |
|---|---|---|---|---|---|---|
| Phosphoinositide-3-Kinase Regulatory Subunit 1 | Pik3r1 | Mm.PT.58.5285167 | 5‘-AGAAAGGACTGGAATGTTCGAC-3‘ | *M.gastrocnemius* | 2.25 | 27 |
| | | | 5‘-GCATCTGCTAAGACGTGTAGC-3‘ | *M.quadriceps* | 2.17 | 26 |
| **Reference genes** | | | | | | |
| **Gene Name** | **Gene Abbreviation** | **PrimeTime qPCR Primer Assay** | **Sequence F/R** | **Tissue** | **PCR Efficiency** | **Quantification cycle value (Cq)** |
| Beta-2-Microglobulin | B2M | Mm.PT.39a.22214835 | 5‘-TGGTCTTTCTGGTGCTTGTC-3‘ | *M.gastrocnemius* | 2.09 | 24 |
| | | | 5‘-GGGTGGAACTGTGTTACGTAG-3‘ | *M.quadraceps* | 2.15 | 24 |
| Peptidylprolyl Isomerase A | Ppia | Mm.PT.39a.2.gs | 5‘-CAAACACAAACGGTTCCCAG-3‘ | *M.gastrocnemius* | 2.09 | 24 |
| | | | 5‘-TTCACCTTCCCAAAGACCAC-3‘ | *M.quadriceps* | 2.13 | 24 |
| Ribosomal Protein Lateral Stalk Subunit P0 | Rplp0 | Mm.PT.58.43894205 | 5‘-TTATAACCCTGAAGTGCTCGAC-3‘ | *M.gastrocnemius* | 2.03 | 23 |
| | | | 5‘-CGCTTGTACCCATTGATGATG-3‘ | *M.quadriceps* | 2.01 | 22 |
| RNA Polymerase II Subunit A | Polr2a | Mm.Pt.39a.22214849 | 5‘-GGTCCTTCGAATCCGCATC-3‘ | *M.gastrocnemius* | 2.15 | 28 |
| | | | 5‘-CAGGGTCATATCTGTCAGCATG-3‘ | *M.quadriceps* | 2.14 | 28 |

## 8.5 *Curriculum Vitae*

**Personal data**

| | |
|---|---|
| Name: | Ottavia Agrifoglio |
| Date of birth: | 04 November 1989 |
| Place of birth: | Catania (Italy) |

**Education**

| | |
|---|---|
| 06.2016 | Abilitazione alla professione di Biologo (Biology qualification exam)<br>University of Catania |
| 03.2015-04.2015 | International internship – Epidemiology and Public Health<br>Queen Mary University of London, Blizard Institute - Barts and the London School of Medicine and Dentistry |
| 10.2013-11.2015 | Laurea Magistrale in Biologia Cellulare e Molecolare (M.Sc. in Cell and Molecular Biology)<br>University of Catania |
| 10.2009-03.2013 | Laurea Triennale in Scienze Biologiche (B. Sc in Biology)<br>University of Catania |
| 09.2008-10.2009 | Facoltà di Lettere Classiche (Faculty of Classical Studies)<br>University of Catania |
| 09.2004-06.2008 | Diploma di Liceo Classico (High School Diploma)<br>Liceo Ginnasio Statale "Mario Cutelli" (Catania, Italy) |
| 09.2000-06.2003 | Licenza media<br>Scuola Media Statale "Dante Aligheri" (Catania, Italy) |
| 09.1995-06.2000 | Licenza elementare<br>Scuola Elementare "Mario Rapisardi" (Catania, Italy) |

**Work experience**

| | |
|---|---|
| 07.2022-09.2024 | Researcher - Rostock University Medical Center, Department of Medicine II, Division of Gastroenterology and Endocrinology |

| | |
|---|---|
| 03.2019-06.2022 | Doctoral student – Research Institute for Farm Animal Biology (FBN – Dummerstorf) |
| 02.2018-07.2018 | Tutorship "Alternanza Scuola Lavoro" – University of Catania and Liceo Classico "N. Spedalieri" |
| 09.2017-10.2017 | Tutorship "Piano Nazionale Lauree Scientifiche per le lauree in biologia e biotecnnologie" – University of Catania |
| 06.2016-07.2017 | Tutorship "Alternanza Scuola Lavoro" – University of Catania and Istituto Superiore "E. Vittorini" |
| 04.2015-11.2015 | Tutorship Hygene and Statistics – University of Catania |

**Publications**

**Agrifoglio O.**, Görs S., Sciascia Q., Li Z., Albrecht E., Achilles S., Statz M., Bastian M., Lindner T., Gauß KF., Rohde S., Rischmüller K., Berlin P., Lamprecht G., Jaster R., Metges CC., Ehlers L. **"**Changes in Protein Metabolism and Early Development of Sarcopenia in Mice With Cholestatic Liver Disease.**"** J Cachexia Sarcopenia Muscle. 2025 Feb;16(1):e13737. doi: 10.1002/jcsm.13737. PMID: 39971588; PMCID: PMC11839266.

**Agrifoglio O.,** Kasprick A., Gross N., Wahlig M., Kauffold E., Woitas A., Vorobyev A., Ehlers L., Ludwig RJ., Bieber K., Jaster R. **"**Dexamethasone's Clinical Efficacy in Experimental Autoimmune Pancreatitis Correlates with a Unique Transcriptomic Signature, Whilst Kinase Inhibitors Are Not Effective.**"** Biomedicines. 2024 Oct 29;12(11):2480. doi: 10.3390/biomedicines12112480. PMID: 39595046; PMCID: PMC11591683.

Ehlers L., Bannert K., Rohde S., Berlin P., Reiner J., Wiese M., Doller J., Lerch MM., Aghdassi AA., Meyer F., Valentini L., **Agrifoglio O.**, Metges CC., Lamprecht G., Jaster R. "Preclinical insights into the gut-skeletal muscle axis in chronic gastrointestinal diseases." J Cell Mol Med. 2020 Aug;24(15):8304-8314. doi: 10.1111/jcmm.15554. Epub 2020 Jul 6. PMID: 32628812; PMCID: PMC7412689**.**

Barchitta M., Maugeri A.**,** **Agrifoglio O**., Favara G., La Mastra C., La Rosa MC., Magnano San Lio R., Agodi A. "Comparison of Self-Administered Web-Based and Interviewer Printed Food Frequency Questionnaires for Dietary Assessment in Italian Adolescents." Int J Environ Res Public Health. 2019 Jun 1;16(11):1949. doi: 10.3390/ijerph16111949. PMID: 31159389; PMCID: PMC6604022.

Barchitta M., Maugeri A., Quattrocchi A., **Agrifoglio O.**, Scalisi A., Agodi A. **"**The Association of Dietary Patterns with High-Risk Human Papillomavirus Infection and

Cervical Cancer: A Cross-Sectional Study in Italy.**"** Nutrients. 2018 Apr 11;10(4):469. doi: 10.3390/nu10040469. PMID: 29641467; PMCID: PMC5946254.

Barchitta M., Maugeri A., Quattrocchi A., **Agrifoglio O.**, Agodi A. "The Role of miRNAs as Biomarkers for Pregnancy Outcomes: A Comprehensive Review." Int J Genomics. 2017;2017:8067972. doi: 10.1155/2017/8067972. Epub 2017 Aug 13. PMID: 28884117; PMCID: PMC5572592.

---

**Participation to congresses**

---

**Agrifoglio, O.;** Görs, S.; Sciascia, Q.; Albrecht, E.; Lindner, T.; Rischmüller, K.; Jaster, R.; Lamprecht, G.; Metges, C. C.; Ehlers, L. „Veränderungen im Proteinstoffwechsel und frühe Entwicklung von Sarkopenie bei Mäusen mit cholestatischer Lebererkrankung" Zeitschrift für Gastroenterologie 2024; 62(09): 706 - 707 DOI: 10.1055/s-0044-1789868

**Agrifoglio O.**, Wahlig M., Kasprick A., Bieber K., Ludwig R., Jaster R. „Effects of tofacitinib and takinb on autoimmune pancreatitis in mice" European Pancreasclub meeting 2024

Agrifoglio O., Wahlig M., Kasprick A., Bieber K., Ludwig R., Jaster R. „Effects of tofacitinib and takinb on autoimmune pancreatitis in mice" Deutsches Pankreasclub Tagung 2024

**Agrifoglio O.**, Görs S., Sciascia Q., Li Z., Statz M., Ehlers L., Jaster R., Lamprecht G., Metges C.C. "Food intake and protein and amino acid metabolism in a murine bile duct ligation model of liver cirrhosis" 59. Wissenshaftlicher Kongress – Deutsche Gesellschaft für Ernährung

L. Netz, R. Jaster, J. Reiner, P. Berlin, K. Bannert, S. Rohde, D. Revskij, **O. Agrifoglio,** C.C. Metges, A.A. Aghdassi, G. Lamprecht, L. Ehlers „Störungen der Darmbarrierefunktion bei experimenteller Cholestase: molekulare Mechanismen und Einfluss von Ghrelin". Z Gastroenterol 2021; 59(08): e180-e181. DOI: 10.1055/s-0041-1733540

**Agrifoglio O.**, Görs S., Li Z., Statz M., Ehlers L., Jaster R., Lamprecht G., Metges C.C. „Sarcopenia in a murine bile duct ligation model of liver cirrhosis" ESVCN Conference 2021

Maugeri A., Barchitta M., **Agrifoglio O.**, Favara G., La Mastra C., La Rosa MC., Magnano San Lio R., Panella M., Cianci A., Agodi A. "The impact of social determinants and lifestyles on dietary patterns during pregnancy: evidence from the "Mamma & Bambino" study". Ann Ig. 2019 Mar-Apr;31(2 Supple 1):81-89. doi: 10.7416/ai.2019.2280. PMID: 30994167.

Barchitta M., Maugeri A., **Agrifoglio O**., Favara G., La Mastra C., La Rosa MC., Magnano San Lio R., Agodi A. "Dietary patterns and school performance: evidence from a sample of

adolescents in Sicily, Italy." Ann Ig. 2019 Mar-Apr;31(2 Supple 1):72-80. doi: 10.7416/ai.2019.2279. PMID: 30994166.

**M. Barchitta, A. Maugeri, MC.** La Rosa, **O. Agrifoglio**, C. La Mastra, A. Agodi. "Adherence to the mediterranean diet is positively associated with LINE-1 methylation levels." European Journal of Public Health, Volume 28, Issue suppl_4, November 2018, cky214.008, https://doi.org/10.1093/eurpub/cky214.008

**A. Maugeri, M. Barchitta, MC.** La Rosa, **O. Agrifoglio**, C. La Mastra, A. Agodi. "Exposure to particulate matter and DNA methylation in women from Catania, Italy." European Journal of Public Health, Volume 28, Issue suppl_4, November 2018, cky213.313, https://doi.org/10.1093/eurpub/cky213.313

Barchitta M., Quattrocchi A., Maugeri A., La Rosa MC., **Agrifoglio O.**, La Mastra C., Scalisi A., Agodi A. "Associazioni tra profili nutrizionali ed il rischio di infezione da HPV e di cercico-carcinoma: studio su una popolazione di donne in Sicilia". In Atti del 50° Congresso Nazionale SItI. Torino, 22-25 Novembre 2017

## 8.6 Acknowledgements

This doctoral thesis was funded through the research project “EnErGie” by the European Social Fund (ESF; references: ESF/14-BM-A55-0007/18 and -0010/18) and the Ministry of Education, Science, and Culture of Mecklenburg-Vorpommern.

I would like to thank all the people who have contributed to the success of this doctoral dissertation. I would like to thank my first supervisor, Professor Cornelia Metges, for the opportunity to carry out this doctorate. Her supervision and feedback opened my mind to new research perspectives and strengthened both my knowledge and my spirit, enriching my professional abilities. My gratitude goes also to my second supervisor, Professor Robert Jaster. Thank you for all the encouragement, patience, constructive feedback, opportunities, and trust, Many thanks also to my mentor, Dr. Quentin Sciascia: thank you for the support (professional and personal) and for cheering on me even when I thought I wanted to quit. Your help was essential. I would also like to thank Dr. Solvig Görs: dear Solvig, thank you for being my “FBN mum”. Thanks for all the explanations, for the brainstorming sessions, for the patience, and for the continued corrections and revisions. Thank you, especially for the cups of tea, the marshmallow mice and chocolate, the nights at the theatre, the lunches, the chat and the ice creams, the little presents for Teresa. You have no idea how welcome you made me feel since day one. I am thankful also to all the technical personnel of the FBN Dummerstorf: Mrs. Karpati, Mrs. Wunsche, Mr. Geick, Mrs. Dwarfs, and Mrs. Mielenz. Their work was crucial for the obtainment of the results shown in this dissertation. Many thanks also to Sophie and Meike, whose help was precious both during the animal trial and in the lab.

I would like to express my gratitude also to my colleagues at the UMR. Firstly, I am grateful to Dr. Luise Ehlers for the help in organizing the mice work and revising the data, the manuscript, and the dissertation. Dear Luise, I know it was hard work and yet you were always there with your positive attitude and your friendly advice. Many thanks to my colleagues of the Gastroenterology Lab: Dr. Rischmüller, Dr. Berlin, Mrs. Bergmann. Your help and feedback were precious, thank you for all that you have done.

Many thanks also to my Italian family in Rostock, always ready to cheer on me: Daria, Grazia, Marzia, thank you for being there and supporting me!

A very special thanks go out to Johannes: thank you for the coffee and snacks, for the chat and the phone calls, the support and the encouragement. My FBN journey would have been so boring without you, I loved sharing my desk with you, even when you came back from the pig facility stinking like…pigs, you know. A special thought goes to the late Prof. Guglielmo Longo (University of Catania). Every time I felt like quitting, I had your voice in mind saying

that my head was stronger than concrete and there was no chance I could not accomplish whatever I put my mind into. You would laugh if you saw me fighting with all those histological slides to get my results. Thank you.

Last but not least, I would like to thank my family: Mum, Dad, Anto, we might be far on the map, but I have always felt you close to me. Thank you for seconding my dreams and ambitions and letting me go to the other side of Europe, I know it is not always easy. All my gratitude goes out to Michael. Thank you for being my strength and stay, for being my first and stronger supporter, for tolerating me even when I was unbearable, for believing in me when I was so exhausted and demotivated to do it. You have no idea how much you helped me to go through this path. And finally, thank you, Teresa, you taught me that the best things in life require patience. I dedicate to you every single word and effort put in this work, my child.

## 8.7 Statement of independence

I hereby declare that I have written this dissertation “Metabolic alterations and early development of sarcopenia in a murine model of cholestatic liver disease” independently and that I have not used any other aids than the ones referenced. The sources of phrases, wording, figures, and tables taken from other works have been clearly cited. I hereby further declare that I have written this dissertation in accordance with the principles of good scientific practice and in accordance with the current “Regeln zur Sicherung guter wissenschaftlicher Praxis und zur Vermeidung Fehlverhaltens” of the University of Rostock.